NASA
Technical
Paper
2384

March 1985

Description and Calibration of the Langley Hypersonic CF_4 Tunnel

A Facility for Simulating Low γ Flow as Occurs for a Real Gas

Raymond E. Midden and
Charles G. Miller III

NASA

NASA Technical Paper 2384

1985

Description and Calibration of the Langley Hypersonic CF_4 Tunnel

A Facility for Simulating Low γ Flow as Occurs for a Real Gas

Raymond E. Midden and
Charles G. Miller III

Langley Research Center
Hampton, Virginia

NASA
National Aeronautics
and Space Administration

Scientific and Technical Information Branch

Summary

The Langley Hypersonic CF_4 Tunnel is the only operational, conventional-type (as opposed to impulse) hypersonic wind tunnel in this country which simulates one of the important aspects of real-gas phenomena experienced during reentry of a blunt vehicle, that is, the decrease in the ratio of specific heats (frequently referred to as gamma or γ) that occurs within the shock layer about the vehicle because of dissociation. A detailed description of this facility is presented which includes discussion of the basic components, instrumentation, and operating procedure. Results from pitot-pressure surveys measured at the nozzle exit and downstream of the exit for reservoir temperatures from 1020°R to 1495°R and reservoir pressures from 1000 to 2550 psi are presented along with sample measurements made with models of various shapes.

At the maximum value of reservoir pressure and temperature, a uniform test core having a diameter of approximately 11 in. (0.55 times the nozzle-exit diameter) exists. The corresponding free-stream Mach number is 5.9, the unit Reynolds number is 4×10^5 per foot, the ratio of specific heats immediately behind a normal shock is 1.10, and the normal-shock density ratio is 12.6. When the facility is operated at reservoir temperatures below 1440°R, the test-core diameter increases to about 14 in. but pitot-pressure variations occur on the centerline, indicating the existence of flow disturbances originating in the upstream region of the nozzle. Although these centerline irregularities are relatively small in magnitude and, in general, result in a perturbation in centerline free-stream Mach number of less than 1.5 percent, they significantly impact the flow about a blunt model tested on the nozzle centerline. Because these disturbances are contained within a small region (0.5-in. radius) about the centerline, properly sized models can be tested off centerline in the uniform flow between the centerline-disturbance region and the nozzle boundary layer or the lip shock originating at the nozzle exit and converging toward the nozzle centerline. Pitot-pressure surveys performed in this region revealed that the flow was uniform. The average pitot pressure, and hence average free-stream Mach number, across the test core was essentially constant between the nozzle exit and 12 in. downstream of the nozzle exit. A comparison of measured and predicted shock detachment distance, pressure distributions, and heat-transfer distributions on models of various shapes positioned off the nozzle centerline and up to 12 in. downstream of the nozzle exit also indicated that the flow in this region was axially and radially uniform. Samples of data obtained in this facility with various models are presented to illustrate the effect of the ratio of specific heats on the flow conditions about the model and the potential significance of knowing the magnitude of this effect.

Introduction

During entry of blunt vehicles into Earth and other planetary atmospheres, values of normal-shock density ratio are encountered that are significantly larger than values generated in conventional-type (as opposed to impulse) hypersonic wind tunnels with air or nitrogen as the test gas. These high values of density ratio result from the dissociation of the atmospheric gas as it passes through the shock and into the high-temperature shock layer. With the onset of dissociation, the shock layer experiences a significant decrease in static temperature, a slight increase in static pressure, and hence a significant increase in density. These phenomena are commonly referred to as real-gas effects.

The importance of real-gas effects has been recognized for well over two decades. Early studies revealed that the primary factor governing the inviscid flow field about blunt bodies at hypersonic speeds is the normal-shock density ratio. (See reference listing of ref. 1.) For example, the bow-shock detachment distance is dependent on the density ratio across the shock and is of practical importance in radiative heat-transfer studies because it determines the volume of gas available to radiate. Also, real-gas effects may significantly impact the aerodynamic characteristics of blunt bodies because of changes in the level of pressure and variations to the pressure distribution over the surface, particularly in regions of compression or expansion.

Unfortunately, the majority of data demonstrating real-gas effects are analytical, and little experimental data exist for verification of various computer codes. This relative scarcity of experimental data at high values of normal-shock density ratio is due, in part, to developmental and hardware problems associated with high-enthalpy facilities capable of generating hypersonic-hypervelocity real-gas flows. Most of these facilities are of an impulse or ballistic-range type. The disadvantages of impulse facilities, as compared with ideal-gas conventional-type wind tunnels, are well recognized. (Examples are short test times, poor test repeatability, flow contamination, complex instrumentation with associated poor reliability and relatively large uncertainties, and departure from equilibrium flow during the nozzle expansion process or within the shock layer of the test model.) An alternate method for generating high normal-shock density ratio at hypersonic conditions, but with relatively low enthalpies, is to employ a test gas having a low ratio of specific heats (frequently referred to as gamma or γ) in a conventional-type wind tunnel (ref. 2). A study of this method is reported in reference 3, in which tetrafluoromethane

(CF_4) was used as the test gas in a small (3-in-diameter test section) pilot model wind tunnel. The CF_4 gas was selected now only because of its low ratio of specific heats but also because of its low boiling point, thermal stability, and low vibrational relaxation time; in addition, it is readily available, nontoxic, and easily reclaimed. These tests with CF_4 demonstrated that values of normal-shock density ratio as high as 12 were obtained at a free-stream Mach number of 6, and measured pitot pressure and nozzle-wall (free-stream static) pressure were in good agreement with prediction. They also demonstrated the need for a larger CF_4 wind tunnel; hence, the Langley 20-Inch Hypersonic Arc-Heated Tunnel (ref. 4) was modified and became the Langley Hypersonic CF_4 Tunnel (ref. 5), which is referred to herein as the CF_4 Tunnel.

The addition of the CF_4 Tunnel to the collection of hypersonic wind tunnels at the Langley Research Center added a new dimension to the research capability at Langley. Valuable information concerning the effect of gamma on the flow about a proposed reentry vehicle could now be obtained experimentally by testing a model both in the CF_4 Tunnel and in the Langley 20-Inch Mach 6 Tunnel (ref. 6), which is referred to herein as the Mach 6 Tunnel. These two facilities provide nearly the same free-stream Mach number in ideal air ($\gamma = 1.4$) as in CF_4 ($\gamma_\infty = 1.2$), but the unit free-stream Reynolds number can be matched only by operating the CF_4 Tunnel near its maximum reservoir pressure of 2500 psia and by operating the Mach 6 Tunnel at a low reservoir pressure (approximately 40 psia). These pressure levels introduce difficulties for both facilities, but they may be relaxed for blunt-body testing in which small mismatches in Mach number and Reynolds number are of little concern. For a blunt body (i.e., a body with a sonic corner) in flight, the thermochemical equilibrium value of gamma within the shock layer will change little between the nose region and the shoulder. Gamma will also be constant within the shock layer over the front of a blunt body tested in the CF_4 Tunnel, thereby simulating the low gamma aspect of an equilibrium real gas. An estimate of the differences attributed to real-gas effects may be provided by testing this same blunt body in the ideal-air flow of the Mach 6 Tunnel. The simulation of low gamma effects in the CF_4 Tunnel for a relatively slender and/or lifting-type reentry vehicle is not as accurate as for a blunt body. This is because a lifting-type vehicle will generally experience longitudinal or circumferential variations in gamma within the flow field during flight, whereas the flow about models of these vehicles in the CF_4 Tunnel will be characterized by a nearly constant gamma. However, this does not diminish the overall importance of performing tests of such shapes in the CF_4 Tunnel because these tests provide an assessment of gamma effects not possible elsewhere. The geometric complexity of most lifting-type vehicles requires the designer to rely heavily on experiment since such shapes are not readily amenable to analytical treatment with flow-field codes.

Results from the preliminary calibration of the Langley Hypersonic CF_4 Tunnel were reported in reference 5. Since this first calibration, a number of changes have been made to facility hardware, instrumentation, and operating procedure, and more detailed calibrations have been performed. The present report presents a general description of the CF_4 Tunnel and its modifications, a discussion of operational experience (both in the text and in the appendix), and results from this more extensive calibration along with examples of results obtained with various models.

Symbols

The symbols enclosed in parentheses denote computer symbols used in table I.

	(A)	speed of sound
C_h		heat-transfer coefficient, lbm/ft^2-sec
C_m		pitching-moment coefficient
C_p		pressure coefficient
	(H)	enthalpy
L		distance from nose tip, in.
M		Mach number
	(NPR)	Prandtl number
p	(P)	pressure, psia
	(Q)	dynamic pressure
$\dot{q}$		heat-transfer rate, Btu/ft^2-sec
R	(NRE)	unit Reynolds number, ft^{-1}
r		radius, in.
	(S)	entropy
s		wetted surface length, in.
T		temperature, °R or °F
t		time, sec
	(U)	velocity
	(VIS)	viscosity

x, y, z		nozzle or model coordinates (rectangular coordinates where x is the horizontal axis, y is the vertical axis, and z is along the nozzle axis, with $z = 0$ at nozzle exit), in.
Z		compressibility factor
α		angle of attack, deg
γ	(GAM)	ratio of specific heats
θ		angle subtended by a circular arc measured from the hemisphere axis, deg
ρ	(RHO)	density, lbm/ft^3
ϕ		circumferential angle measured from the most leeward meridian, deg

Subscripts:

b		base or shoulder
eff	(EFF)	effective
n		model nose
sph		hemisphere stagnation point
$t, 1$	(T1)	reservoir conditions
$t, 2$	(T2)	stagnation conditions behind normal shock
w		wall
∞	(1)	free-stream static conditions
2		static conditions behind normal shock

Abbreviations:

BL	boundary layer
CA	chromel-alumel
$\mathfrak{q}$	nozzle centerline
ESP	electronically scanned pressure
IC	iron-constantan

A bar over a symbol denotes the average value.

Facility

Description

The Langley Hypersonic CF_4 Tunnel is a conventional type, blowdown wind tunnel that uses tetrafluoromethane (CF_4) (manufactured as Dupont Freon-14) as the test gas. This facility, which was originally the Langley 20-Inch Hypersonic Arc-Heated Tunnel (ref. 4), is shown schematically and photographically in figure 1. Basic components include a CF_4 storage trailer, high-pressure storage field, pressure regulator, lead-bath heaters, nozzle, test section, diffuser, vacuum system, and CF_4 reclaimer. These basic components will now be discussed briefly.

High-pressure CF_4 system. The high-pressure CF_4 system consists of a compressor capable of producing pressures up to 5000 psia, two bottlefields, a storage trailer, a pressure regulator, and applicable control valves. One bottlefield consists of a single bottle, and the other consists of three storage bottles; each bottle has a volume of 30 ft^3 and a design pressure of 5000 psia. The storage bottles are generally maintained at pressures between 2500 and 3500 psia and are located outside the building that houses the test section; hence, they are at ambient (outside) temperature. The supply trailer is rated for a maximum pressure of 2500 psia. The desired pressure of CF_4 from the storage bottles into the heaters is controlled by an externally loaded dome pressure regulator. All piping downstream of the storage bottles, including piping between the heaters and settling chamber, is AISI type 304 or 316 stainless steel.

Heaters. The CF_4 test gas is heated to a maximum temperature of approximately 1530°R by two lead-bath heaters in parallel. A sketch of a lead-bath heater is shown in figure 2. Each heater contains 20 000 lb of molten lead that is heated by eighteen 3-kW heating elements. The test gas flows through 44 spirally wound stainless-steel tubes, each having an inside diameter of 0.25 in. and outside diameter of 0.375 in., immersed in the molten-lead container. The maximum design pressure for the heater is 3000 psia. The 220-V resistance heaters are controlled thermostatically in a manner that continuously regulates power to the heaters. Each heater requires approximately 6 hr to achieve operating temperature from the ambient temperature and has a 45-min recovery time for a 500°R drop in temperature. The flow rate through the heaters ranges from approximately 3 to 10 lbm/sec. These heaters are enclosed in a small, heavily insulated room with its own ventilation system within the tunnel test room.

Settling chamber and nozzle. An in-line filter has recently been installed between the heaters and the settling chamber to trap particles greater than 10 microns in diameter. This flow-through, cylindrical filter is fabricated from 316 stainless steel (housing and mesh), is 2 ft long, has a diameter of 6 in., and is rated

for 3000 psia and 1500°R. The settling chamber is of conventional design and consists of a pressure vessel, diffusing cone, and fine-mesh screens (figs. 3 and 4). The pressure vessel is 12 in. long, has an inside diameter of 7.0 in., and has a wall thickness of 2.5 in. Flow enters the settling chamber through the perforated cone and then passes through a pair of screens or a screen and porous-plate combination before entering the nozzle. (Components of the settling chamber are shown in the photograph of fig. 4.) The piping between the heaters and settling chamber, the in-line filter, and the settling chamber are all wrapped with electric-resistance heaters and an outer layer of insulation. These components are heated to the desired reservoir temperature for the CF_4 test gas primarily for the following reasons: (1) to minimize thermal gradients in the CF_4 adjacent to the reservoir wall for reasons discussed in reference 7, (2) to minimize heat loss from the CF_4 test gas in its travel from the heater to the nozzle, and (3) to reduce thermal shock to the reservoir and nozzle such as that which occurs when a cool surface is suddenly subjected to a rapid increase in temperature.

The contoured, axisymmetric nozzle has a throat diameter of 0.446 in. (see fig. 3) and exit diameter of 20 in. This nozzle was designed by using the methods of references 3 and 8 to generate Mach 6 flow in CF_4 at the nozzle exit. The settling chamber and nozzle throat section were designed for a maximum pressure of 3000 psia and a temperature of 1600°R.

Test section. The flow exhausts from the nozzle into an open-jet test section approximately 6 ft long with an internal diameter of 5 ft (fig. 5). Models are supported at the nozzle exit by a pneumatically driven injection mechanism. The angle of attack may be varied over a range from $-10°$ to $50°$ with a $0.1°$ uncertainty, but it is not variable during a run. The injection time (the time required for the model to move from its retracted position to the nozzle centerline) is variable from approximately 0.3 to 0.7 sec, and the retraction time is less than 1 sec. The test section is protected from overpressure by a deadweight relief valve designed to open at 1 psi. Operable windows measuring 24 by 30 in. are located on opposite sides of the test section for flow-visualization purposes (primarily schlieren); a 24- by 30-in. fixed window is also located on the top of the test section, with two 12-in-diameter windows inclined 45° positioned on each side of this large window (fig. 1(b)).

Vacuum system. After traversing the open test section, the test gas is collected by a diffuser, passed through a water-cooled heat exchanger to reduce its temperature, and dumped into two vacuum spheres that have been evacuated to a pressure of approximately 0.01 psia by three vacuum pump-blower combinations. The vacuum spheres have diameters of 17 ft and 51 ft for a combined total volume of 72 000 ft^3. A fourth vacuum pump-blower combination is used to evacuate the nozzle and test section to approximately 0.01 psia prior to a run.

Reclaimer. A schematic drawing of the reclaimer is shown in figure 6. After having collected CF_4 from a single run or several runs, the spheres are evacuated with vacuum pumps that exhaust directly into the reclaimer system. The contaminated CF_4 gas first passes through a heat exchanger for initial cooling, then through a separator (filter) for oil and water removal, and then through a second heat exchanger. It next travels into a liquid nitrogen (LN_2) cooled condenser (fig. 6) in which the CF_4 is liquefied (LCF_4) and the gaseous impurities are exhausted to atmosphere. The nominal operating pressure of the condenser is 0.5 to 2 psig. The liquid CF_4 is then compressed to approximately 5000 psia, passed through a vaporizer to be converted to a gas, and returned to the storage bottles. Liquid nitrogen is supplied to the condenser from a 4000-gal trailer maintained at a pressure of 40 psig.

Operating Procedure

To prepare for a run, the settling chamber, nozzle, test section, diffuser, and vacuum spheres are evacuated to a pressure of about 0.01 psia. The lead-bath heaters are set to the desired temperature for the CF_4 test gas, and the pressure regulator is set to the desired reservoir pressure. (For reasons to be discussed subsequently, argon is maintained in the heaters at about 30 psig during the night and other periods of inactivity. This inert gas is removed prior to the first run of the day (or after tunnel shutdown) by venting to atmosphere. The lines and heater tubes are then evacuated and filled with CF_4. Generally, a short-duration blowdown run is made to remove any residual particles in the lines and settling chamber.) Test flow is initiated by actuating a preset program that automatically opens the appropriate valves. Following the establishment of steady flow, which requires about 3 sec, the model is injected into the flow. After desired data are obtained, the model is retracted and the tunnel is shut down. The nominal run time is 10 sec; however, a maximum run time of approximately 30 sec is possible. The time interval between runs is normally 45 to 60 min. This time is required to evacuate the spheres to the desired pressure, pump up the CF_4 storage bottlefield either from the reclaimer or the CF_4 trailer, and allow the heaters to recover. The gas collected in the spheres may be reclaimed while tests are in progress. In an effort to minimize impurities, the facility is maintained under vacuum and is opened to the atmosphere only when necessary (e.g., to perform a model change).

Instrumentation

An extensive modernization of the data acquisition system for the CF_4 Tunnel has recently been completed. This stand-alone system is schematically shown in figure 7.

The reservoir pressure $p_{t,1}$, temperature $T_{t,1}$, and pitot pressure $p_{t,2}$ at or just downstream of the nozzle exit are routinely measured for each run. The reservoir pressure is measured with a strain-gauge pressure transducer having a full-scale rating of 3000 psia. This transducer, which is calibrated periodically over the range from 0 to 3000 psia, is believed to provide values of $p_{t,1}$ that are accurate to within ± 2 percent. The reservoir temperature is measured with two chromel-alumel thermocouples (primary and backup) inserted through the wall of the settling chamber and positioned near the center of the chamber. Measured values of $T_{t,1}$ are also believed to be accurate to within ± 2 percent. A flat-faced cylindrical probe, having an inside diameter of 0.06 in. and outside diameter of 0.09 in., that is coupled with either an electronically scanned pressure (ESP) silicon sensor (ESP-32 model 780, manufactured by Pressure Systems, Incorporated (PSI)) or with a variable-capacitance diaphragm transducer (manufactured by Datametrics), is used to measure the pitot pressure during a run. This probe may be positioned at the desired axial and radial station, and the pitot-pressure measurement is believed to be accurate to within ± 2 percent.

Basic model measurements include forces and moments, surface pressures, surface heat-transfer rates, and shock shapes. A total of 138 channels of instrumentation are available for measuring model pressures. Of this number, 128 channels are electronically scanned and the remaining 10 are variable-capacitance diaphragm transducers. Each electronically scanned pressure (ESP) module contains 32 sensors (referred to as ESP-32 by PSI), and these modules are mounted inside the tunnel at the base of the strut to minimize tubing length between the model and sensor. (The ESP-32 combines 32 pressure transducers, internal multiplexing, and amplification to provide a scanner for a high data rate. An integral, pneumatically controlled slide allows the transducers to be calibrated on line. This on-line calibration consists of applying three accurately known pressures (actually vacuum levels) to the sensors; these levels are generally selected to cover the expected surface pressure levels for a run.) The sample rate for the ESP system is 10 samples per second for each of the 128 channels, or 20 samples per second for 64 channels. This fast response system has been used to measure pressures ranging from the test-section pitot pressure (a maximum of 3.5 psia) to pressures nearly as low as the free-stream static pressure (a minimum of 0.03 psia).

Surface heat-transfer rates are measured by using either the conventional thin-skin transient calorimeter technique or thin-film resistance gauges (ref. 9). For both techniques, the model is rapidly injected into the flow for a short period of time, usually 2 to 3 sec, and then is retracted. A potentiometer referred to as a slide wire is used to determine the position of the model during its injection into the flow. One hundred channels are available for chromel-alumel thermocouples, and 100 channels are also available for iron-constantan thermocouples; a reference temperature of 32°F is accurately maintained for both types of thermocouples. One hundred channels of constant-current circuitry interfaced to a 12-bit analog-to-digital (A/D) system controlled by a Hewlett-Packard 9826 desktop computer are available for thin-film resistance gauges.

The ESP-32 (model 780 PSI system) contains its own signal-processing system and thus is interfaced directly to the controller, a Hewlett-Packard 9845 desktop computer with extended memory of nearly 1 megabyte. Peripheral equipment includes an 8-in-diameter, dual-disc mass storage unit and a multipen plotter. The output signals from the variable-capacitance pressure transducers, thermocouples, and strain-gauge force balance are fed into a 128-channel, 14-bit, amplifier per channel, analog-to-digital (A/D) system (system 620/series 100 manufactured by the NEFF Instrument Corporation). The amplifier gain and the filter may be varied for each channel via plug-in units. Like the PSI system, the NEFF system is interfaced to the computer via a pacing unit and real-time clock that allows different sampling rates to be used during a run (e.g., a relatively slow sampling rate prior to model insertion and a much faster rate once the model is in the flow). Data from the NEFF system are usually sampled at 50 samples per second for each channel following model insertion, but rates as high as 150 samples per second are possible. The cables, patchboard, and NEFF A/D system are calibrated as one by using an accurately known output of a voltage calibration standard located at the tunnel test section.

Measurement Techniques

To minimize the amount of CF_4 test gas used, the run duration is generally tailored to the type of measurement. Time histories of reservoir pressure and temperature, pitot pressure, and slide-wire output are shown in figure 8 for a representative run. Also shown in this figure is the response of a thin-film resistance heat-transfer gauge injected into the flow. The pitot-pressure time history of figure 8(c) demonstrates that approximately 3 sec are required to establish a steady-flow condition at the nozzle exit, and the duration of steady flow for this particular run is approximately 7 sec. This

flow duration of 7 sec is satisfactory for force and moment and heat-transfer tests. However, because of lag time, the run duration must sometimes be increased for measuring pressures near the free-stream static pressure, particularly with variable-capacitance diaphragm transducers. The measured values of pitot pressure presented herein correspond to steady-flow test times of 6 to 8 sec.

Shock shapes are usually recorded with a pulsed white-light, single-pass schlieren system. However, they may also be recorded with the dual-plate holographic interferometer system shown schematically in figure 9 and discussed in detail in reference 10. Holograms are recorded by using a pulsed ruby laser that provides a 50-mJ pulse of 20 nsec duration. A 6-mW He-Ne alignment laser is positioned behind the ruby laser, and a third laser (50-mW argon) is used for reconstruction. The holograms may be used to produce shadowgraphs, schlieren photographs, or interferograms of the test flow. Representative schlieren and interferogram photographs are presented in figure 10.

Another flow diagnostic used in this facility is the oil-flow technique. Usually, models are painted black, sprayed with a mixture of oils of various viscosities mixed with white artist pigment, and then injected rapidly into the flow. Movement of the oil is photographed while the model is in the flow. In some wind tunnels, the model can be removed from the tunnel and the flow patterns photographed after the run. This allows oil-flow patterns to be photographed in detail all around the model. Such a procedure is not possible in the CF_4 Tunnel, primarily because of the lip shock originating at the nozzle exit. As the model is retracted from the inviscid test core and passes through the nozzle boundary layer and across this lip shock, the patterns are significantly distorted; thus, there is a necessity for real-time photography.

Survey Rakes

Pitot-pressure surveys at and downstream of the nozzle exit were measured with a vertical rake having 41 pitot probes spaced 0.5 in. apart; a photograph of this survey rake is shown in figure 11(a). The center probe was coincident with the nozzle centerline; hence, the rake extended 10 in. above and below the nozzle centerline. Pitot probes were flat-faced tubes having an inside diameter of 0.06 in., an outside diameter of 0.09 in., and a length of 1 in. The inviscid test-core diameter is defined as the region in which the pitot pressure is within ± 2 percent of the average value of the center 19 probes, excluding the 3 centermost probes for reasons to be discussed subsequently. For the present conditions, a 2-percent uncertainty in the pitot pressure corresponds to a 0.2- to 0.25-percent uncertainty in free-stream Mach number.

Total temperature surveys were measured with a 21-probe rake containing tubes spaced 1 in. apart, each of which contained a chromel-alumel thermocouple (fig. 11(b)). The center probe was coincident with the nozzle centerline; hence, this rake extended horizontally 10 in. to either side of the nozzle centerline. A single probe housing a platinum-rhodium thermocouple was attached to the rake and was mounted 1 in. above the center probe. This multishielded platinum-rhodium thermocouple probe was designed to reduce the corrections (ref. 11) to the measured temperature to near 0, thereby providing an accurate measurement of the total temperature $T_{t,2}$ that could be compared with the measured reservoir temperature $T_{t,1}$.

Calculated Flow Properties

Free-stream and postnormal shock thermodynamic and transport properties were determined from a procedure based on the expressions presented in references 3, 12, and 13. Basic inputs to this procedure are measured reservoir pressure $p_{t,1}$ and temperature $T_{t,1}$ and pitot pressure $p_{t,2}$. From the measured reservoir pressure and temperature, the corresponding value of density is obtained by using the equation of state (ref. 13) that accounts for intermolecular force effects. The entropy is determined from the temperature and density, and then an isentropic, one-dimensional expansion is performed. Thermodynamic equilibrium is assumed throughout the flow process; justification for not including vibrational nonequilibrium effects is discussed in reference 3. The flow is expanded to an estimated value of free-stream temperature, and the remaining free-stream thermodynamic properties of interest are obtained from the isentropic condition and the equations presented in reference 13. The free-stream velocity, and hence Mach number, is determined from the conservation of energy, and the usual normal shock relations are employed to obtain static conditions immediately behind the shock. Stagnation conditions behind the shock are obtained by bringing the flow to rest isentropically and from consideration of the conservation of energy. Values of free-stream temperature are tried until the calculated stagnation-point (pitot) pressure agrees with the measured pitot pressure. It should be noted that this measured pitot pressure was free of rarefaction effects for the present flow conditions and pitot-probe geometry (ref. 11); that is, no correction for rarefied flow effects was required on the input value of pitot pressure.

For the range of reservoir conditions of this study, the compressibility factor, which represents the degree of departure from ideal-gas behavior, varied from approximately 1.03 to 1.12. (See fig. 12.) Imperfect-gas effects at the free-stream conditions and behind the normal shock are negligible (i.e., the compressibility factor

is unity). Because measured and calculated values of $T_{t,2}$ are compared in this report, it should be noted that the calculated value of $T_{t,2}$ for the present conditions is 2 to 3 percent less than that of $T_{t,1}$ because of the large intermolecular force effects in the reservoir. This is unlike an ideal-gas facility, such as the Langley 20-Inch Mach 6 Tunnel, in which $T_{t,2} = T_{t,1}$. An error analysis for the present flow conditions shows that a 2-percent error in reservoir pressure does not influence the predicted value of $T_{t,2}$, nor does a 2-percent error in pitot pressure. A 2-percent error in $T_{t,1}$ yields a 2.2-percent error in $T_{t,2}$, and both of these errors are of the same magnitude as the uncertainty in the measurements.

Monitoring the mass of CF_4 within the high-pressure storage bottles before and after a test or series of tests provides a measure of the efficiency of the reclaimer system. The mass is deduced from the measured bottlefield pressure and ambient (outside) temperature. As shown in figure 12, a significant departure from ideal CF_4 behavior occurs for the nominal bottlefield pressure of 3000 psia and temperature range from 490°R to 560°R. Figure 12 demonstrates the importance of accounting for intermolecular force effects in the determination of reclaimer efficiency and the quantity of CF_4 available for testing.

Test Conditions

Tests with the pitot-pressure survey rake were performed for a range of reservoir pressures from 1000 to 2550 psia and temperatures from 1020°R to 1495°R. The survey rake was positioned at the nozzle exit and at various distances downstream of the exit up to 12 in. To provide an insight to the values of free-stream and post-normal shock flow quantities generated in the CF_4 Tunnel, sample printouts of calculated flow quantities corresponding to several combinations of measured $p_{t,1}$, $T_{t,1}$, and $p_{t,2}$ are presented in table I. The input value of $p_{t,2}$ used to calculate these flow conditions represents an average of the measured pitot pressure across the inviscid test core, excluding the three center probes for reasons to be discussed subsequently. Naturally, the purity of the test gas is a concern in the determination of flow conditions and in the analysis of results. For this reason, samples of the gas were collected periodically and analyzed for purity; these samples were found to be at least 99.9 percent pure in all cases.

Results and Discussion

A major function of the CF_4 Tunnel is to provide information on simulating an important aspect of real-gas (dissociated) flow over blunt bodies, that is, the decrease in gamma (γ) that occurs within the shock layer. For blunt bodies with a sonic corner, gamma within the shock layer over the front of the body will be nearly constant both in flight and in the CF_4 Tunnel. Because continuum flows for blunt bodies at hypersonic conditions are relatively insensitive to variations in Mach number and Reynolds number, tests in the CF_4 Tunnel provide a simulation of the effect of gamma or normal-shock density ratio. It should be noted, however, that for more slender configurations, measurements in CF_4 represent only an approximation of γ effects. This happens because for a reacting gas, such as that occurring during reentry, γ within the shock layer may change appreciably along or around the body as the flow expands or is compressed; however, γ within the shock layer of a slender model in the CF_4 Tunnel remains essentially constant throughout the flow field. Nevertheless, important information concerning the effects of γ can be obtained in the CF_4 Tunnel that cannot be obtained in other ground test facilities. To do so experimentally, that is, to determine explicitly the effect of a departure from ideal-air conditions, the model must be tested both in air and in CF_4. These tests, which involve two hypersonic wind tunnels, should be performed at the same free-stream Mach number and Reynolds number so that γ is the only variable. The CF_4 Tunnel and the 20-Inch Mach 6 Tunnel, an ideal-air facility, provide this capability; these facilities are compatible from the viewpoint of model size, range of angle of attack, instrumentation, and data reduction.

Pitot-pressure surveys with the 41-probe vertical survey rake are generally measured following a significant modification to facility hardware or periodically to monitor facility performance closely. This has resulted in a large volume of calibration data, samples of which are presented herein. In this section, the effect of reservoir pressure on flow characteristics at the test section will be discussed first, followed by discussions of the effect of reservoir temperature and of the effect of axial distance downstream of the nozzle exit. This will be followed by some basic examples illustrating the use of this facility to examine the effect of either normal-shock density ratio or γ on shock detachment distance, pressure distributions, heat-transfer distributions, and aerodynamic coefficients.

Pitot-Pressure and Total Temperature Surveys

Effect of reservoir pressure. Pitot-pressure surveys measured at the nozzle exit for nominal reservoir temperatures of 1045°R and 1450°R are shown in figure 13. The most noticeable feature of these profiles at $T_{t,1} \approx 1045$°R (fig. 13(a)) is the "dip-spike" characteristic that occurs in a small region about the nozzle centerline. This phenomenon was repeatable on a run-to-run basis, as shown in figure 13(a), and was observed for each test series with the 41-probe survey rake for

these reservoir conditions. The profiles of figure 13(a) indicate that flow disturbances exist in the upstream region of the nozzle and focus along the nozzle centerline, typical of axisymmetric contoured nozzles. For $T_{t,1} \approx 1045°R$, the variation in nominal reservoir pressure had no appreciable effect on the pitot-pressure profile, including the pitot-pressure variation on the centerline; these profiles indicate that the inviscid test-core diameter is approximately 14 to 15 in. (The nozzle boundary-layer thickness is approximately 2.5 to 3 in.)

Reasonably flat and symmetrical (about the nozzle centerline) pitot-pressure profiles are observed at the higher reservoir temperature ($T_{t,1} \approx 1450°R$, as seen in fig. 13(b)). These profiles were measured during the same test series as those of figure 13(a) and exhibit the same good run-to-run repeatability. Although there is some indication of the dip-spike characteristic at the lowest reservoir pressure, it was absent for $p_{t,1} > 1500$ psia. The pitot-pressure profiles at the higher temperature (fig. 13(b)) have a saddlelike distribution, in which a region of higher pitot pressure surrounds an inner, uniform pitot-pressure region. For the highest reservoir pressure in figure 13(b), the percentage variations in pitot pressure for various core diameters are given in the following table:

$p_{t,2}$, percent	Core diameter, in.
±1.0	6
±1.9	8
±2.0	10
±2.3	12
±3.0	14

The results of figure 13 show that the average pressure ratio across the inviscid test core $\bar{p}_{t,2}/p_{t,1}$ measured at the nozzle exit is essentially independent of stagnation pressure for these two values of reservoir temperature. This independence of $\bar{p}_{t,2}/p_{t,1}$, and hence free-stream Mach number M_∞, on $p_{t,1}$ was also observed at other values of $T_{t,1}$.

The effect of reservoir pressure on the total temperature profile measured horizontally at the nozzle exit is shown in figure 14. These profiles show that the total temperature is constant across a 16-in-diameter core for $T_{t,1} \approx 1190°R$ for both reservoir pressures. The profiles of figure 14 give no indication of a disturbance on the nozzle centerline and indicate that the thermal boundary-layer thickness is approximately 2 in. As discussed previously, a temperature probe was mounted to the total temperature rake and was located 1 in. above the center probe to provide an accurate measurement of the total temperature $T_{t,2}$. The time history of the temperature measured with this probe (fig. 15) shows that the probe had a relatively slow response time. (It should be noted that the total temperature rake (and probe) was injected into the flow following flow establishment in the nozzle, whereas the pitot-pressure survey rake was positioned at the nozzle exit prior to flow initiation.) The measured value of $T_{t,2}$ is compared with the measured reservoir temperature $T_{t,1}$ in figure 15 and is observed to become asymptotic with $T_{t,1}$ about 4 sec after the probe reached its final position. Measured $T_{t,2}$ was generally 0.5 to 2 percent lower than measured $T_{t,1}$, thereby in agreement (within experimental accuracy) with calculated $T_{t,2}$.

Effect of reservoir temperature. Pitot-pressure surveys at the nozzle exit for several reservoir temperatures for a reservoir pressure of approximately 2000 psia are shown in figure 16. These profiles illustrate that the magnitude of the pitot-pressure variation on the nozzle centerline region decreases with increasing reservoir temperature and is absent at the highest reservoir temperature ($T_{t,1} = 1475°R$). They also illustrate that the symmetrical pitot-pressure profiles take on a saddlelike characteristic about the nozzle centerline with increasing $T_{t,1}$ and that the test-core diameter remains constant for this variation in $T_{t,1}$.

Calculated values of free-stream Mach number, normal-shock density ratio, and unit free-stream Reynolds number are shown in figure 17 as a function of reservoir temperature for a range of reservoir pressure. These flow parameters were calculated by using the average pitot pressure across the inviscid test core measured with the 41-probe survey rake. The three center pitot-pressure probe measurements, corresponding to the nozzle centerline region, were omitted in the determination of the average value of pitot pressure. The open symbols in figure 17 denote that the porous plate was removed from the reservoir, whereas the closed symbols denote that the plate was installed. As shown in figure 17, installation of the porous plate did not affect the pitot pressure, and hence the calculated flow parameters, measured at the nozzle exit. The Mach number, density ratio, and ratio of Reynolds number to reservoir pressure are observed to be functions of reservoir temperature only (i.e., essentially independent of reservoir pressure). The results of figure 17(a) illustrate that relatively high reservoir temperatures ($T_{t,1} > 1350°R$) are required to lower the Mach number in CF_4 sufficiently to match the free-stream Mach numbers of the Mach 6 Tunnel ($5.7 < M_\infty < 6$ in air). Although increasing the reservoir temperature to match M_∞ causes a corresponding increase in density ratio (fig. 17(b)), which is desirable in many studies, it causes a decrease in Reynolds number for a given reservoir pressure (fig. 17(c)). To match Mach number and Reynolds number simultaneously between these two facilities, the CF_4 Tunnel must be operated at its maximum pressure and temperature.

Equations, tables, or charts that provide test-section flow parameters in terms of the reservoir conditions are often very useful, particularly in planning a study. Because the flow parameters shown in figure 17 were essentially functions of reservoir temperature only, these results were amenable to curve fits. The empirical equations resulting from second-order, least-squares curve fits to the free-stream Mach number, free-stream unit Reynolds number, normal-shock density ratio, and pitot pressure in the CF_4 Tunnel are as follows:

$$M_\infty = 11.2894 - (6.8577 \times 10^{-3})T_{t,1} + (2.1885 \times 10^{-6})T_{t,1}^2 \quad (\pm 0.7 \text{ percent}) \qquad (1)$$

$$R_\infty/p_{t,1} = (2.7917 \times 10^3) - 3.4692T_{t,1} + (1.1445 \times 10^{-3})T_{t,1}^2 \quad (\pm 5.0 \text{ percent}) \qquad (2)$$

$$\rho_2/\rho_\infty = 5.6577 + (7.6343 \times 10^{-3})T_{t,1} - (2.0800 \times 10^{-6})T_{t,1}^2 \quad (\pm 0.2 \text{ percent}) \qquad (3)$$

$$p_{t,2}/p_{t,1} = (2.9264 \times 10^{-1}) + (1.6287 \times 10^{-3})T_{t,1} - (7.0722 \times 10^{-7})T_{t,1}^2 \quad (\pm 4.0 \text{ percent}) \qquad (4)$$

where $p_{t,1}$ and $p_{t,2}$ are in psia, $T_{t,1}$ is in °R, and R_∞ is in ft^{-1}.

These equations are valid for

$$1020°R \leq T_{t,1} \leq 1500°R$$
$$960 \text{ psi} \leq p_{t,1} \leq 2550 \text{ psi}$$
$$z = 0$$

Pitot-pressure profiles at several nozzle axial stations. Pitot-pressure surveys measured at the nozzle exit and at several axial stations downstream of the exit are shown in figure 18 for $T_{t,1} \approx 1190°R$ and two values of $p_{t,1}$. For $p_{t,1} \approx 1000$ psia (fig. 18(a)), the nozzle centerline disturbance (dip-spike characteristics resulting from weak waves embedded within the nozzle flow) decreases in magnitude between $z = 0$ and 4 in. and appears to have vanished at $z = 8$ in. This same trend is observed for $p_{t,1} \approx 1495$ psia (fig. 18(b)), but there is some indication that a greater distance downstream of the nozzle exit is required at the higher reservoir pressure for the disturbance to vanish.

The profiles of figure 18 also show that the available test core decreases in diameter with distance downstream of the nozzle exit. This decrease in test-core diameter is due to the lip shock that originates at the exit of the nozzle and converges toward the nozzle centerline. The radial location of the lip shock for a given distance downstream of the exit is revealed by a sudden, large increase in pitot pressure with increasing radial distance from the centerline, as observed in figure 18. Pitot-pressure profiles measured between $z = 4$ and 12 in. show that the test-core diameter decreases with increasing z as follows:

z, in.	Approximate test-core diameter, in.
4	14
8	12
12	10

The range of axial station $0 \leq z \leq 12$ in. will accommodate most models tested in the CF_4 Tunnel; however, the small available test-core diameter at $z = 12$ in., coupled with the desirability to test off the nozzle centerline to avoid the disturbances focused in this region, may present problems for some models which occupy the region $z > 8$ in.

The results of figure 19, in which the free-stream Mach number is plotted as a function of distance downstream from the nozzle exit, show that the Mach number is essentially constant over the present range of z. It should be noted that the results of figure 19 are for a constant value of reservoir temperature equal to 1200°R. To eliminate $T_{t,1}$ as a variable in figure 19, curve fits were applied to the calculated values of Mach number as a function of reservoir temperature for each axial station z. The Mach number was determined by using the average pitot pressure across the inviscid test core as discussed previously. Thus, each test symbol in figure 19 is the result of the evaluation of M_∞ at $T_{t,1} = 1200°R$ from a curve-fit expression obtained from at least six data points at each z for the case of the porous plate in or out of the reservoir. Again, the effect of the porous plate on flow conditions is negligible.

Before leaving this section, a brief look at the repeatability of pitot-pressure profiles between test series will be made. In figure 20, pitot-pressure profiles measured at the nozzle exit are shown for three test series. These results are for two reservoir pressures and nearly the same reservoir temperature for each run at each $p_{t,1}$. The repeatability at $p_{t,1} \approx 1590$ psia (fig. 20(b)) is quite good, and this includes the dip-spike characteristic in the nozzle centerline region and the decrease in radial pitot pressure expected in the nozzle boundary layer; however, repeatability at the lower reservoir pressure (fig. 20(a)) is not as good. Actually, the pitot-pressure profiles for series 1 and 3 are in good agreement. The results for the second series correspond to a lower reservoir temperature than the other two, but this alone is not expected to account for the differences observed.

Consideration of CF_4 liquefaction. The calculated (or theoretical) saturation curve for CF_4 is shown in figure 21, along with the current free-stream

static pressure and temperature operating range for the tunnel. This range corresponds to reservoir pressures from 1000 to 2600 psia and temperatures from 1115°R to 1485°R. Figure 21 shows that the present free-stream operating conditions are theoretically free of liquefaction.

Placement of models within the test core. Two flow disturbances in the CF_4 Tunnel, mentioned previously, require that particular attention be given to where models are located in the test section. To avoid flow disturbances focused on the nozzle centerline and the potential degradation of the flow over a model mounted on the centerline, models are routinely tested off centerline between this disturbance and the boundary layer. The second disturbance to be avoided is the lip shock that originates at the nozzle exit. Care must be taken to ensure that impingement by the lip shock on the model and its shock structure at all angles of attack is avoided. When this lip shock intersects the bow shock of a hemisphere model, the bow-shock shape is significantly altered, as shown in figure 22. Another example of the presence of this lip shock is shown in figure 8(e), which shows the apparent impingement of the lip shock on a thin-film heat-transfer gauge during model injection. These two flow disturbances (nozzle centerline disturbance and lip shock) have a significant impact on the size of the model and the ranges of angles of attack and sideslip that can be accommodated in the CF_4 Tunnel.

Pitot-pressure profiles at various lateral stations. To examine the flow in the region where models are generally tested, vertical pitot-pressure profiles were measured at several lateral stations from the nozzle centerline. Profiles measured at the nozzle exit ($z = 0$) and 8 in. downstream of the exit are shown in figure 23 for a reservoir pressure of 1500 psia and temperature of 1250°R. The profiles at both axial stations show that the flow is uniform (free of any disturbances) away from the centerline. Similar lateral surveys measured at other reservoir conditions revealed that the flow between the nozzle centerline and the nozzle boundary layer or the lip shock is quite uniform (pitot-pressure variation less than ±2 percent) and satisfactory for model testing.

Representative Results From Model Tests in the CF_4 Tunnel

Representative shock shapes, pressure distributions, heat-transfer distributions, and aerodynamic coefficients measured on various models in the CF_4 Tunnel are presented in this section to illustrate the types of tests performed, the typical model size, and the limitations of the facility. They also illustrate the significance of the variation of normal-shock density ratio or reduction in γ on flow characteristics about different types of models (blunt and relatively slender).

Shock shapes. Shock shapes measured at Mach 6 in air ($\rho_2/\rho_\infty \approx 5.2$) and CF_4 ($\rho_2/\rho_\infty \approx 12.0$) are shown in figure 24 for a hemisphere (ref. 14), a representative planetary aeroshell (ref. 14), the Shuttle orbiter (ref. 15), and a proposed generic planetary aerocapture vehicle (ref. 16). These comparisons clearly illustrate the strong dependence of shock detachment distance on the normal-shock density ratio. The differences in shock detachment distance due to the differences in density ratio are expected to influence flow characteristics about the model. One flow characteristic affected is the swallowing of high-entropy streamlines, resulting from the blunt nose, by the boundary layer. This swallowing will, naturally, influence the boundary layer, and hence the heat-transfer rate to the surface. The effect of density ratio on entropy-layer swallowing characteristics may be significant for the orbiter and biconic configurations. Another flow characteristic for the orbiter that is influenced by the density ratio is the location of the bow-shock/wing intersection. At the large values of density ratio that occur during Earth reentry (typically 12 to 16), the bow shock from the nose region will intersect the wing at a more inboard location than that observed in tests in a conventional hypersonic air tunnel. Limited results obtained at $\alpha = 20°$ in air and CF_4 show that, in terms of wing half-span, the bow-shock/wing intersection occurs about 10 percent more inboard for CF_4 (ref. 15).

An effective value of gamma, which accounts for a variation in density ratio, may be used as input to a perfect-gas inviscid flow-field code to provide an accurate prediction of the "real-gas" shock detachment distance for blunt bodies, as illustrated in figures 24(a) and 24(b). This use of effective gamma has been demonstrated previously (refs. 1 and 17) for hemispheres and blunt bodies with sonic corners. However, the tests with the relatively slender biconic model also demonstrated that the measured shock shape at $\rho_2/\rho_\infty \approx 12.0$ could be accurately (within ±5 percent) predicted with a perfect-gas, inviscid flow-field code when effective gamma was used as an input (ref. 16).

Pressure distributions. Pressure distributions on two of the four configurations presented in figure 24 are given in figure 25. The 4-in-diameter hemisphere tested off the nozzle centerline is compared with prediction (ref. 18) in figure 25(a). The agreement is quite good and lends credibility to the prediction method, to the quality of the flow conditions, and to the accurate prediction of free-stream and postshock flow conditions

for the CF_4 Tunnel. The measured pressure distributions at Mach 6 in air and CF_4 are compared in figure 25(b) for the planetary aeroshell (ref. 14) and in figure 25(c) for a straight (as opposed to bent), spherically blunted 13°/7° biconic configuration (ref. 16). The results for the aeroshell show that $p_w/p_{t,2}$ is lower for the higher density ratio over most of the surface except near the base. (The effect of differences in Mach number and Reynolds number between air and CF_4 are assumed negligible.) The pressure distributions on the biconic configuration are presented to illustrate the effect of density ratio or γ on the aft-cone pressure along the most windward ray and along the midmeridian ray. The windward pressure distribution is of particular interest since it shows the larger expansion downstream of the fore-cone/aft-cone junction experienced for a low γ flow. This expansion is followed by an increase in pressure in the direction of the base. The overexpansion-recompression trend along the windward ray of the aft cone is accurately predicted by the perfect-gas, inviscid flow-field code with an effective value of γ as the input. This effect of density ratio on the pressure distribution may reasonably be expected to affect the pitching-moment coefficient.

All supersonic or hypersonic wind tunnels with contoured axisymmetric nozzles must be examined for effects of centerline disturbances (discussed previously) on the flow about models positioned on the centerline. Pressure distributions are shown in figures 26(a) and 26(b) for a 4-in-diameter hemisphere positioned both on the nozzle centerline and 3 in. below the centerline for two values of reservoir pressure. Surface pressures were nondimensionalized by the pitot pressure measured with a single probe at the same axial location as the model nose. For the cases where the hemisphere was tested off centerline, measured surface pressure distributions were in excellent agreement over a range of z from 0.5 to 7.5 in.; that is, no effect of axial variation was observed. However, testing the hemisphere on the nozzle centerline near the nozzle exit ($z = 0.5$ in.) caused a severe degradation in the pressure distribution. When the hemisphere was moved farther downstream of the nozzle exit (see figs. 26(c) and 26(d)), but remained on the nozzle centerline, the effect diminished considerably depending on reservoir pressure. For $p_{t,1} \approx 1540$ psia, the effect of this disturbance on the hemisphere pressure was small at $z = 4$ in. and essentially vanished at $z = 7.5$ in. However, at the lower reservoir pressure ($p_{t,1} \approx 1000$ psia), the effect of the disturbance was evident for $0.5 \leq z \leq 7.5$ in. While on the subject of testing models on the nozzle centerline, the effect of the nozzle-centerline disturbance on the shock shape and heating distribution for the 4-in-diameter hemisphere is shown in figures 27(a) and 27(b), respectively; the model centerline is coincident with the nozzle centerline. Note the discontinuity in shock shape at the stagnation region (fig. 27(a)) and the irregular heating distribution in this region (fig. 27(b)). For the preceding reasons, most testing in the CF_4 Tunnel is performed with the model positioned off centerline. This certainly limits the model size and available range of angle of attack, which must be considered in designing models and planning test programs for this facility.

Heat transfer. Heat-transfer distributions measured on the 4-in-diameter hemisphere positioned off the nozzle centerline are shown in figure 28 for two values of reservoir pressure. These heat-transfer rates were obtained by using the thin-skin transient calorimeter technique for which chromel-alumel thermocouples were spot-welded to the inside surface of the thin (0.020 to 0.030 in.) stainless-steel shell. The measured heating distributions are observed to be in reasonably good agreement with the predicted heating levels given in unpublished data by H. Harris Hamilton II of the Langley Research Center, which are based on the thermodynamic properties of reference 19. A concern with these measurements was the possible effect of flow contamination. Although flow contamination is not expected to have an appreciable effect on measured surface pressures and forces and moments, solid particles carried by the flow can result in a substantial increase in heating rate beyond that for clean flow. The results of figure 28 demonstrate that the present level of flow contaminants does not have an appreciable influence on measured heat-transfer rates.

As discussed previously, steps have been made to reduce the level of flow contamination. One indication of the success of these steps is the excellent survival rate for thin-film resistance heat-transfer gauges that faced into the flow. Several studies have been performed in which five hemispheres or disks having thin-film gauges on the front surface were mounted in a rake and injected into the flow (ref. 9). These delicate gauges were usually in the flow for 2 to 3 sec, and sometimes longer. To date, approximately 15 gauges have been tested, some as many as five times, and only 1 gauge has been destroyed.

Two concerns when testing very small models (with a diameter less than 0.5 in.) are possible vibrational nonequilibrium effects and possible rarefaction effects. For vibrational equilibrium to exist within the shock layer of a model, the relaxation distance must be less than the shock detachment distance. The smallest models tested in the CF_4 Tunnel to date are 0.3-in-diameter hemispheres. For these hemispheres, the vibrational relaxation time must be less than the shock detachment distance divided by the flow velocity in the shock layer, which at the stagnation region is approximately

3.5×10^{-6} sec, to provide equilibrium flow in the post-normal shock region at the present CF_4 test conditions. This relaxation time is close to the value given in reference 3; thus, to minimize vibrational nonequilibrium flow effects, the model size should be such that the shock detachment distance is greater than about 0.01 in. (That is, if the model is a hemisphere, the diameter should exceed 0.30 in.)

An example of the sensitivity of the stagnation-point heat-transfer rate for a hemisphere in the low Reynolds number flow regime to the density ratio is shown in figure 29. This figure shows the ratio of the heat-transfer rate to the value predicted with classical boundary-layer theory and plotted as a function of postshock Reynolds number and density ratio. The experimental data in this figure were obtained with small (0.3-in-diameter) quartz hemispheres having thin-film gauges deposited over the stagnation region. They were tested in the CF_4 Tunnel and in the Langley 31-Inch Mach 10 Tunnel (formerly known as the Langley Continuous-Flow Hypersonic Tunnel). Predicted values of the stagnation-point heating for CF_4 were obtained by using Hamilton's data and reference 19; these predictions were made for a 4-in-diameter hemisphere and were scaled to the quartz hemispheres by $(r_{n,\mathrm{sph}}/r_{n,\mathrm{quartz\ sph}})^{1/2}$. Reference 21 was used to predict the stagnation-point heat-transfer rate to the quartz hemispheres for air. For the flow conditions in CF_4, low Reynolds number effects increase stagnation-point heating by 15 to 18 percent over predicted values based on classical boundary-layer theory. The results of figure 29 also imply that low Reynolds number effects may occur for the 4-in-diameter hemisphere. Again, this is another area that the researcher should be aware of when testing relatively small models.

Another example of the effect of density ratio or γ is shown in figure 30, in which heat-transfer distributions measured along the windward centerline of a 0.006-scale Shuttle orbiter model are presented for several angles of attack. These data (ref. 15) were obtained in the Langley 20-Inch Mach 6 Tunnel over a wide range of free-stream Reynolds number and also in the CF_4 Tunnel. The orbiter heating is nondimensionalized by the measured heat-transfer rate to the 4-in-diameter hemisphere that was tested at the same flow conditions in both facilities as the orbiter model. A significant increase in the heat-transfer coefficient occurs for the higher density ratio (decreasing γ) at $\alpha = 20°$ and 30°. The influence of density ratio or γ on heating is less at $\alpha = 40°$, a result of greater effective model bluntness. Thus at the angle-of-attack range for the hypersonic portion of the early orbiter flights ($\alpha \approx 40°$), the effect of density ratio on heating was relatively small.

Aerodynamic coefficients. The effect of γ on the aerodynamic coefficients of a 0.004-scale orbiter model in the CF_4 Tunnel and in the 20-Inch Mach 6 Tunnel is illustrated in figure 31. Also shown in figure 31, which is taken from reference 22, are the calculated values of the STS-1 flight pitching-moment curve (ref. 22) for zero deflection of the elevons and body flap. The CF_4 data and predicted flight C_m show a nose-up pitching moment compared with the air results. This nose-up pitching-moment increment of approximately 0.03 is almost identical to the difference between preflight predictions and flight results in the high hypersonic regime. The comparisons in figure 31 illustrate that the CF_4 Tunnel can make a significant contribution toward understanding the effect of γ on the aerodynamic characteristics of a proposed entry vehicle.

Concluding Remarks

The Langley Hypersonic CF_4 Tunnel is presently the only operational, conventional-type (as opposed to impulse) hypersonic wind tunnel in this country which simulates a decrease in the ratio of specific heats (gamma or γ) within the shock layer, such as that which occurs during blunt body reentry because of real-gas effects (dissociation). A detailed description of this facility is presented that includes a discussion of the basic components, instrumentation, and operating procedure.

Pitot-pressure surveys were measured at the nozzle exit and downstream of the exit for reservoir temperatures from 1020°R to 1495°R and reservoir pressures from 1000 to 2550 psia. At the maximum value of reservoir pressure and temperature, a uniform test core having a diameter of approximately 11 in. (0.55 times the nozzle-exit diameter) exists. The corresponding free-stream Mach number is 5.9, the unit Reynolds number is 4×10^5 per foot, the ratio of specific heats immediately behind a normal shock is 1.10, and the normal-shock density ratio is 12.6. Routine operation of this facility at the maximum reservoir temperature is detrimental to the hardware and corresponds to a higher level of flow contamination than at lower temperatures; however, there is a trade-off when the facility is operated at lower reservoir temperatures. Irregularities occur in the pitot-pressure profiles near the nozzle centerline at the lower reservoir temperatures, indicating the existence of flow disturbances originating in the upstream region of the nozzle. These irregularities, which are typical of axisymmetric contoured nozzles, are relatively small in magnitude and, in general, result in a perturbation in centerline free-stream Mach number of less than 1.5 percent. Nevertheless, models tested on the nozzle centerline experienced a significant degradation of properties within the flow field. Because these disturbances are contained within a small region (0.5 in.

radius) about the centerline, properly sized models can be tested off centerline in the uniform flow between the centerline disturbance region and the nozzle boundary layer or the lip shock originating at the nozzle exit and converging toward the nozzle centerline.

The contamination level during the steady test-flow period following nozzle flow establishment has been reduced to an acceptably low level as observed from heat-transfer measurements and as indicated by the survival of thin-film resistance gauges. The average pitot pressure, and hence average free-stream Mach number, across the test core was essentially constant between the nozzle exit and 12 in. downstream of the nozzle exit. Thus, models tested off the nozzle centerline in the CF_4 Tunnel will experience a flow quality and a contamination level similar to that found in most hypersonic wind tunnels that use air as the test gas.

Comparison of measured and predicted shock detachment distance, pressure distributions, and heat-transfer distributions on various models positioned off the nozzle centerline indicated the absence of significant flow nonuniformity and lent credibility to the method used to predict free-stream and postshock flow conditions. Basically, the CF_4 Tunnel is a constant Mach number facility with a limited range of Reynolds number; but, when coupled to the Langley 20-Inch Mach 6 Tunnel, it allows the effect of γ to be determined experimentally for a given Mach number and Reynolds number. This capability to simulate an important aspect of real-gas flows is illustrated by measurements made with blunt bodies typical of planetary aeroshells, the Shuttle orbiter, and a proposed biconic aerocapture vehicle.

Langley Research Center
National Aeronautics and Space Administration
Hampton, VA 23665
November 16, 1984

Appendix

Operating Experience

As expected in such an undertaking, a number of problems were encountered in the conversion of the Langley 20-Inch Hypersonic Arc-Heated Tunnel to the Langley Hypersonic CF_4 Tunnel. Two such problems unique to CF_4 operation will be discussed in this appendix.

During the shakedown of the facility, an unexpected drop in reservoir pressure occurred during a sequence of tests. The source of this problem was traced to a collection of rustlike particles blocking the stainless-steel screen located within the settling chamber. The tubing from the high-pressure storage field and through the lead-bath heaters is 316 stainless steel, and pure CF_4 supposedly does not react with this tubing material at the present temperatures. However, CF_4 contaminated with water vapor or oil may react at the present conditions to form HF, which will corrode 316 stainless steel. Examination of a section of tube removed from the lead-bath heater revealed that the tubing was corroding and the products of this corrosion resulted in the blockage of the screen. A source of water vapor into the supply line was discovered and eliminated. Prior to this blockage of the screen, a diaphragm in the CF_4 compressor ruptured allowing oil to enter the tubing; hence, an oil detector was installed in the supply line to provide an immediate warning of the presence of oil. With the sources of water vapor and oil eliminated and the screen removed from the settling chamber, testing was resumed. This corrosion of the tube wall did not measurably reduce the wall thickness; that is, the wall thickness remained at acceptable limits for the safe operation of the facility.

Sometime later, the screens were reinstalled and particle collectors in the form of Dupont Teflon disks were positioned at the nozzle exit for each run. (Samples of these collectors are shown in fig. 32.) The level of contamination on a given day decreased with each successive run, but it increased somewhat with increasing pressure and increased dramatically with increasing temperature. When the tunnel was idle for a period of several days, the first run made after this period was exceptionally dirty. Thus, to reduce the level of contamination, the routine operational temperature of the facility was reduced to below 1250°R and an abbreviated run with the model retracted was made at the beginning of each day to "clean out" the piping and settling chamber. To obtain a time history of the contamination level, a Teflon disk was rotated behind a slit in a metal disk such that it completed about three-fourths of a revolution from the time that the valve opened to initiate the flow in the nozzle to the time that it closed (fig. 33). These disks illustrate that the majority of the contaminants arrived at the nozzle exit during the flow-establishment process; and the test period, which began about 3 sec later, was essentially free of contaminants. The present level of flow contamination is not expected to influence significantly the pressure or force and moment measurements on models, and the effect on heat-transfer measurements is negligible as discussed previously.

The CF_4 reclaimer was designed and manufactured specifically for this tunnel. At the time of fabrication, no experience existed for such a system. Consequently, several problems were encountered during the initial operation of this reclaimer.

The reclaimer was installed into the vacuum system which was used for the arc-heated tunnel. Initial operation with the reclaimer revealed a blockage problem, attributed to water and oil contaminants solidifying in the primary heat exchanger and condenser (fig. 6), thereby blocking the line. Some of these solid particles entered the liquid pump, resulting in damaged intake and exhaust valves. Although a small molecular sieve filter preceded the primary heat exchanger, the water and oil contaminants still found their way to the condenser and liquid pump. The primary source of water was concluded to be from the air within the facility and water vapor collected in the walls of the nozzle, test section, and diffuser. To avoid subjecting the reclaimer to this water, a separate vacuum pump was used to evacuate the facility. The exhaust system of the vacuum pumps used to evacuate the vacuum spheres (fig. 1) was not designed for low vacuum and contained a number of leaks. Checks were performed to locate and correct these leaks, thereby minimizing other sources of water vapor. Also, the exhaust system was evacuated prior to a reclaiming cycle. The source of oil is the vacuum pumps. A small booster pump, which increased the reclaimer pressure from approximately 0.5 to 2 psi and from 4 to 5 psi, was removed as a potential source of contaminants. No adverse effect on system performance was observed because of the decrease in operating pressure. The filter capability was improved by installing two large filters ahead of the primary heat exchanger, with one filter filled with C. M. Kemp Vapoilsorb and the other with activated charcoal; two Balston coalescing oil filters were also installed. The first heat exchanger was changed from water cooled to LN_2 cooled, and thus it served as a cold trap. In addition, the heat exchangers were wrapped with resistance heaters so that they could be dried out between reclaimer cycles. These modifications eliminated the reclaimer blockage problem and greatly reduced the water and oil contamination level at the condenser.

During the shakedown, the reclaimer demonstrated an intermittent behavior of reclaiming and nonreclaim-

ing. This behavior was traced to a faulty vent valve and led to the replacement of butterfly valves with gate valves wherever practical. Presently, the reclaimer operates smoothly, free of hardware problems, at an efficiency of 70 to 75 percent, compared with the manufacturer's design efficiency of 90 to 95 percent. Analysis of the waste gas from the condenser showed that only 1 percent of the gas was CF_4.

References

1. Miller, Charles G., III: *Shock Shapes on Blunt Bodies in Hypersonic-Hypervelocity Helium, Air, and CO_2 Flows, and Calibration Results in Langley 6-Inch Expansion Tube.* NASA TN D-7800, 1975.
2. Chapman, Dean R.: *Some Possibilities of Using Gas Mixtures Other Than Air in Aerodynamic Research.* NACA Rep. 1259, 1956. (Supersedes NACA TN 3226.)
3. Jones, Robert A; and Hunt, James L. (Appendix A by James L. Hunt, Kathryn A. Smith, and Robert B. Reynolds and appendix B by James L. Hunt and Lillian R. Boney): *Use of Tetrafluoromethane To Simulate Real-Gas Effects on the Hypersonic Aerodynamics of Blunt Vehicles.* NASA TR R-312, 1969.
4. Schaefer, William T., Jr.: *Characteristics of Major Active Wind Tunnels at the Langley Research Center.* NASA TM X-1130, 1965.
5. Midden, R. E.; and Miller, C. G.: *Description and Preliminary Calibration Results for the Langley Hypersonic CF_4 Tunnel.* NASA TM-78800, 1978.
6. Miller, Charles G., III; and Gnoffo, Peter A.: *Pressure Distributions and Shock Shapes for $12.84^\circ/7^\circ$ On-Axis and Bend-Nose Biconics in Air at Mach 6.* NASA TM-83222, 1981.
7. Jones, Robert A.; and Feller, William V.: *Preliminary Surveys of the Wall Boundary Layer in a Mach 6 Axisymmetric Tunnel.* NASA TN D-5620, 1970.
8. Johnson, Charles B.; Boney, Lillian R.; Ellison, James C.; and Erickson, Wayne D.: *Real-Gas Effects on Hypersonic Nozzle Contours With a Method of Calculation.* NASA TN D-1622, 1963.
9. Miller, Charles G., III: *Comparison of Thin-Film Resistance Heat-Transfer Gages With Thin-Skin Transient Calorimeter Gages in Conventional Hypersonic Wind Tunnels.* NASA TM-83197, 1981.
10. Burner, Alpheus W.; and Midden, Raymond E.: *Holographic Flow Visualization at the Langley CF_4 Tunnel.* NASA TM-74051, 1977.
11. Beckwith, Ivan E.; Harvey, William D.; and Clark, Frank L. (With Appendix A by Ivan E. Beckwith, William D. Harvey, and Christine M. Darden and appendix B by William D. Harvey, Lemuel E. Forrest, and Frank L. Clark): *Comparisons of Turbulent-Boundary-Layer Measurements at Mach Number 19.5 With Theory and an Assessment of Probe Errors.* NASA TN D-6192, 1971.
12. Hunt, James L.; and Boney, Lillian R.: *Thermodynamic and Transport Properties of Gaseous Tetrafluoromethane in Chemical Equilibrium.* NASA TN D-7181, 1973.
13. *Properties and Applications of the "Freon" Fluorocarbons.* Tech. Bull. X-88F, E. I. du Pont de Nemours & Co., Sept. 3, 1968. (Revised Feb. 3, 1969.)
14. Miller, Charles G., III: *Measured Pressure Distributions, Aerodynamic Coefficients, and Shock Shapes on Blunt Bodies at Incidence in Hypersonic Air and CF_4.* NASA TM-84489, 1982.
15. Miller, C. G.: Experimental Investigation of Gamma Effects on Heat Transfer to a 0.006 Scale Shuttle Orbiter at Mach 6. AIAA-82-0826, June 1982.
16. Miller, C. G.; Blackstock, T. A.; Helms, V. T.; and Midden, R. E.: An Experimental Investigation of Control Surface Effectiveness and Real-Gas Simulation for Biconics. AIAA-83-0213, Jan. 1983.
17. Miller, Charles G., III: *A Comparison of Measured and Predicted Sphere Shock Shapes in Hypersonic Flows With Density Ratios From 4 to 19.* NASA TN D-8076, 1975.
18. Sutton, Kenneth: Characteristics of Coupled Nongray Radiating Gas Flows With Ablation Product Effects About Blunt Bodies During Planetary Entries. Ph. D. Thesis, North Carolina State Univ. at Raleigh, 1973. (Available as NASA TM X-72078.)
19. Sutton, Kenneth: *Relations for the Thermodynamic and Transport Properties in the Testing Environment of the Langley Hypersonic CF_4 Tunnel.* NASA TM-83220, 1981.
20. Gilbert, Leon M.; and Goldberg, Leon: A Reynolds Number Scaling Theory for Hypersonic Ablation. AIAA Paper 67-155, Jan. 1967.
21. Fay, J. A.; and Riddell, F. R.: Theory of Stagnation Point Heat Transfer in Dissociated Air. *J. Aeronaut. Sci.*, vol. 25, no. 2, Feb. 1958, pp. 73–85, 121.
22. Calloway, Robert L.: Real-Gas Simulation for the Shuttle Orbiter and Planetary Entry Configurations Including Flight Results. AIAA-84-0489, Jan. 1984.

TABLE I. SAMPLE OF FREE-STREAM AND POSTNORMAL SHOCK FLOW CONDITIONS FOR THE LANGLEY HYPERSONIC CF_4 TUNNEL

(a) Low reservoir pressure

RESERVOIR STAGNATION CONDITIONS

PT1	TT1	RHOT1	ZT1	HT1	ST1
N/M^2	DEG K	KG/M^3		J/KG	J/KG-K
6.922E+06	6.700E+02	1.057E+02	1.034E+00	6.647E+05	3.245E+03
PSI	DEG R	LBM/FT^3		BTU/LBM	S/R
1.004E+03	1.206E+03	6.599E+00	1.034E+00	2.859E+02	3.435E+01

FREESTREAM CONDITIONS

P1	T1	RHO1	Z1	H1	A1
N/M^2	DEG K	KG/M^3		J/KG	M/S
1.891E+02	1.797E+02	1.114E-02	1.000E+00	2.698E+05	1.441E+02
PSI	DEG R	LBM/FT^3		BTU/LBM	FPS
2.743E-02	3.234E+02	6.956E-04	1.000E+00	1.161E+02	4.728E+02
U1	M1	NRE1	GAM1	NPR1	Q1
M/S		1/M			N/M^2
8.887E+02	6.167E+00	9.010E+05	1.224E+00	8.101E-01	4.400E+03
FPS		1/FT			PSI
2.916E+03	6.167E+00	2.746E+05	1.224E+00	8.101E-01	6.382E-01
VIS1	VIS1	GAM1	GAMEFF		
N-S/M^2	LBM/FT-S				
1.099E-05	7.386E-06	1.224E+00	1.127E+00		

STATIC CONDITIONS BEHIND NORMAL SHOCK

P2	T2	RHO2	Z2	H2	A2
N/M^2	DEG K	KG/M^3		J/KG	M/S
8.245E+03	6.625E+02	1.317E-01	1.000E+00	6.618E+05	2.629E+02
PSI	DEG R	LBM/FT^3		BTU/LBM	FPS
1.196E+00	1.193E+03	8.225E-03	1.000E+00	2.847E+02	8.626E+02
U2	M2	NRE2	GAM2	NPR2	RATIO
M/S		1/M			
7.517E+01	2.859E-01	3.084E+05	1.104E+00	7.505E-01	1.182E+01
FPS		1/FT			
2.466E+02	2.859E-01	9.401E+04	1.104E+00	7.505E-01	1.182E+01

STAGNATION CONDITIONS BEHIND NORMAL SHOCK

PT2	TT2	RHOT2	ZT2	HT2	GAMT2
N/M^2	DEG K	KG/M^3		J/KG	
8.626E+03	6.653E+02	1.372E-01	1.000E+00	6.646E+05	1.104E+00
PSI	DEG R	LBM/FT^3		BTU/LBM	
1.251E+00	1.198E+02	8.567E-03	1.000E+00	2.859E+02	1.104E+00

TABLE I. Continued

(b) Moderate reservoir pressure

RESERVOIR STAGNATION CONDITIONS

PT1	TT1	RHOT1	ZT1	HT1	ST1
N/M^2	DEG K	KG/M^3		J/KG	J/KG-K
1.039E+07	6.772E+02	1.539E+02	1.055E+00	6.697E+05	3.213E+03
PSI	DEG R	LBM/FT^3		BTU/LBM	S/R
1.507E+03	1.219E+03	9.606E+00	1.055E+00	2.881E+02	3.401E+01

FREESTREAM CONDITIONS

P1	T1	RHO1	Z1	H1	A1
N/M^2	DEG K	KG/M^3		J/KG	M/S
2.899E+02	1.827E+02	1.680E-02	9.999E-01	2.709E+05	1.452E+02
PSI	DEG R	LBM/FT^3		BTU/LBM	FPS
4.204E-02	3.288E+02	1.049E-03	9.999E-01	1.166E+02	4.763E+02
U1	M1	NRE1	GAM1	NPR1	Q1
M/S		1/M			N/M^2
8.930E+02	6.152E+00	1.343E+06	1.221E+00	8.051E-01	6.699E+03
FPS		1/FT			PSI
2.930E+03	6.152E+00	4.094E+05	1.221E+00	8.051E-01	9.716E-01
VIS1	VIS1	GAM1	GAMEFF		
N-S/M^2	LBM/FT-S				
1.117E-05	7.505E-06	1.221E+00	1.127E+00		

STATIC CONDITIONS BEHIND NORMAL SHOCK

P2	T2	RHO2	Z2	H2	A2
N/M^2	DEG K	KG/M^3		J/KG	M/S
1.256E+04	6.675E+02	1.991E-01	1.000E+00	6.668E+05	2.639E+02
PSI	DEG R	LBM/FT^3		BTU/LBM	FPS
1.821E+00	1.202E+03	1.243E-02	1.000E+00	2.869E+02	8.658E+02
U2	M2	NRE2	GAM2	NPR2	RATIO
M/S		1/M			
7.534E+01	2.855E-01	4.649E+05	1.104E+00	7.495E-01	1.185E+01
FPS		1/FT			
2.472E+02	2.855E-01	1.417E+05	1.104E+00	7.495E-01	1.185E+01

STAGNATION CONDITIONS BEHIND NORMAL SHOCK

PT2	TT2	RHOT2	ZT2	HT2	GAMT2
N/M^2	DEG K	KG/M^3		J/KG	
1.313E+04	6.704E+02	2.074E-01	1.000E+00	6.696E+05	1.104E+00
PSI	DEG R	LBM/FT^3		BTU/LBM	
1.905E+00	1.207E+03	1.295E-02	1.000E+00	2.881E+02	1.104E+00

TABLE I. Concluded

(c) High reservoir pressure

RESERVOIR STAGNATION CONDITIONS

PT1	TT1	RHOT1	ZT1	HT1	ST1
N/M^2	DEG K	KG/M^3		J/KG	J/KG-K
1.749E+07	6.700E+02	2.512E+02	1.101E+00	6.567E+05	3.145E+03
PSI	DEG R	LBM/FT^3		BTU/LBM	S/R
2.537E+03	1.206E+03	1.568E+01	1.101E+00	2.825E+02	3.330E+01

FREESTREAM CONDITIONS

P1	T1	RHO1	Z1	H1	A1
N/M^2	DEG K	KG/M^3		J/KG	M/S
4.448E+02	1.734E+02	2.715E-02	9.999E-01	2.660E+05	1.419E+02
PSI	DEG R	LBM/FT^3		BTU/LBM	FPS
6.451E-02	3.122E+02	1.695E-03	9.999E-01	1.144E+02	4.655E+02
U1	M1	NRE1	GAM1	NPR1	Q1
M/S		1/M			N/M^2
8.839E+02	6.230E+00	2.260E+06	1.229E+00	8.223E-01	1.061E+04
FPS		1/FT			PSI
2.900E+03	6.230E+00	6.887E+05	1.229E+00	8.223E-01	1.538E+00
VIS1	VIS1	GAM1	GAMEFF		
N-S/M^2	LBM/FT-S				
1.062E-05	7.136E-06	1.229E+00	1.128E+00		

STATIC CONDITIONS BEHIND NORMAL SHOCK

P2	T2	RHO2	Z2	H2	A2
N/M^2	DEG K	KG/M^3		J/KG	M/S
1.986E+04	6.545E+02	3.212E-01	1.000E+00	6.538E+05	2.614E+02
PSI	DEG R	LBM/FT^3		BTU/LBM	FPS
2.881E+00	1.178E+03	2.005E-02	1.000E+00	2.813E+02	8.576E+02
U2	M2	NRE2	GAM2	NPR2	RATIO
M/S		1/M			
7.470E+01	2.858E-01	7.537E+05	1.105E+00	7.521E-01	1.183E+01
FPS		1/FT			
2.451E+02	2.858E-01	2.297E+05	1.105E+00	7.521E-01	1.183E+01

STAGNATION CONDITIONS BEHIND NORMAL SHOCK

PT2	TT2	RHOT2	ZT2	HT2	GAMT2
N/M^2	DEG K	KG/M^3		J/KG	
2.078E+04	6.574E+02	3.346E-01	1.000E+00	6.566E+05	1.105E+00
PSI	DEG R	LBM/FT^3		BTU/LBM	
3.014E+00	1.183E+03	2.089E-02	1.000E+00	2.825E+02	1.105E+00

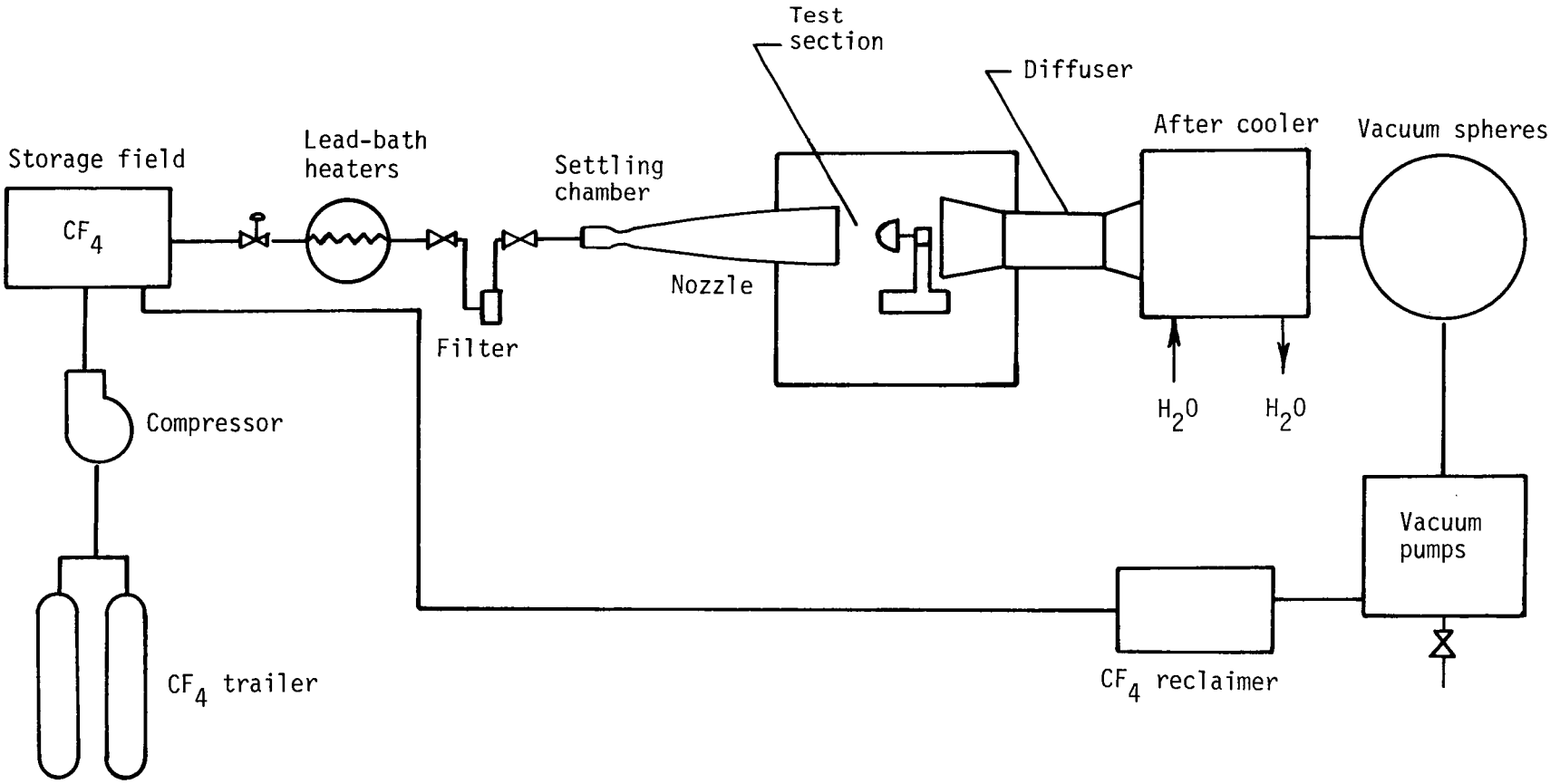

(a) Schematic drawing.

Figure 1. Schematic drawing and photograph of the Langley Hypersonic CF_4 Tunnel.

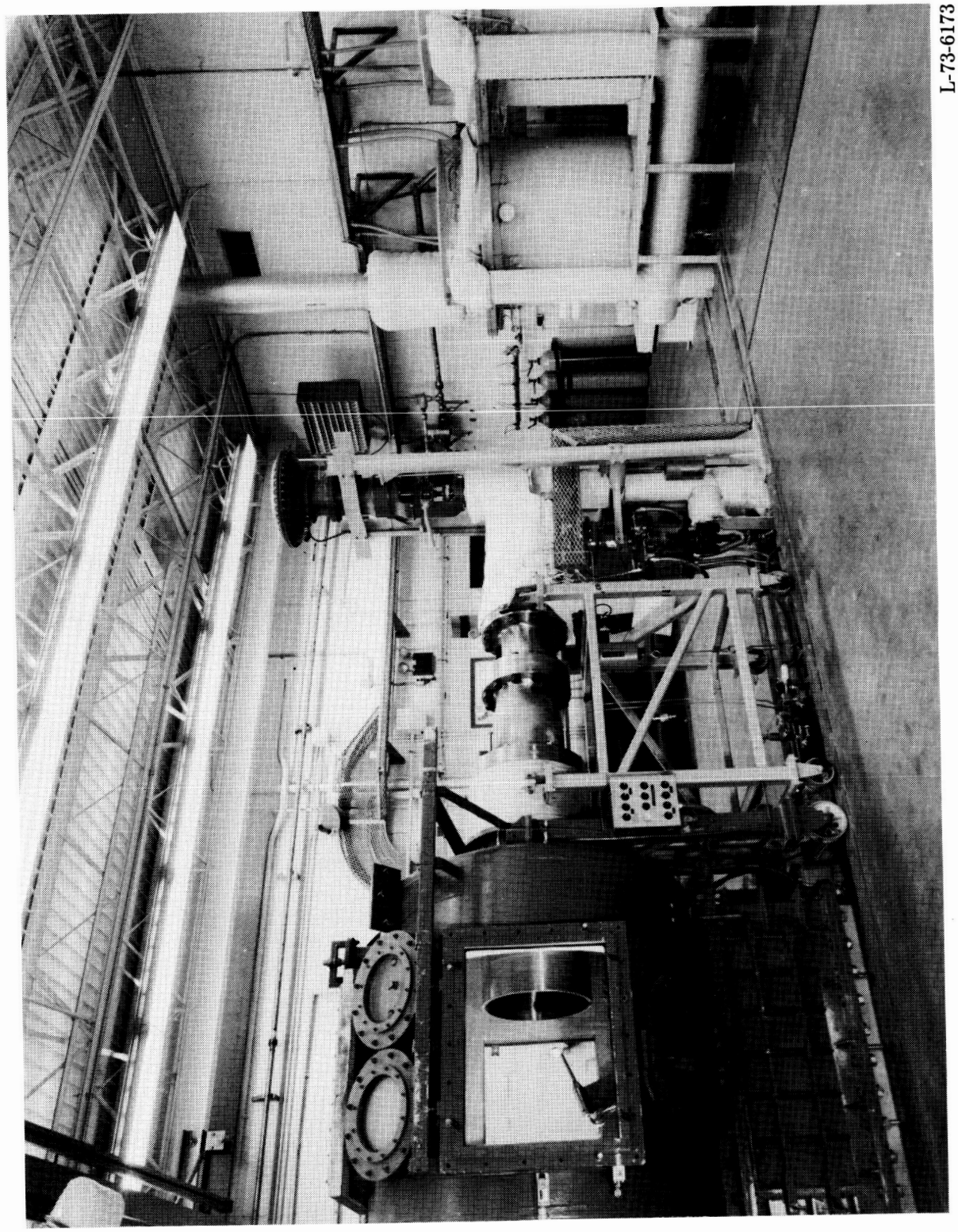

L-73-6173

(b) Photograph.

Figure 1. Concluded.

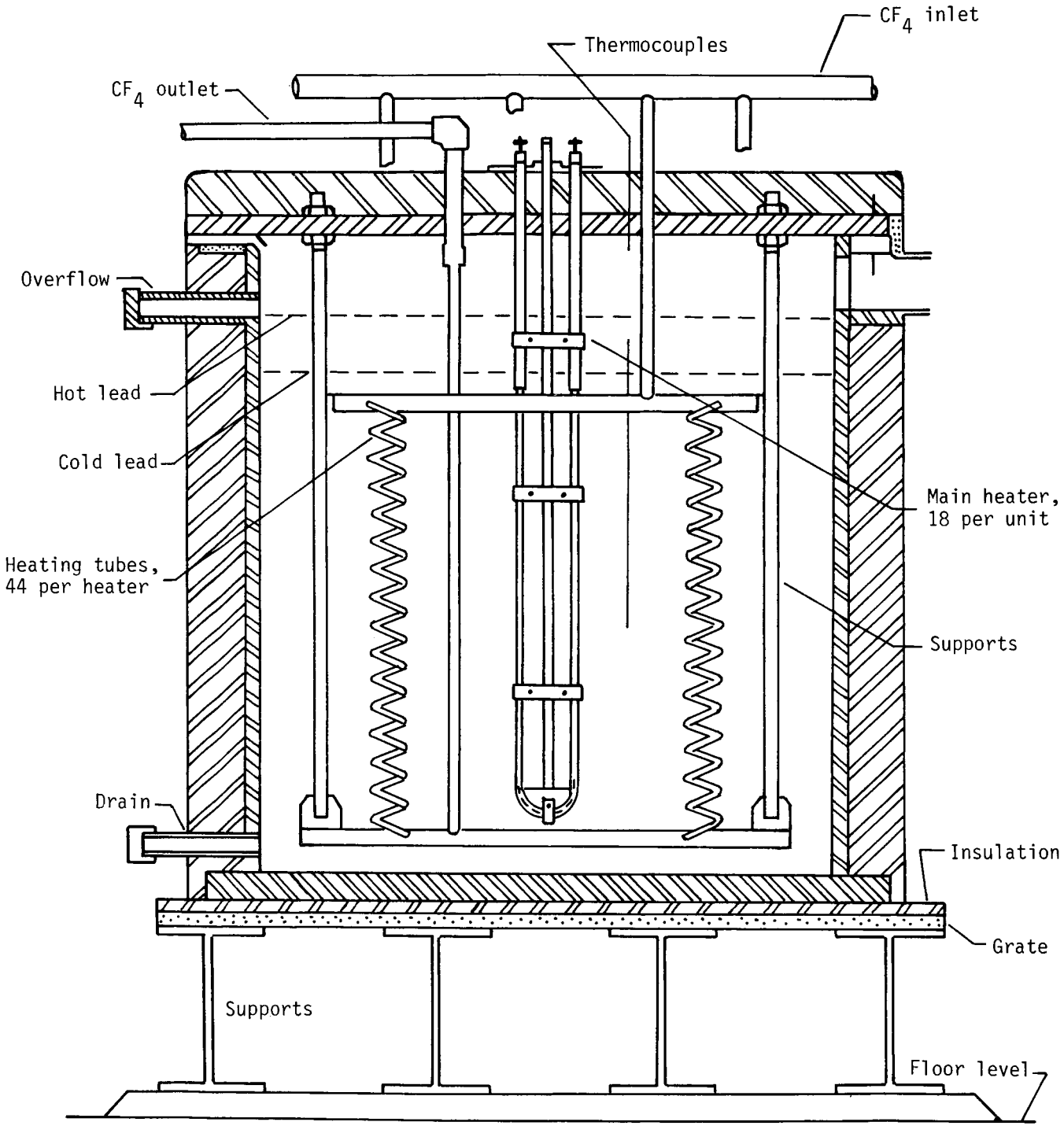

Figure 2. Sketch of lead-bath heater.

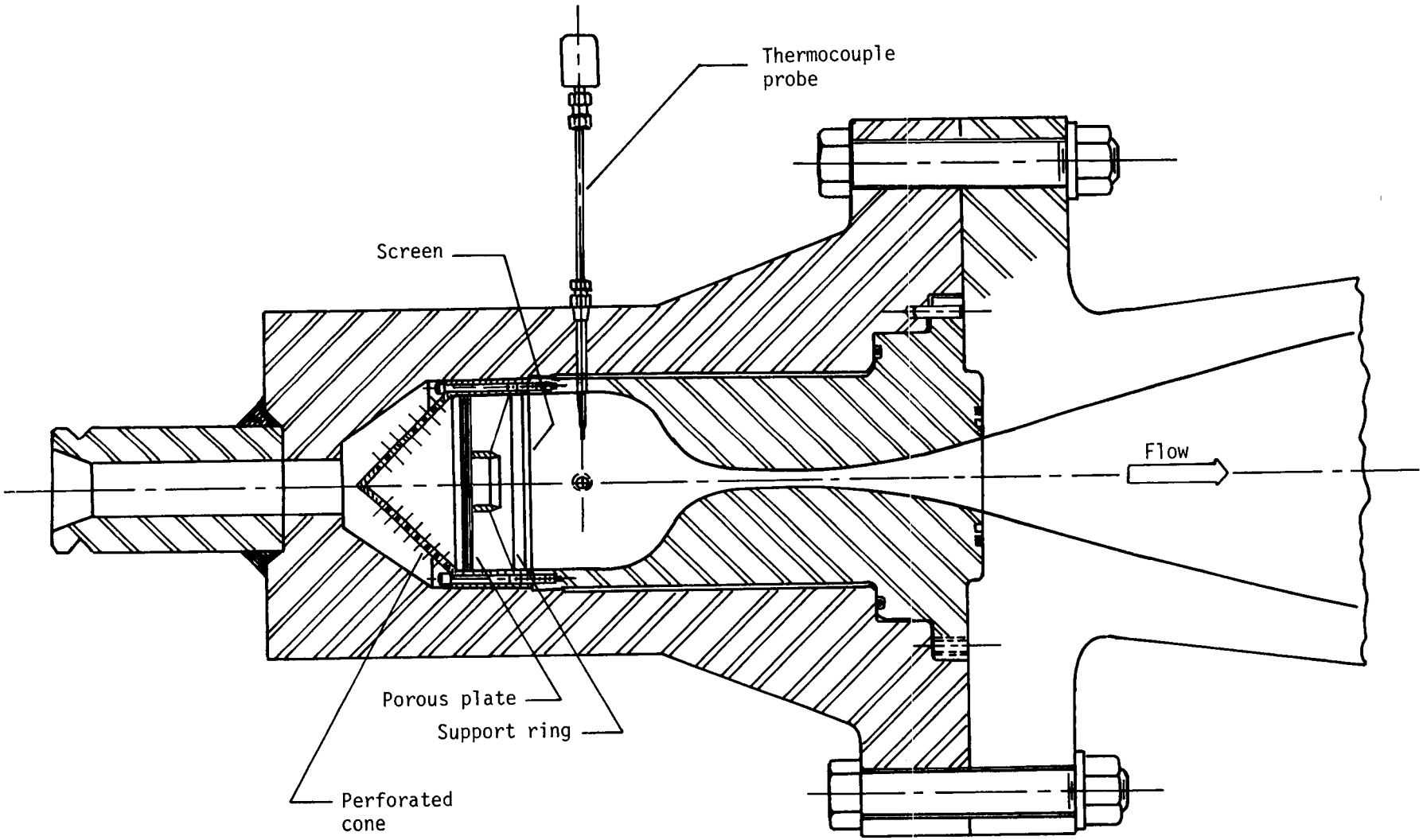

Figure 3. Sketch of settling chamber and nozzle throat section.

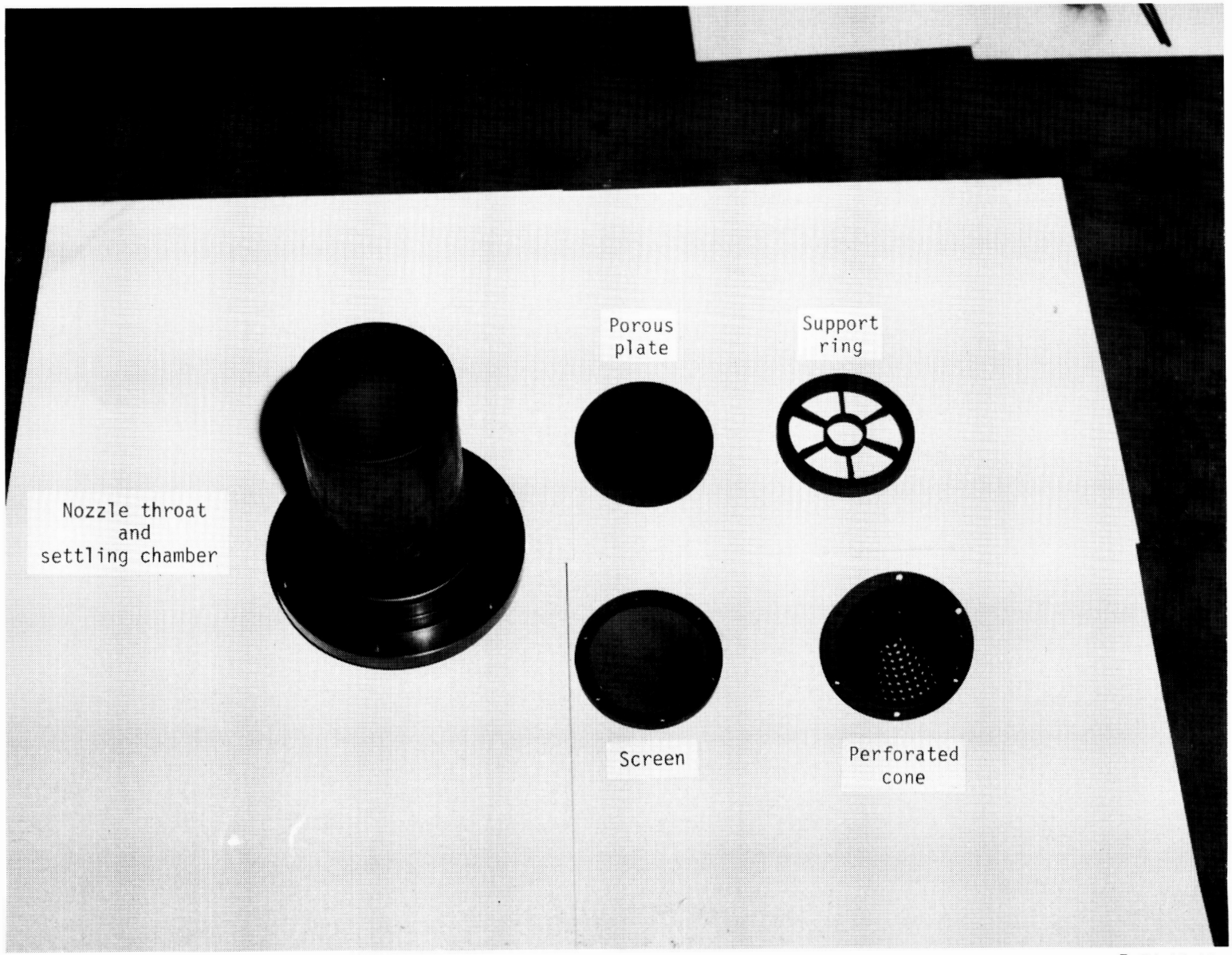

L-81-10,488

Figure 4. Photograph of settling-chamber components.

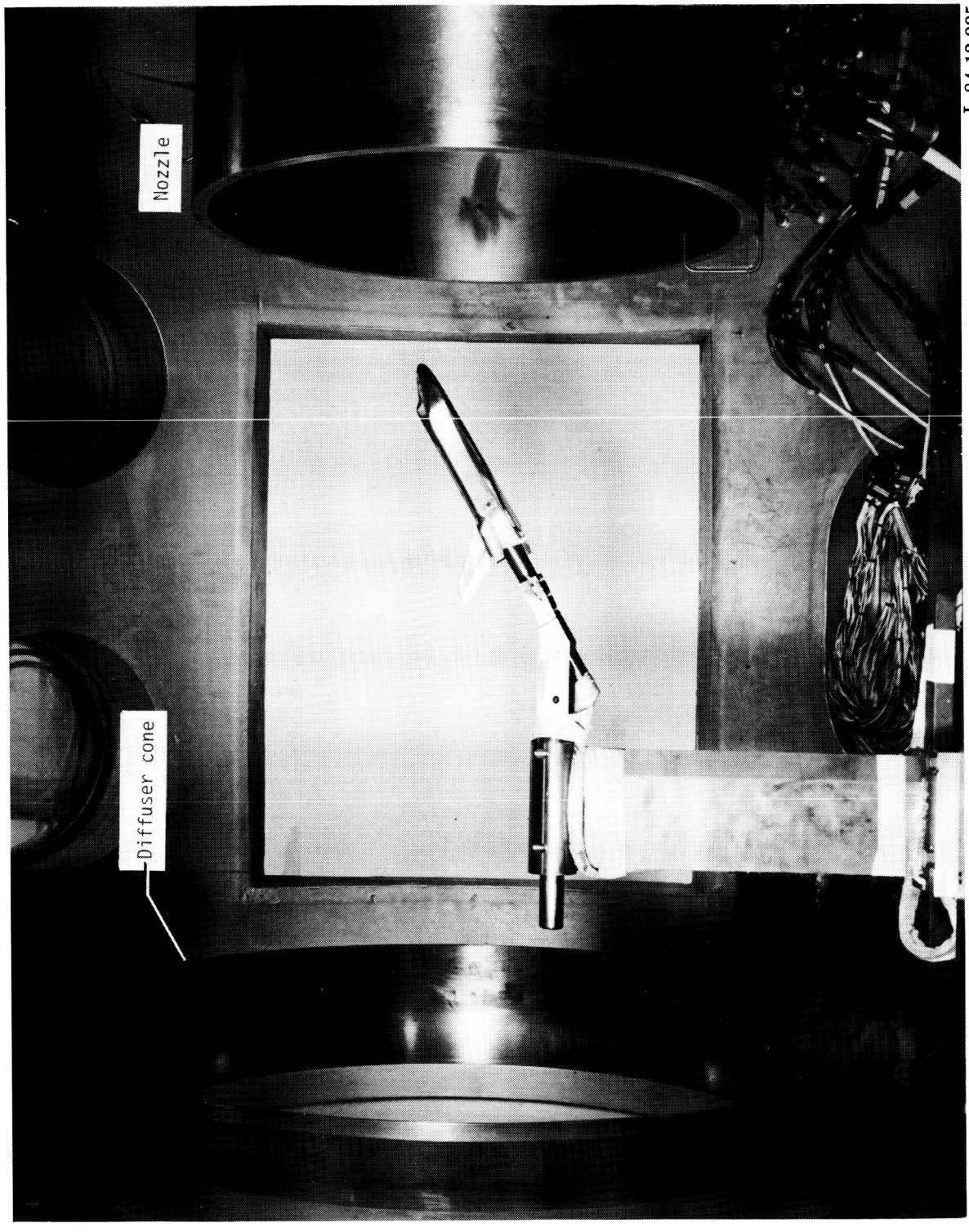

Figure 5. Photograph of test section.

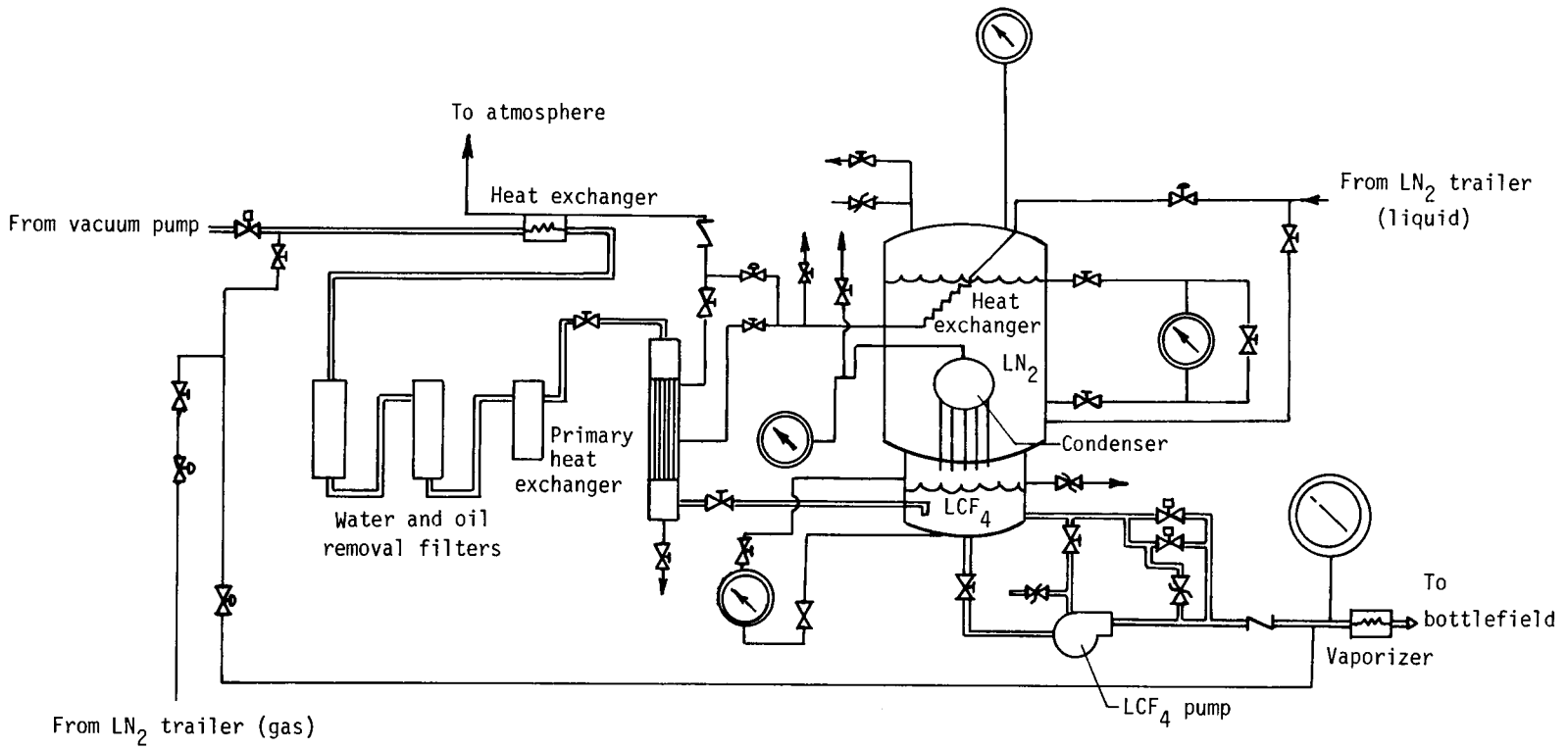

Figure 6. Schematic drawing of CF_4 reclaimer system.

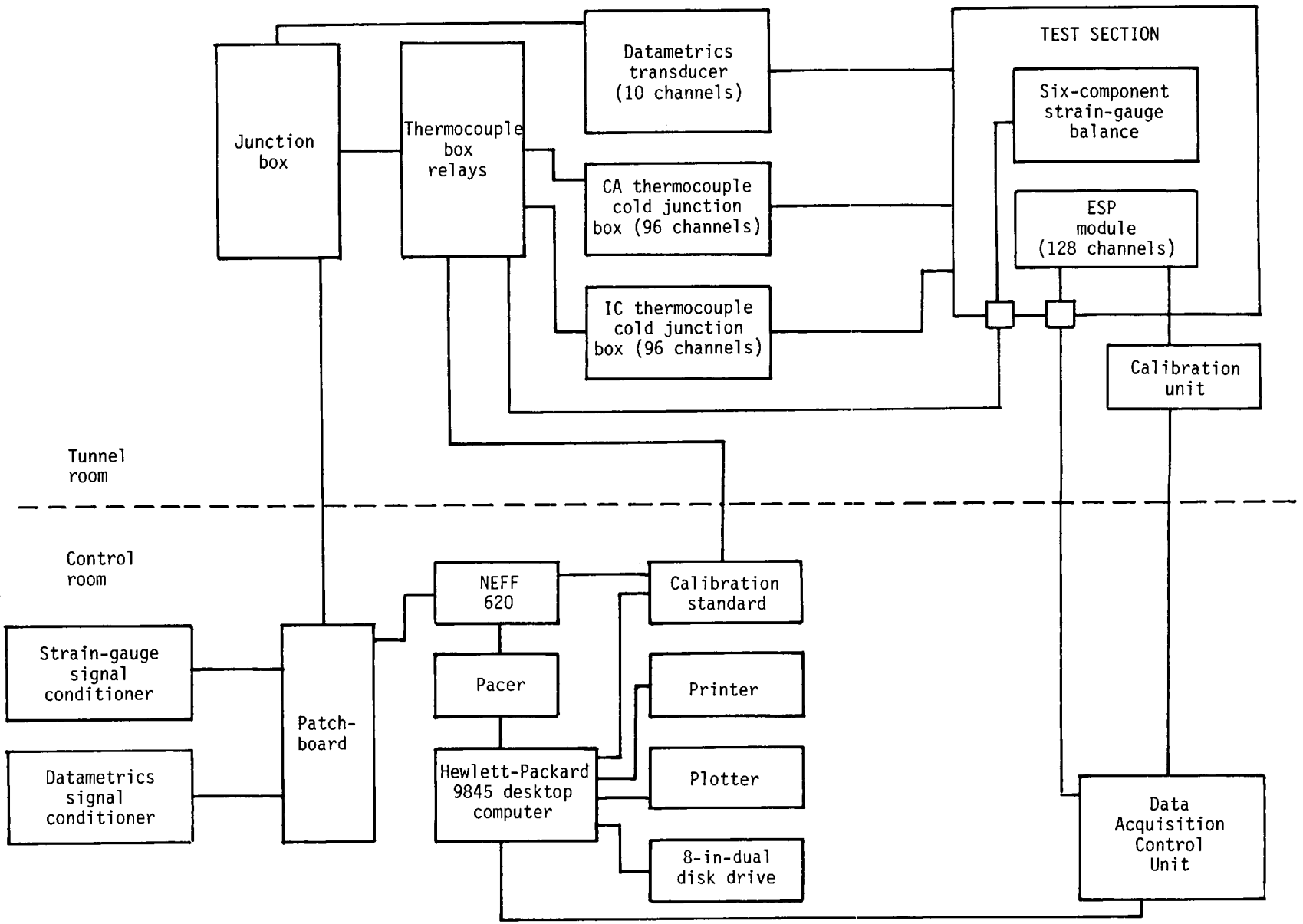

Figure 7. Block diagram of instrumentation for the CF_4 Tunnel.

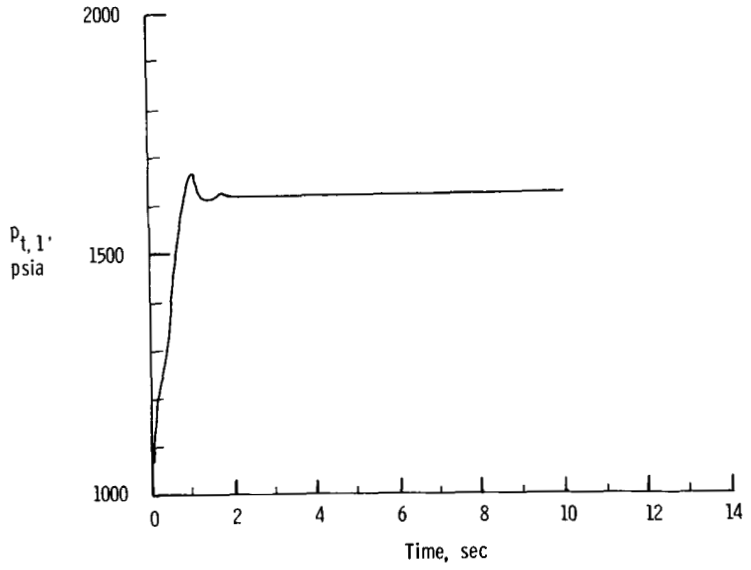

(a) Reservoir pressure.

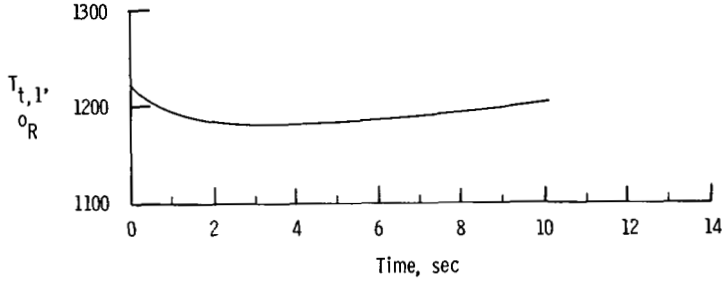

(b) Reservoir temperature.

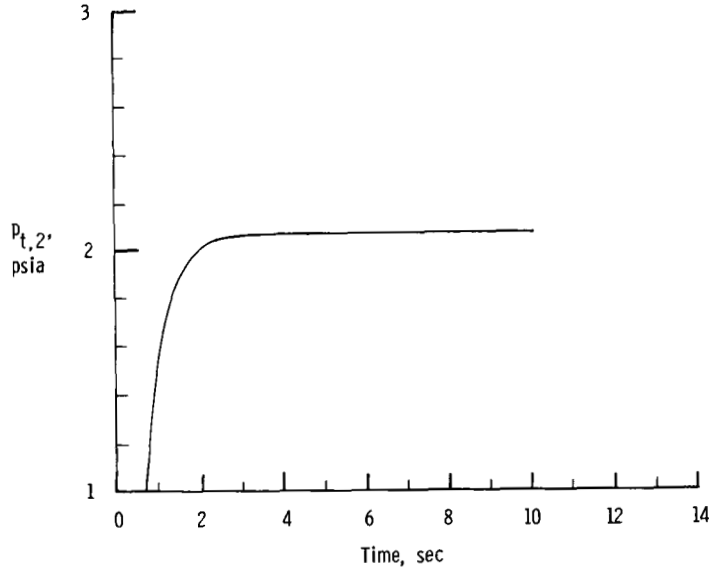

(c) Pitot pressure.

Figure 8. Sample time histories of basic tunnel flow quantities ($p_{t,1}$, $T_{t,1}$, and $p_{t,2}$), model-position indicator, and thin-film gauge measurements at test section.

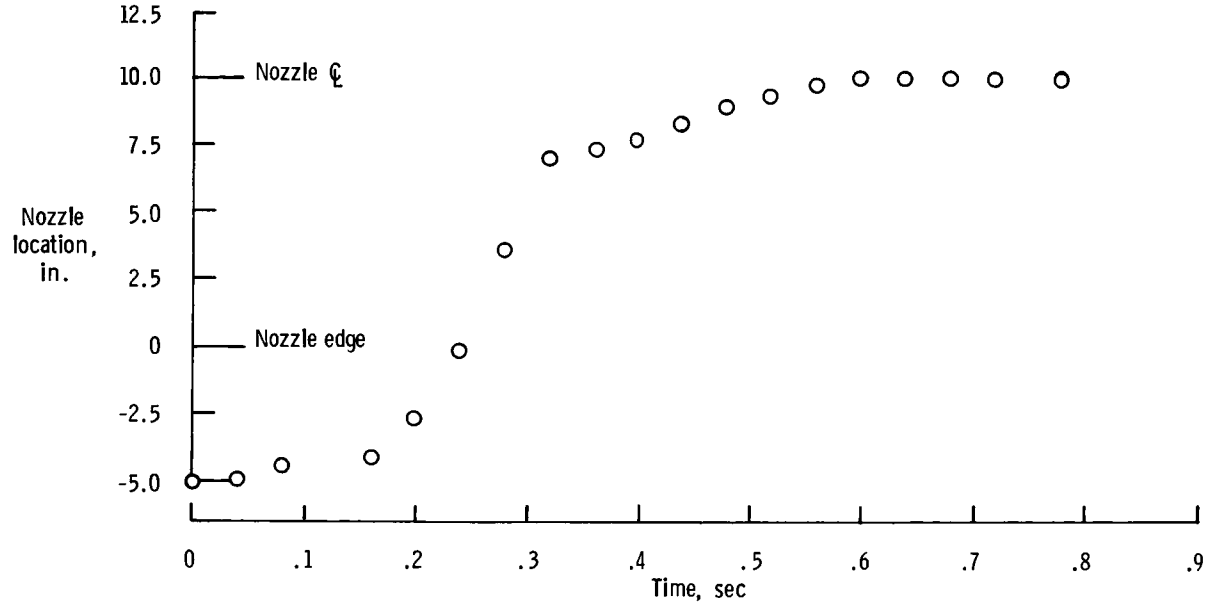

(d) Slide wire.

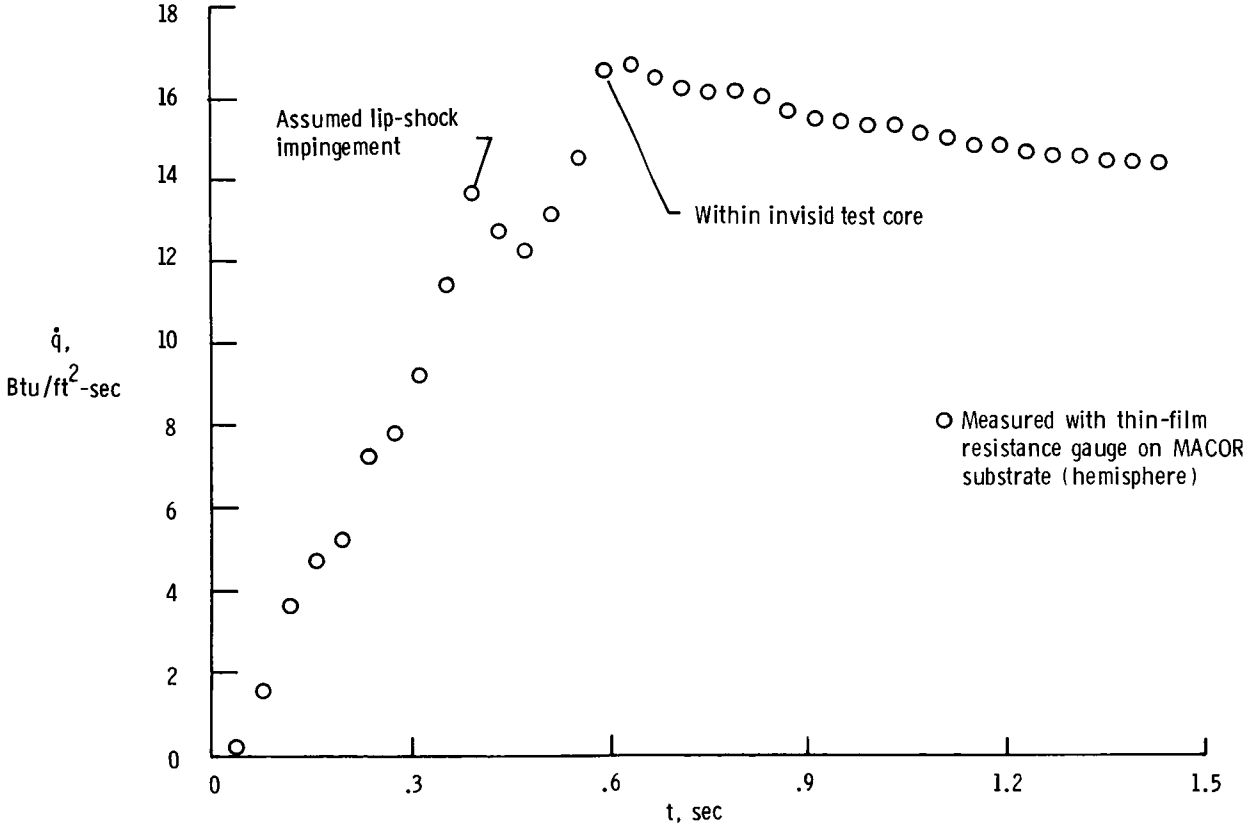

(e) Heat-transfer rate to MACOR hemisphere. (MACOR is a trademark of the Corning Glass Works.) Note change in time scale.

Figure 8. Concluded.

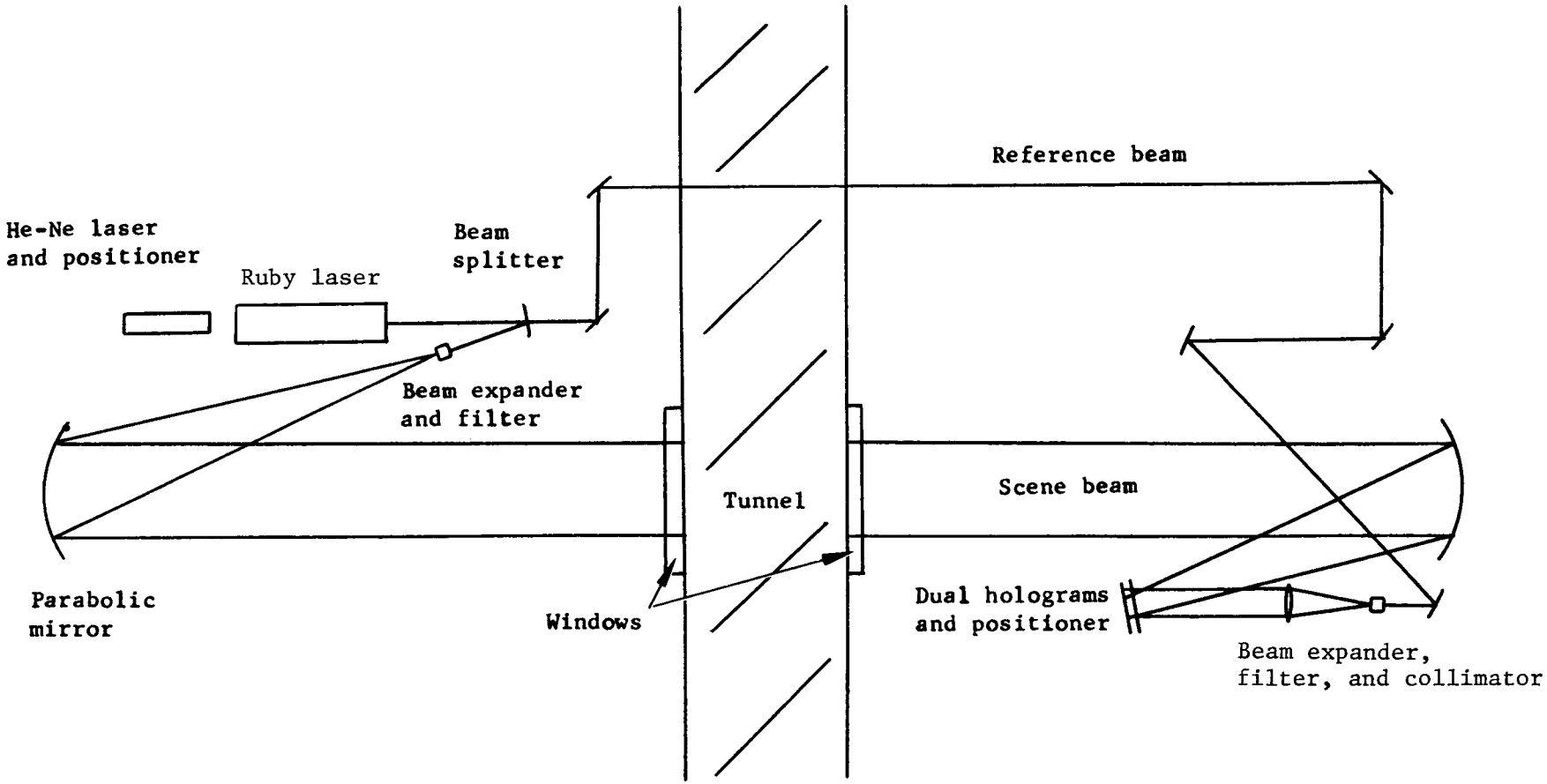

Figure 9. Holographic setup at the CF_4 Tunnel (ref. 10).

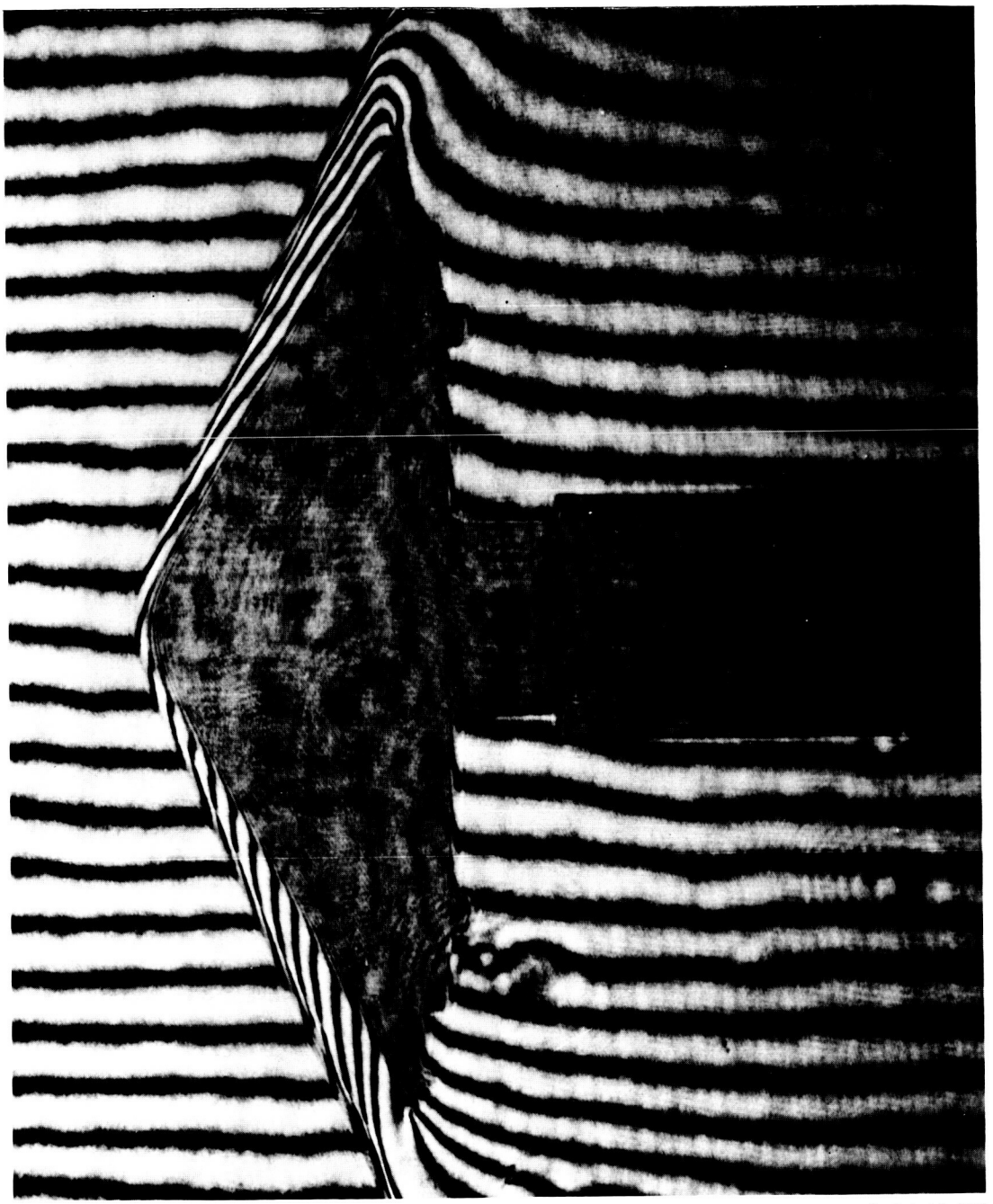

L-84-12,906

(a) Interferogram of sphere cone.

Figure 10. Representative interferogram of sphere cone and schlieren of proposed planetary aerocapture vehicle.

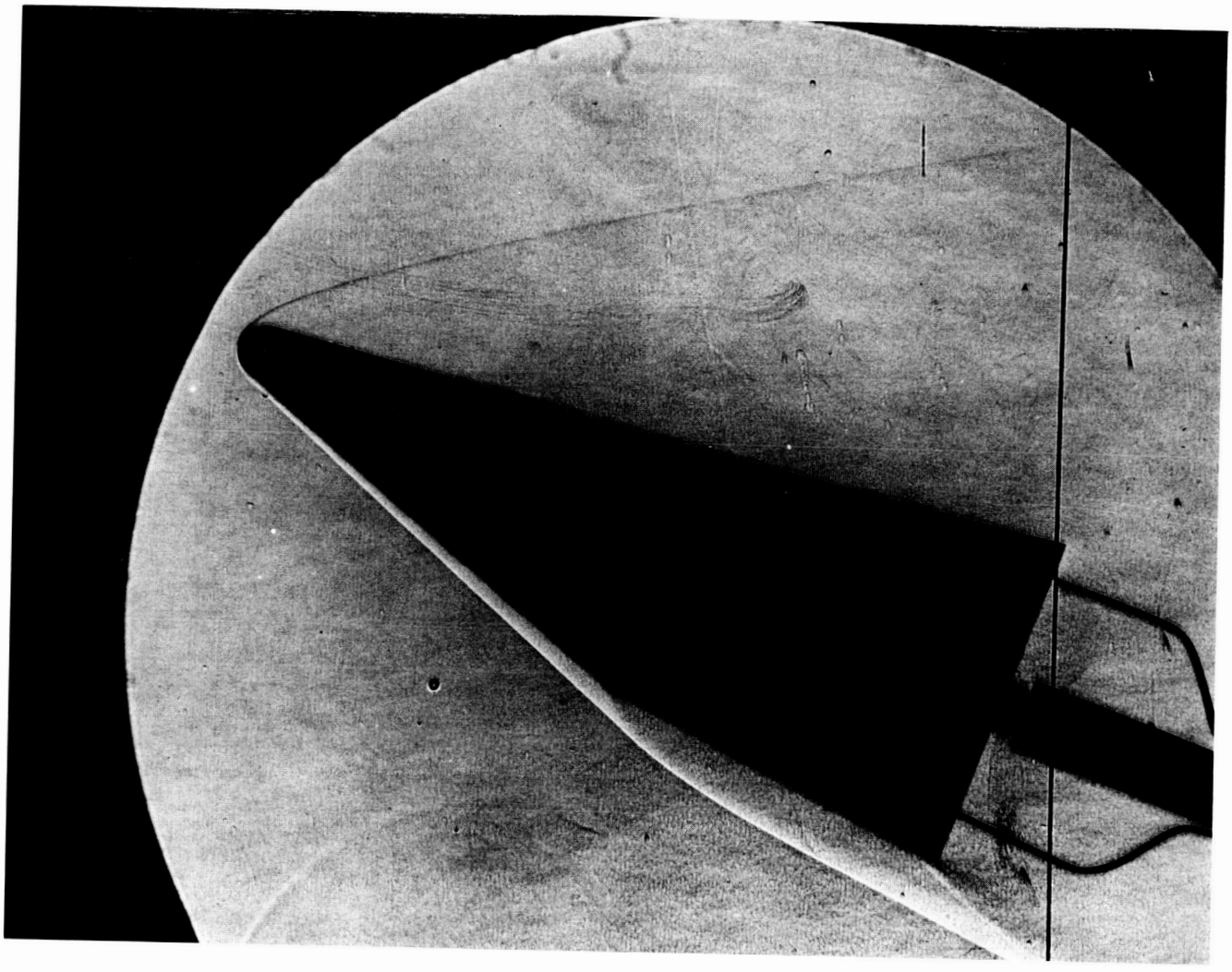

L-84-12,907

(b) Schlieren of proposed planetary aerocapture vehicle.

Figure 10. Concluded.

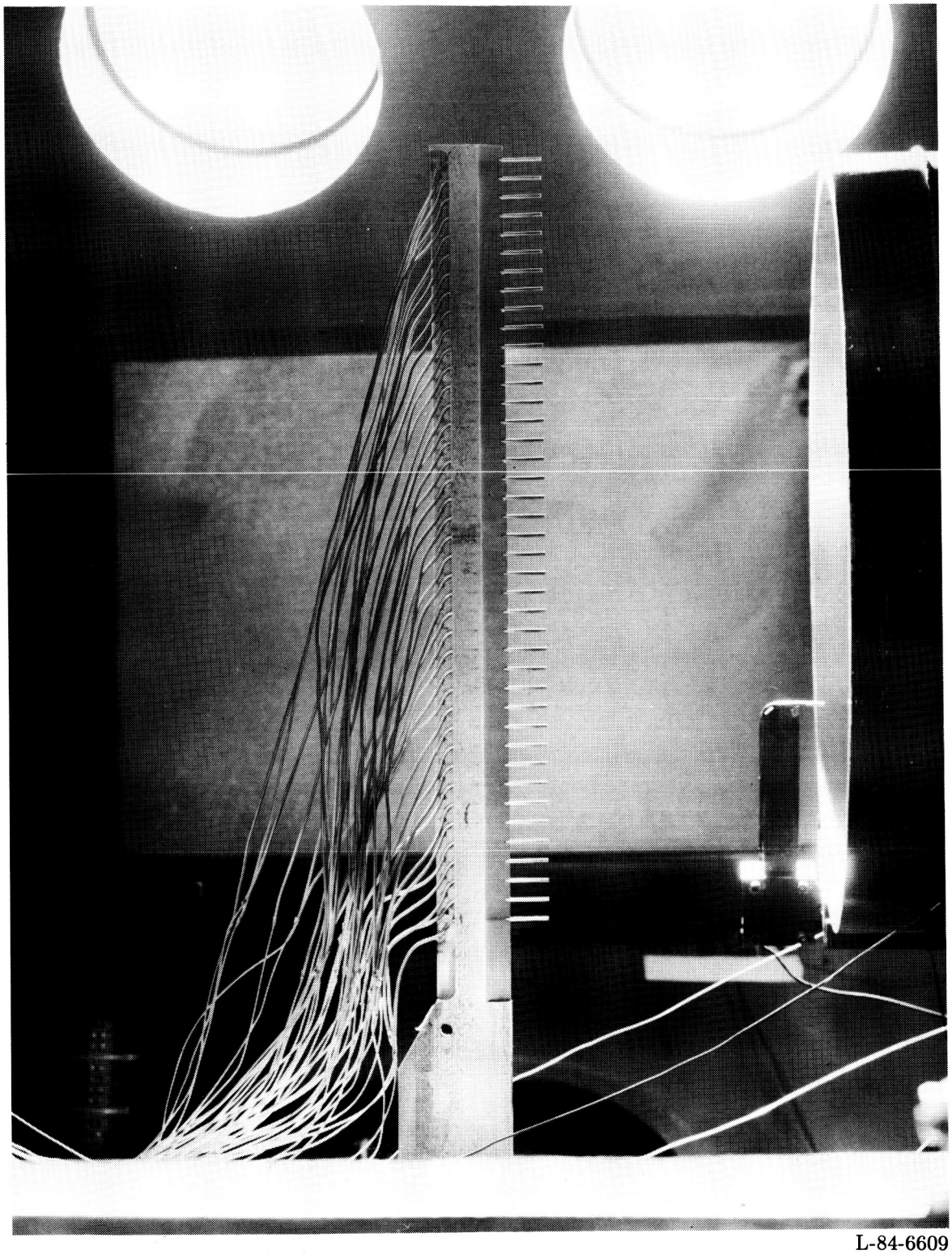

L-84-6609

(a) 41-probe pressure survey rake.

Figure 11. Photographs of 41-probe pitot-pressure rake and 21-probe temperature survey rake.

L-84-8382

(b) Temperature rake.

Figure 11. Concluded.

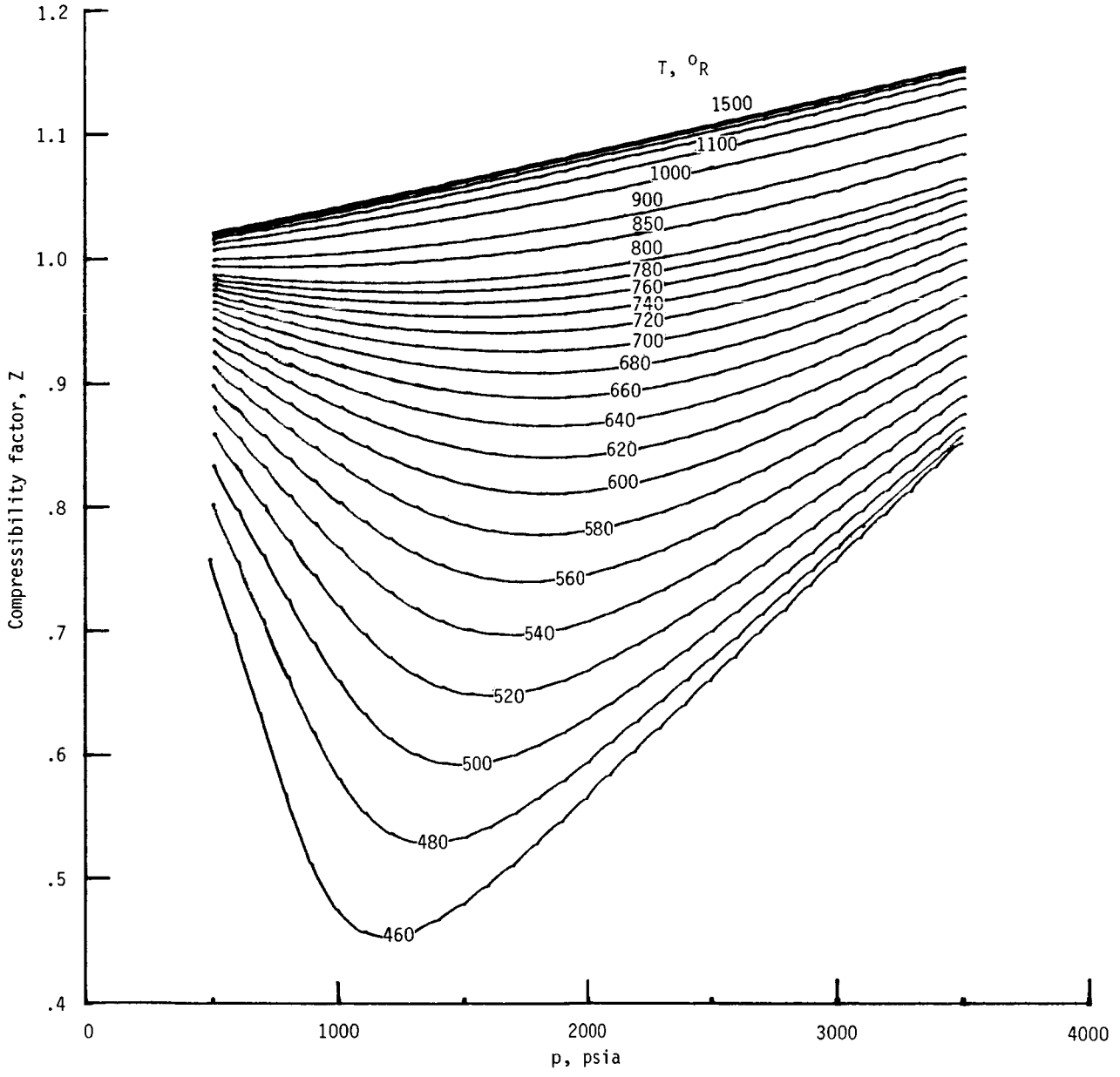

Figure 12. Compressibility factor for CF_4 gas as a function of pressure and temperature.

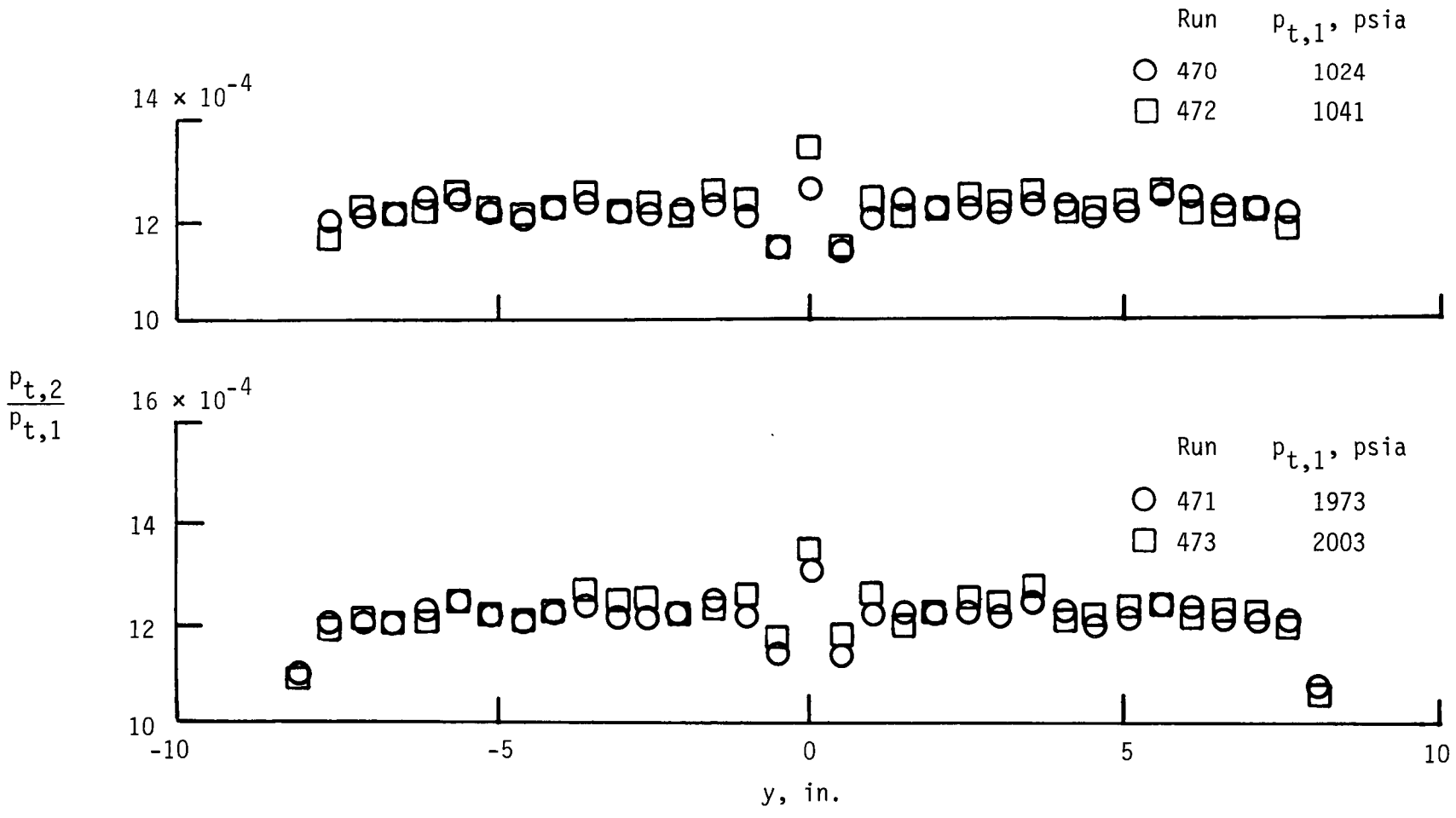

(a) $T_{t,1} \approx 1045°\text{R}$.

Figure 13. Vertical pitot-pressure profiles at nozzle exit for various reservoir pressures at a given reservoir temperature.

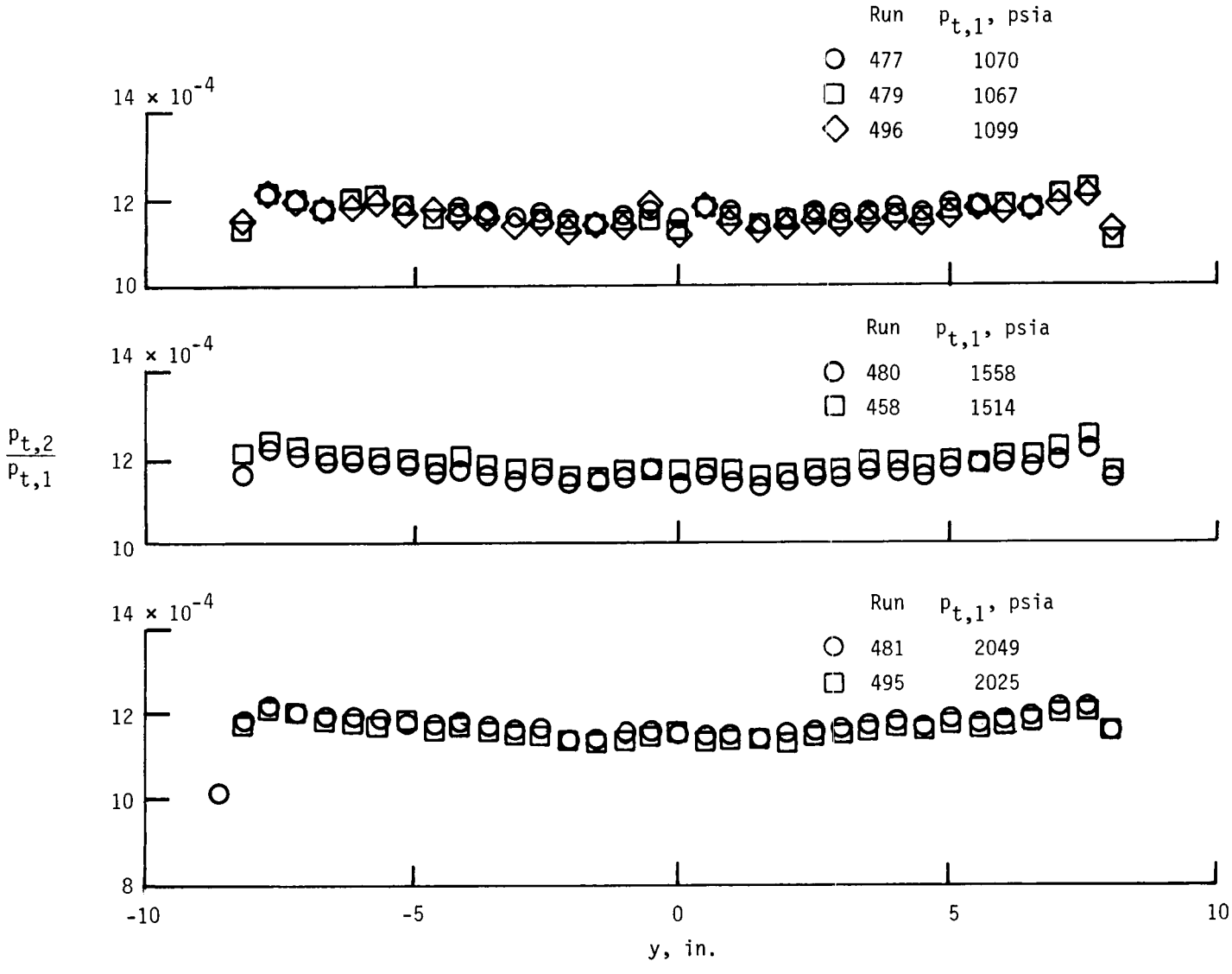

(b) $T_{t,1} \approx 1450°R$.

Figure 13. Concluded.

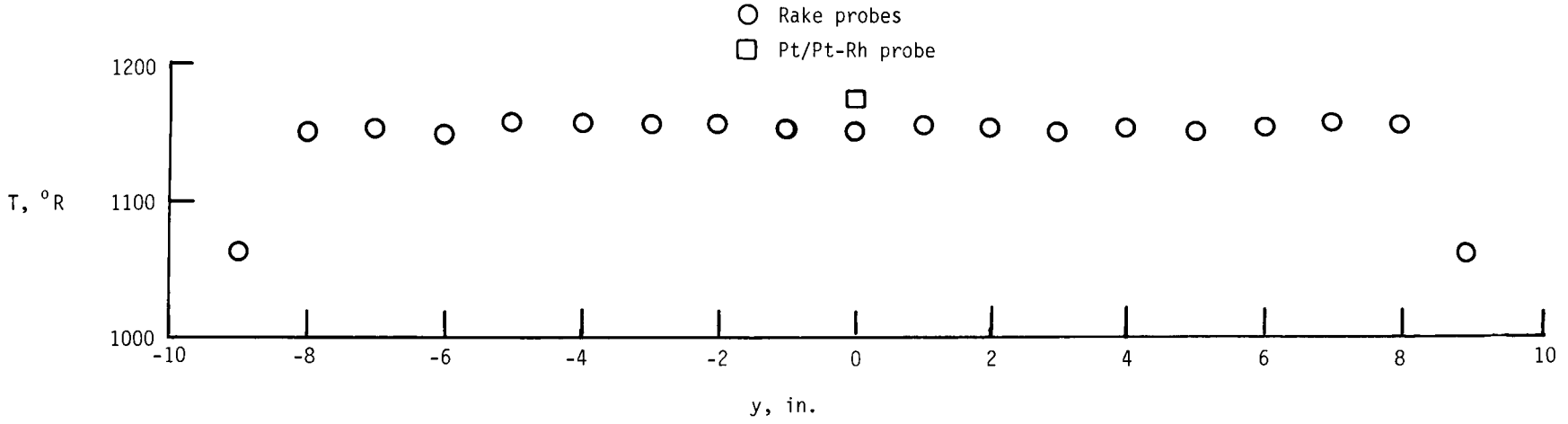

(a) $p_{t,1} = 1516$ psia.

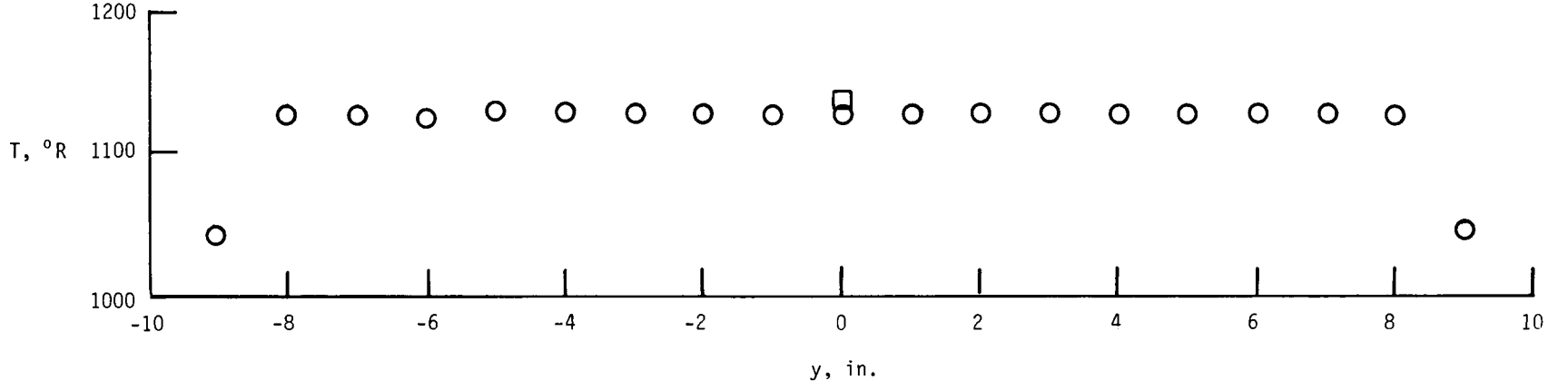

(b) $p_{t,1} \approx 2393$ psia.

Figure 14. Total temperature profile at nozzle exit. $T_{t,1} = 1186°$R.

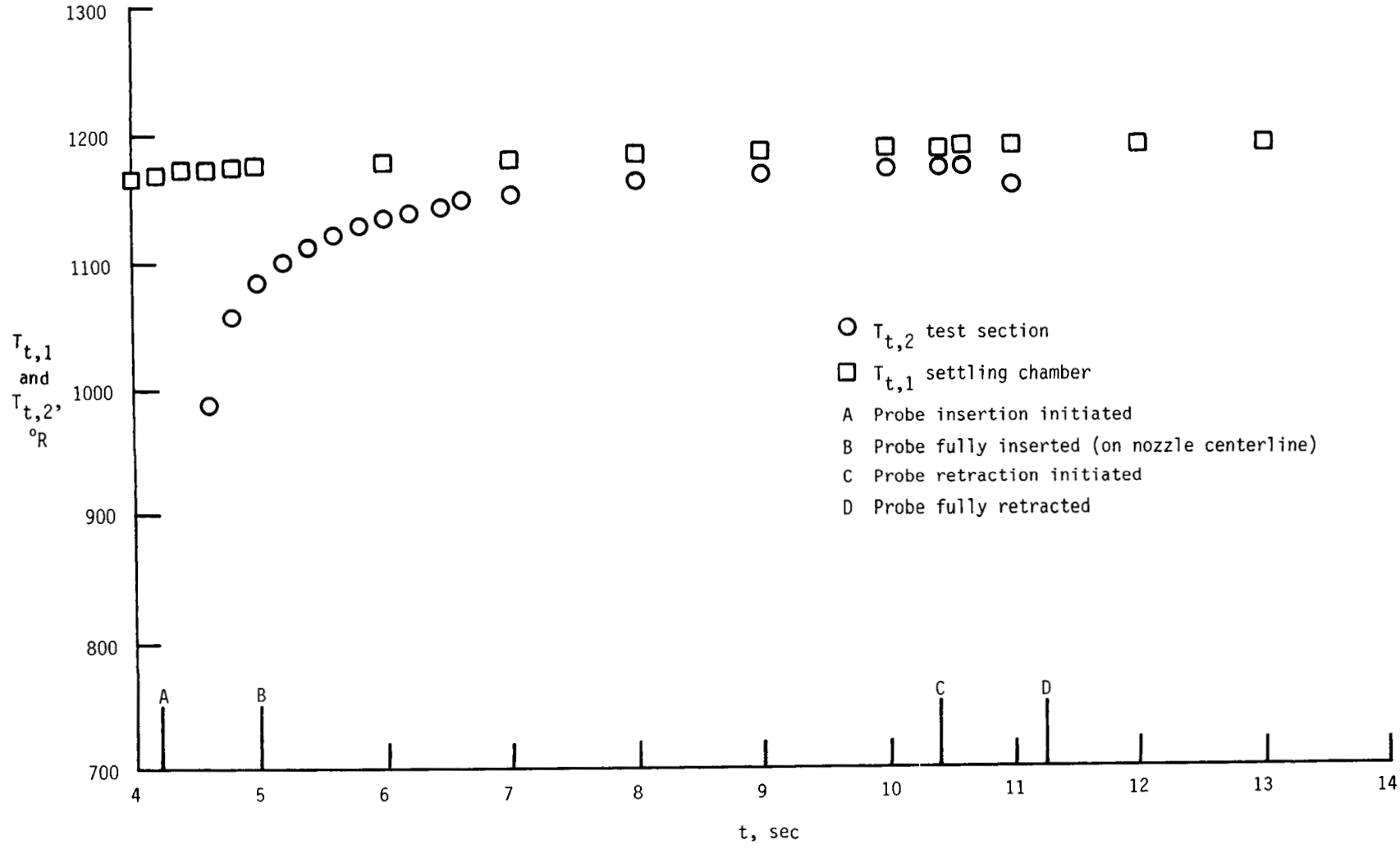

Figure 15. Reservoir temperature and stagnation temperature at nozzle exit as function of time.

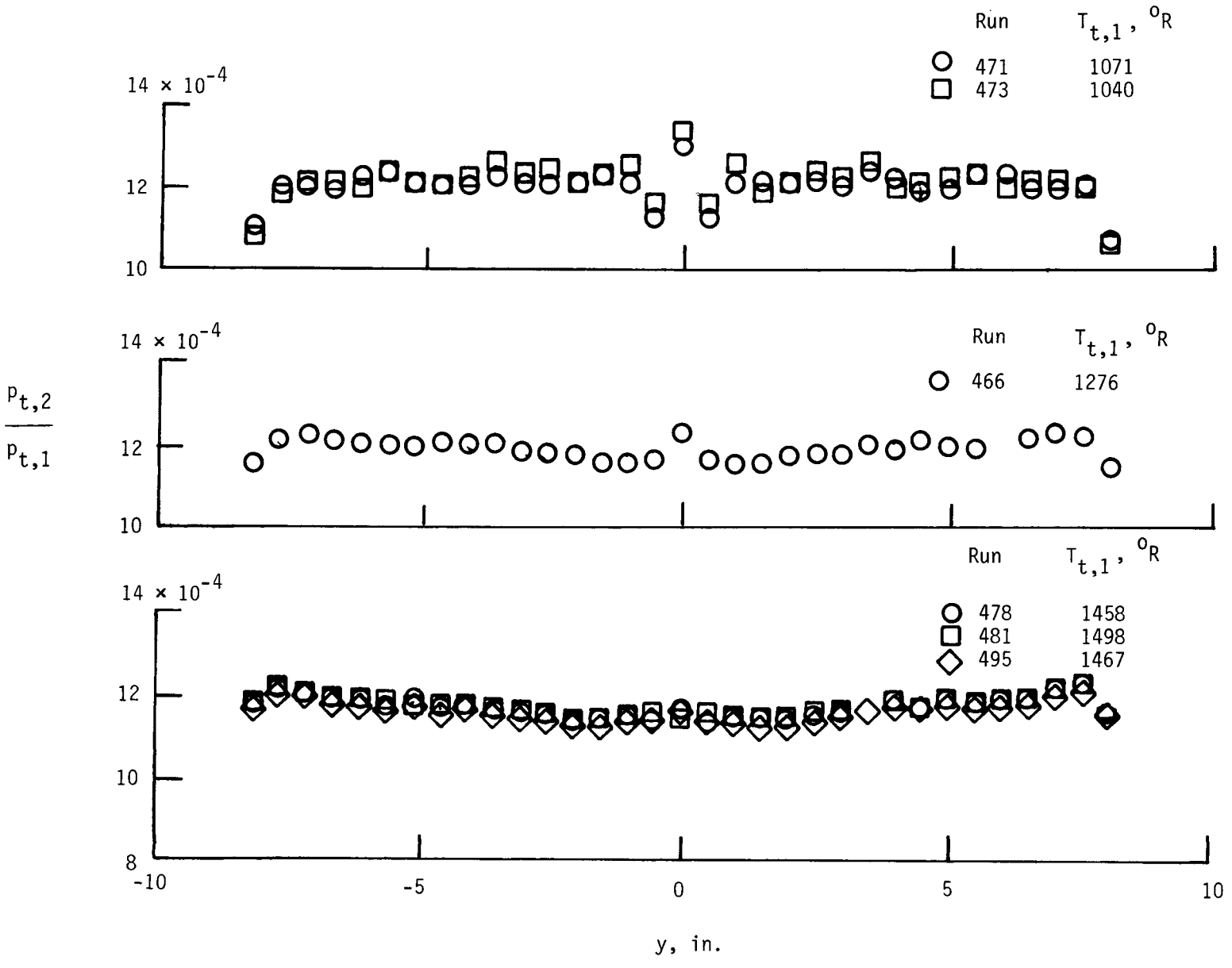

Figure 16. Pitot-pressure profile at nozzle exit for $p_{t,1} \approx 2000$ psia and various values of reservoir temperature.

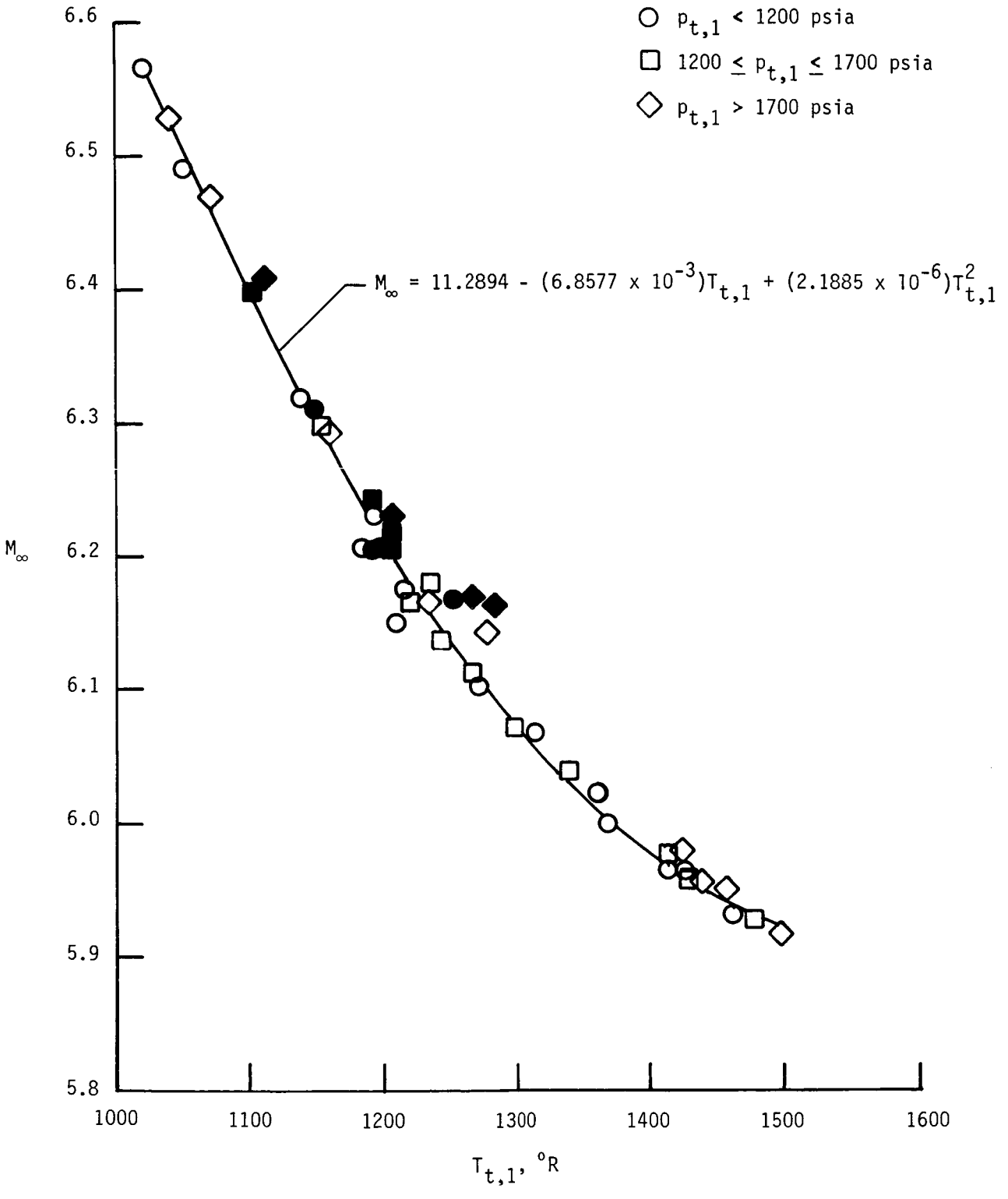

(a) Free-stream Mach number.

Figure 17. Free-stream Mach number, normal-shock density ratio, and free-stream Reynolds number at nozzle exit as function of reservoir temperature. Open symbols indicate porous plate was removed; closed symbols indicate porous plate was installed.

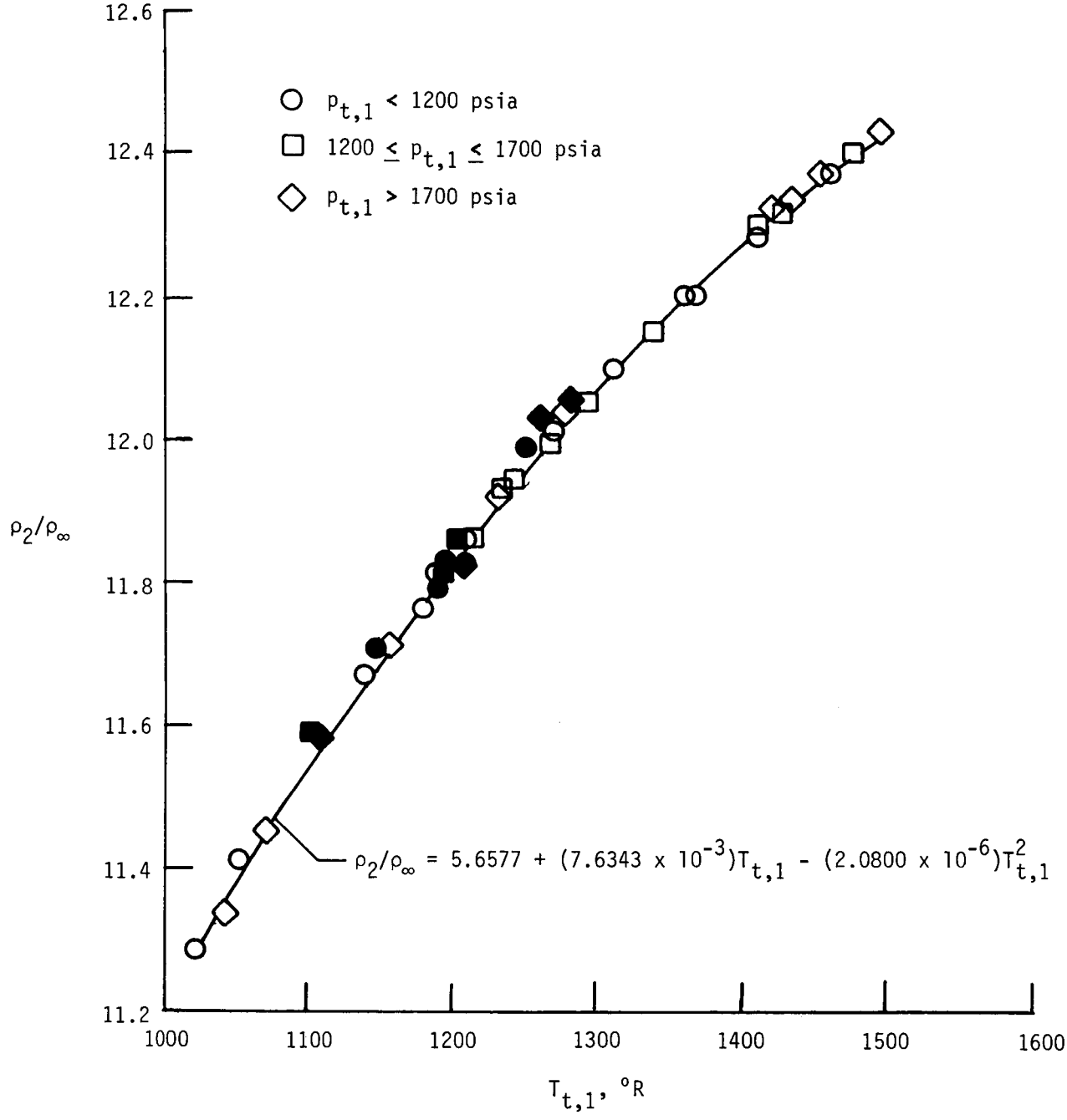

(b) Normal-shock density ratio.

Figure 17. Continued.

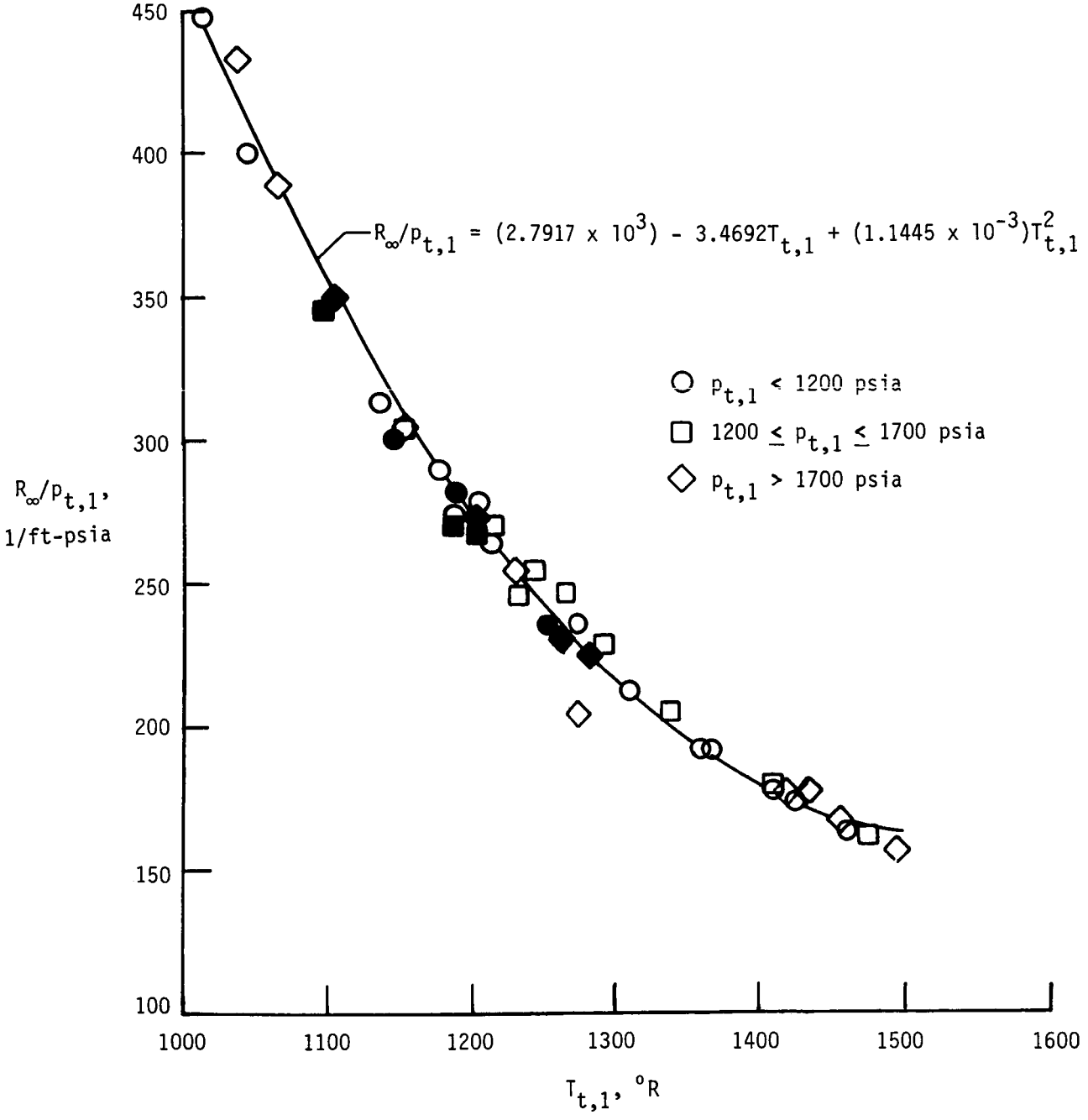

(c) Free-stream Reynolds number.

Figure 17. Concluded.

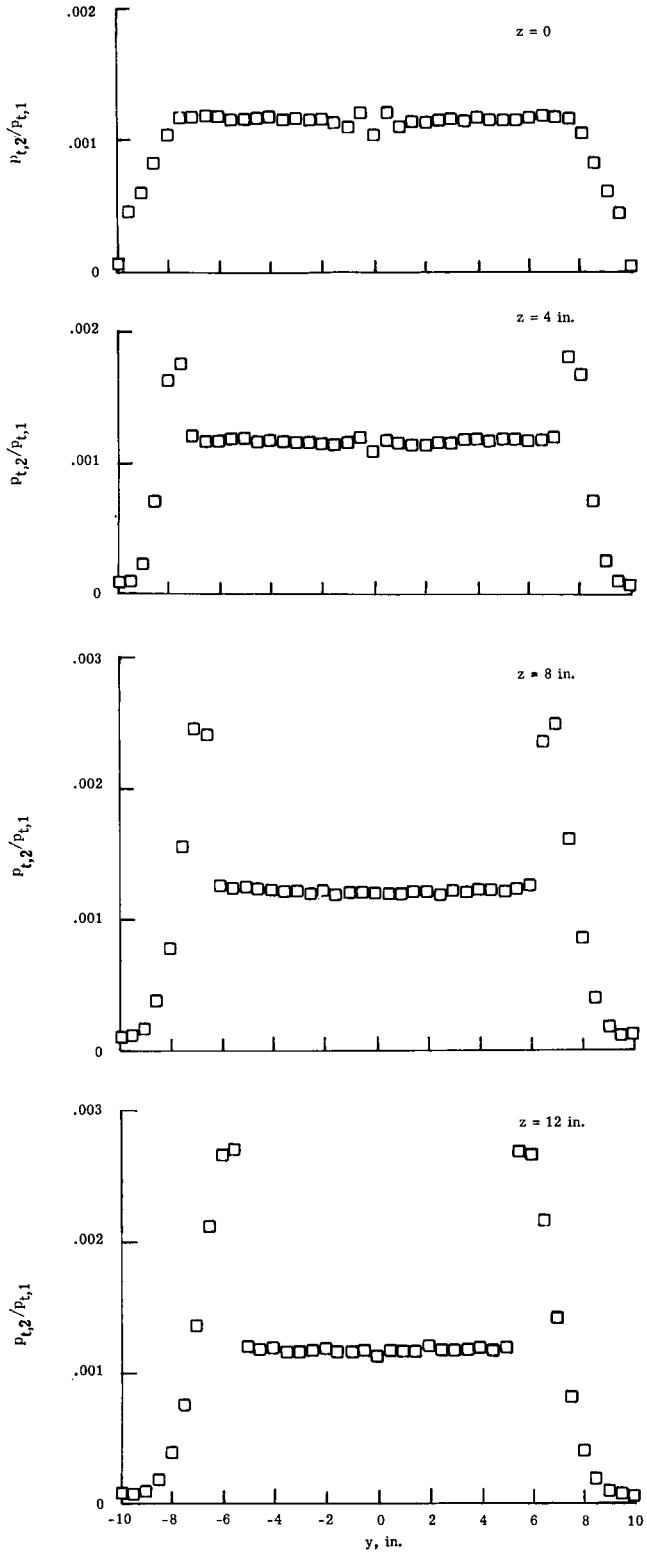

(a) $p_{t,1} \approx 1000$ psia.

Figure 18. Pitot-pressure profiles at various axial stations downstream of nozzle exit. $T_{t,1} \approx 1190°\text{R}$.

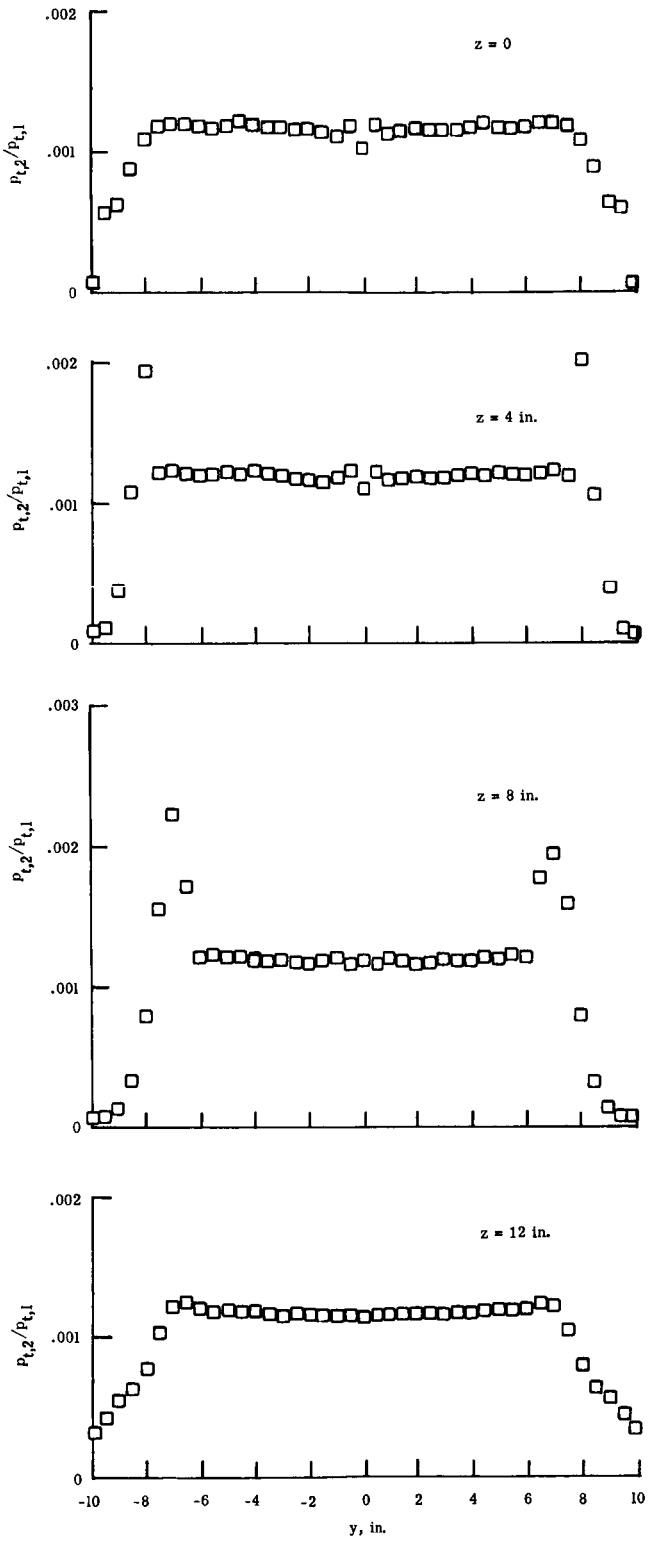

(b) $p_{t,1} \approx 1495$ psia.

Figure 18. Concluded.

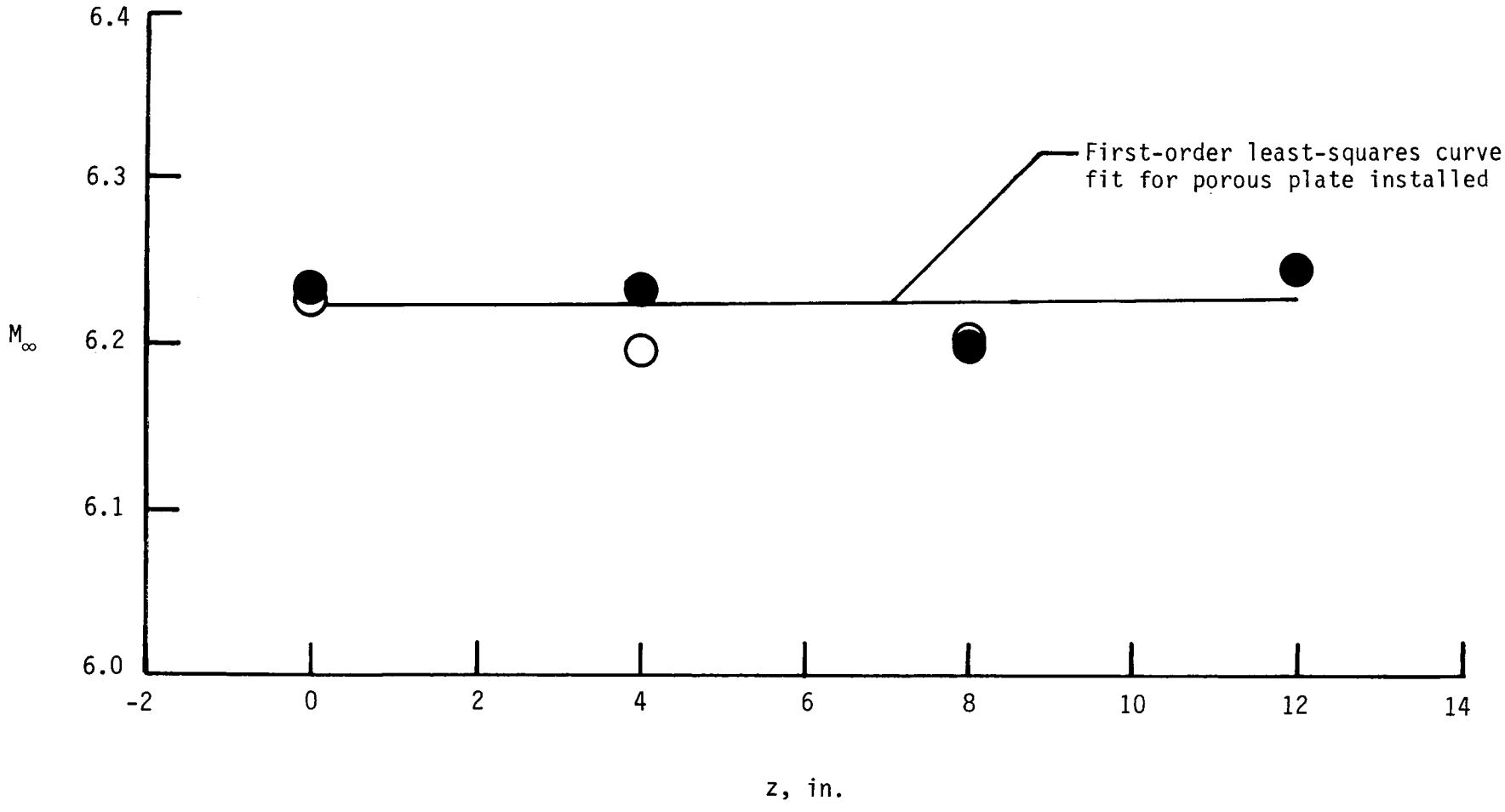

Figure 19. Average free-stream Mach number across inviscid test core at various distances downstream of nozzle exit. $T_{t,1} = 1200°R$. Open symbols indicate porous plate was removed; closed symbols indicate porous plate was installed.

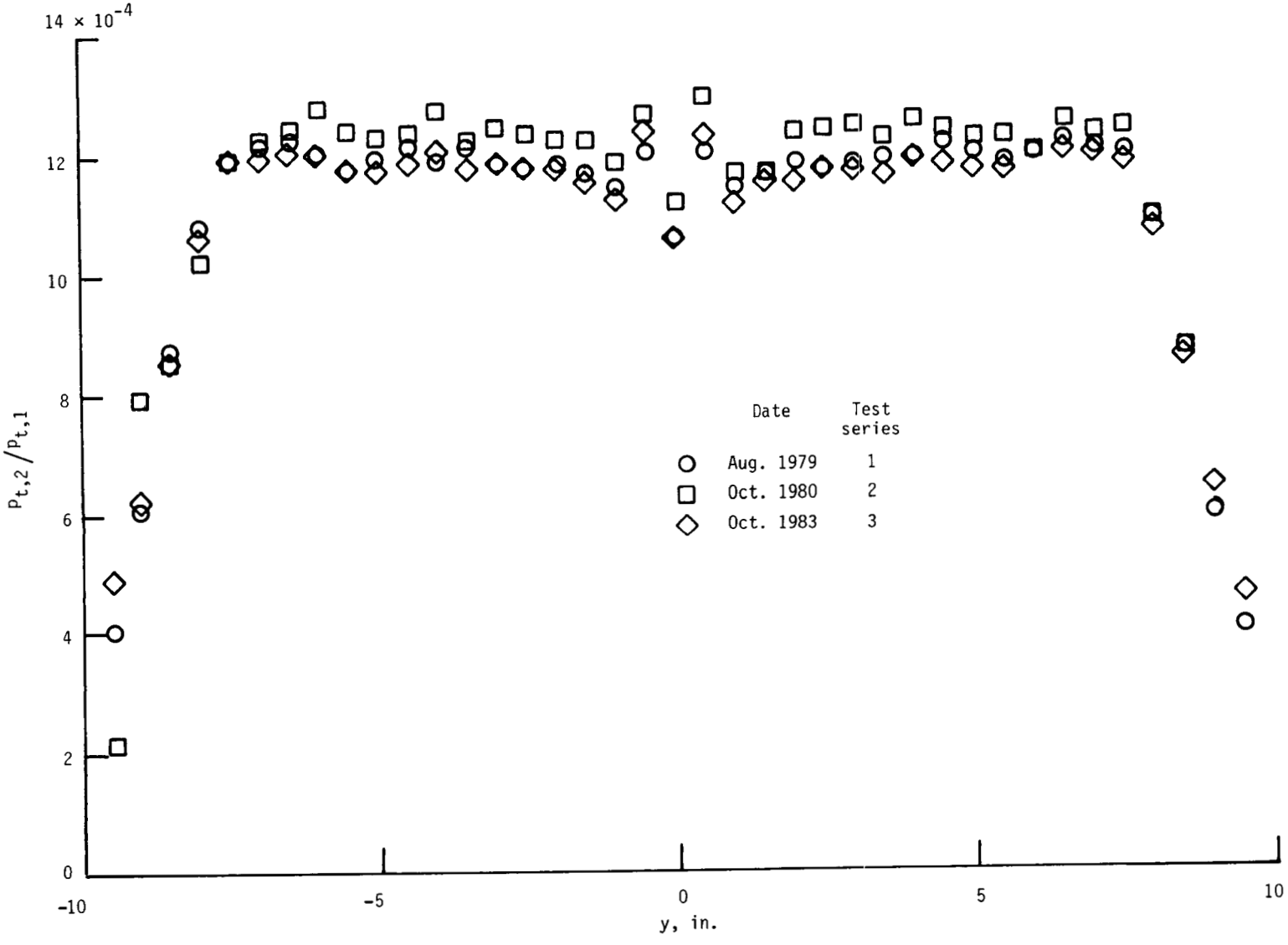

(a) $p_{t,1} \approx 1089$ psia; $T_{t,1} \approx 1179°$R.

Figure 20. Repeatability of pitot-pressure profiles for three test series.

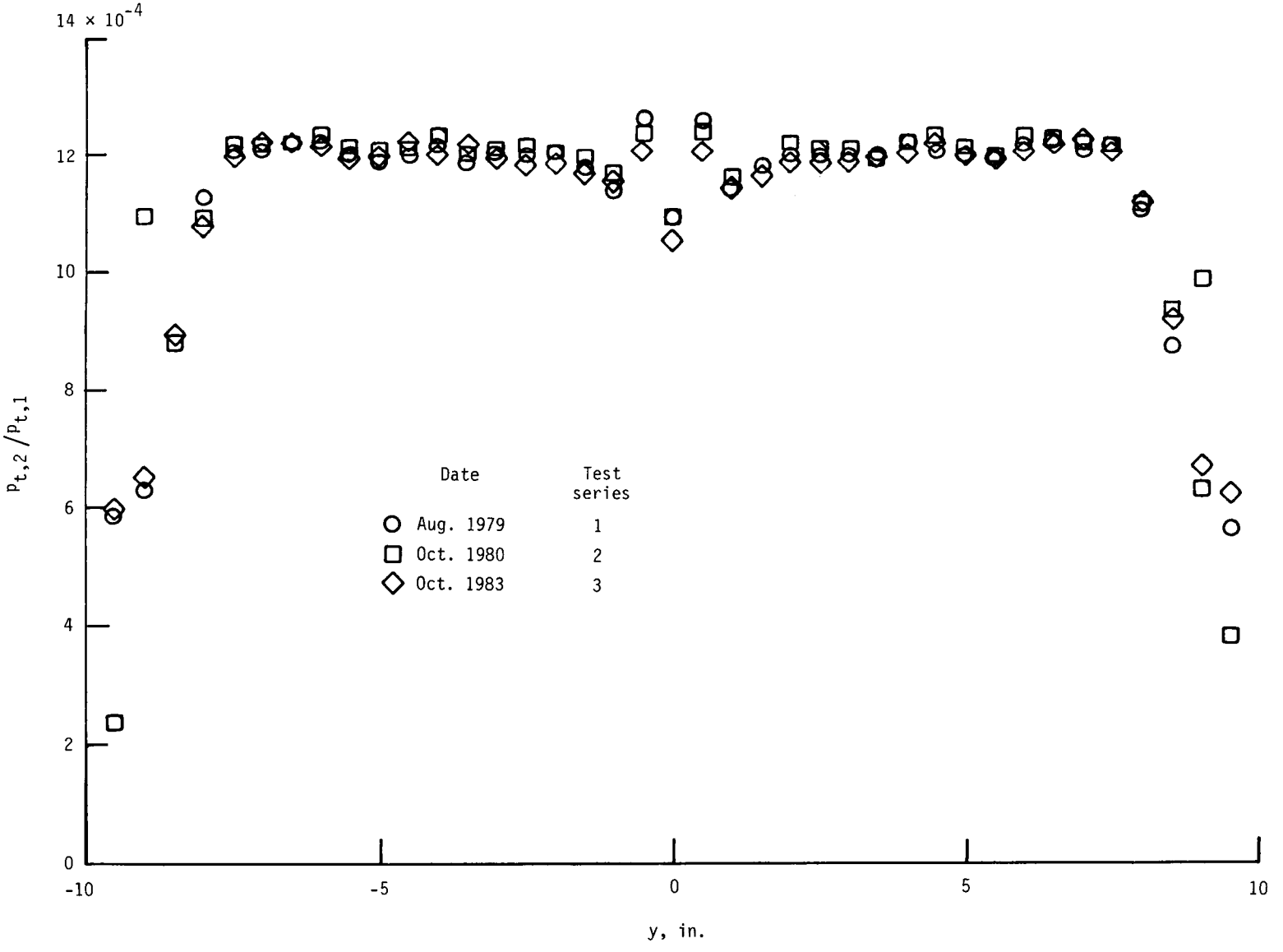

(b) $p_{t,1} \approx 1590$ psia; $T_{t,1} \approx 1150°$R.

Figure 20. Concluded.

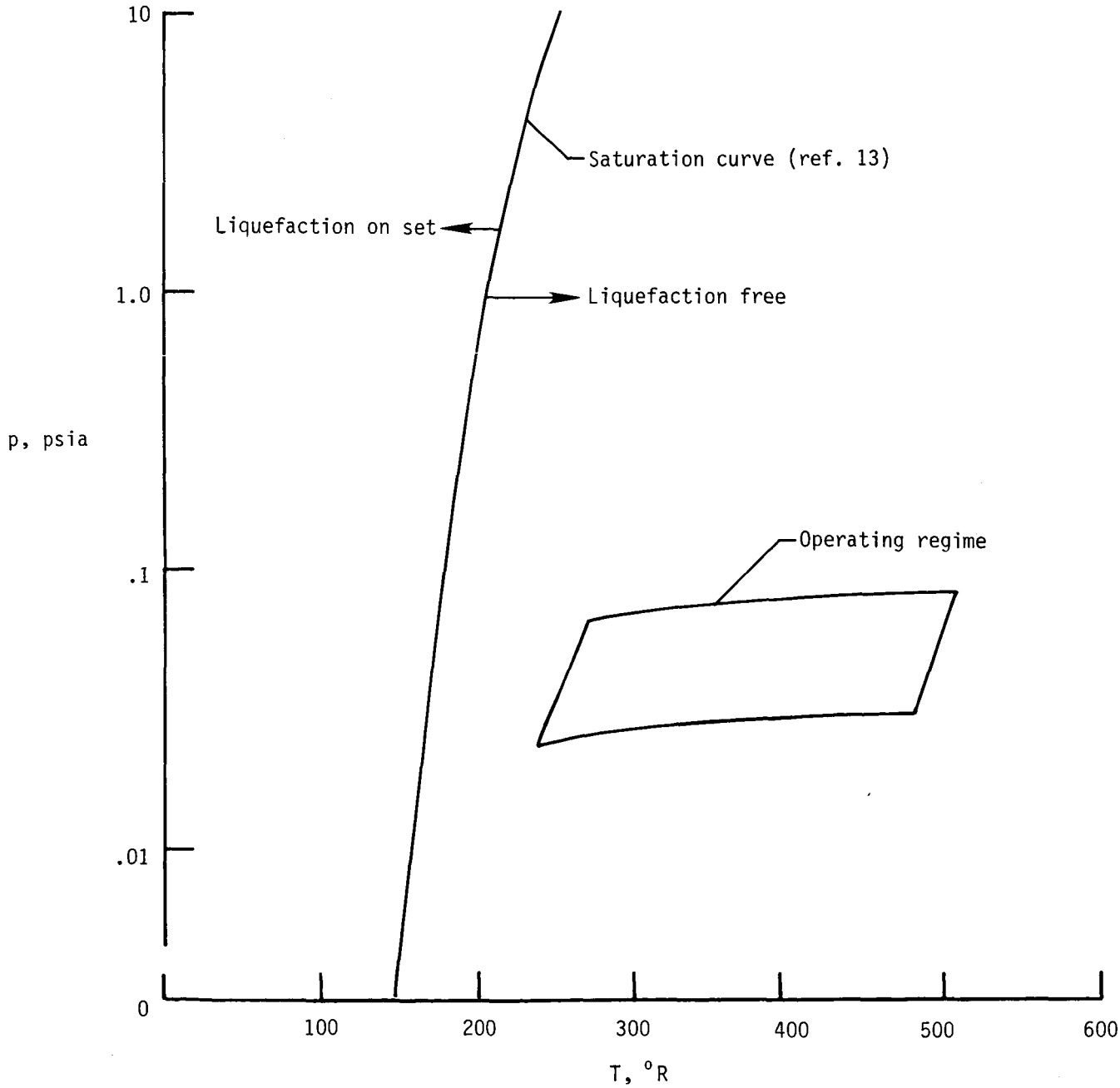

Figure 21. Free-stream pressure-temperature operating regime for the CF_4 Tunnel.

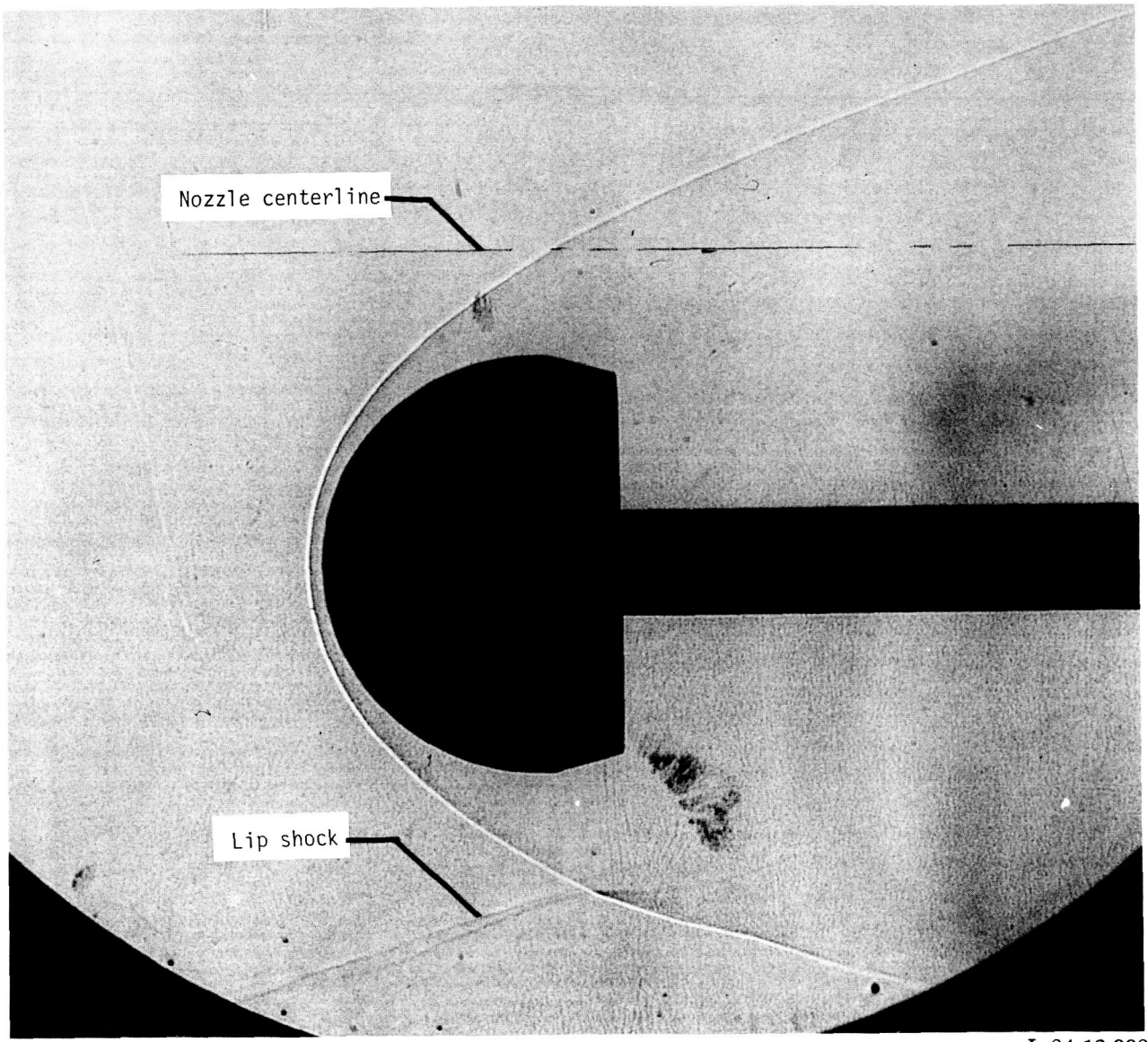

L-84-12,908

Figure 22. Schlieren photograph illustrating interaction of lip shock from nozzle exit and bow shock of test model.

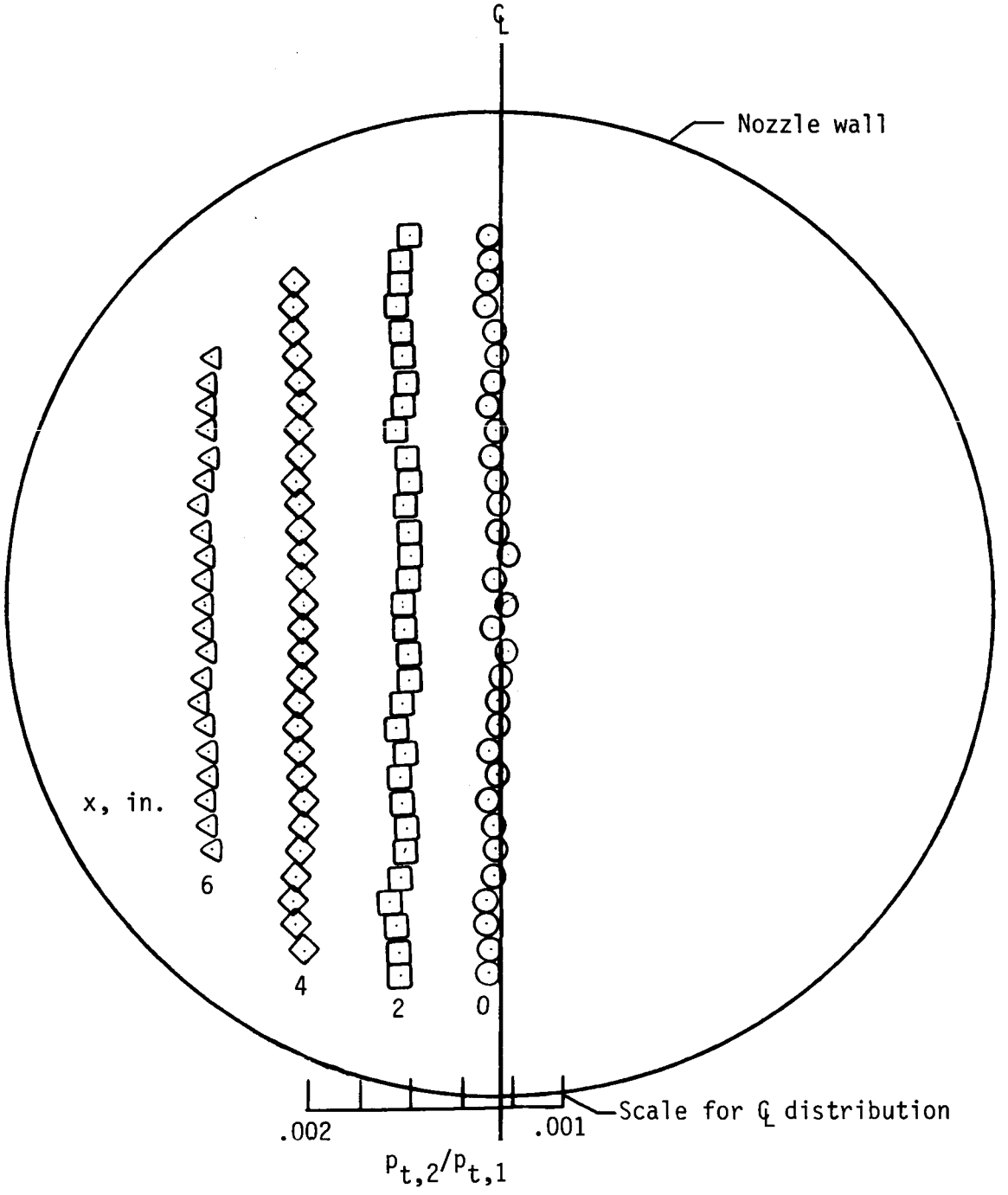

(a) $z = 0$.

Figure 23. Vertical pitot-pressure profiles at lateral stations for given axial station. View from nozzle throat; $p_{t,1} = 1500$ psia; $T_{t,1} \approx 1250°$R.

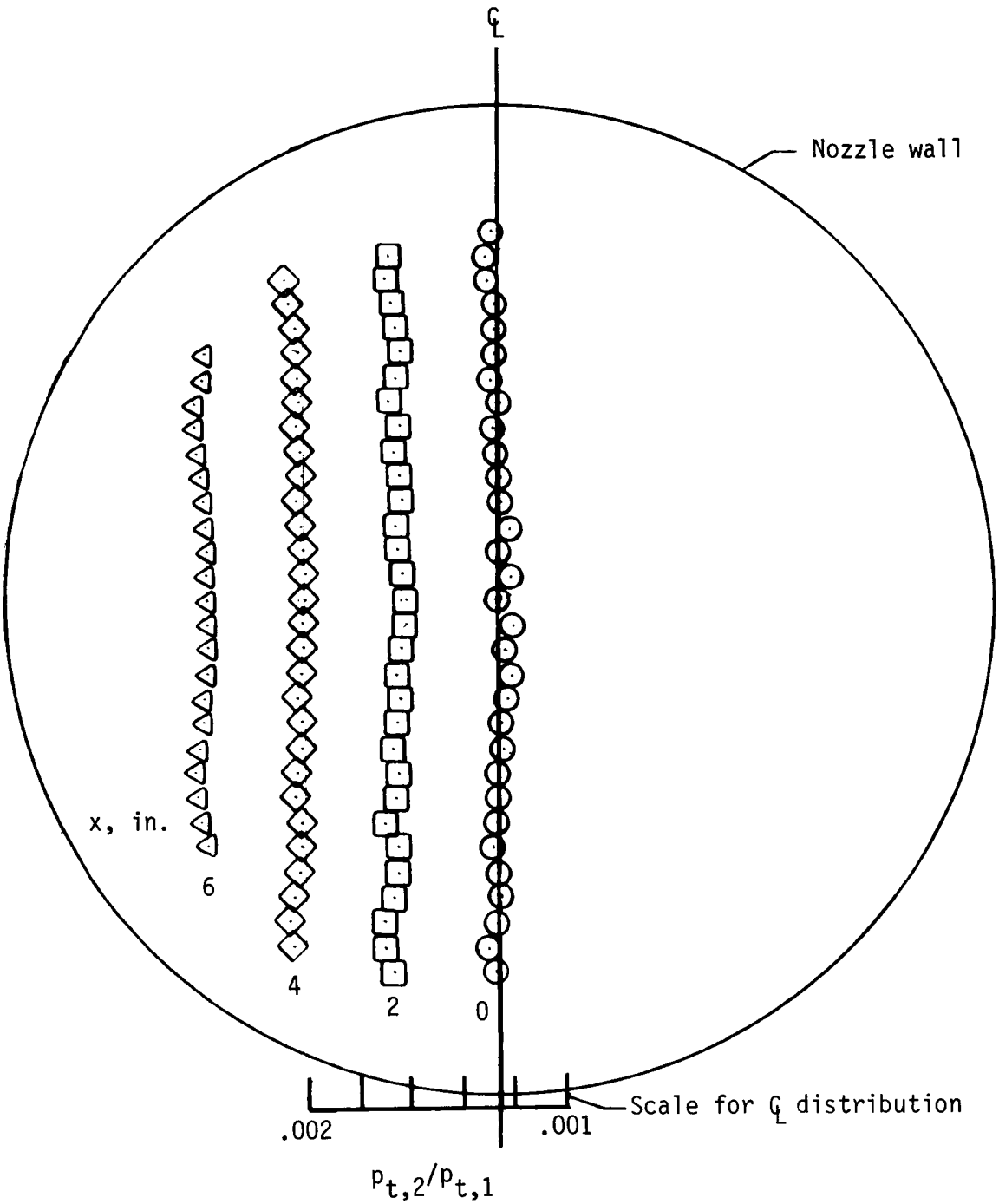

(b) $z = 4$ in.

Figure 23. Continued.

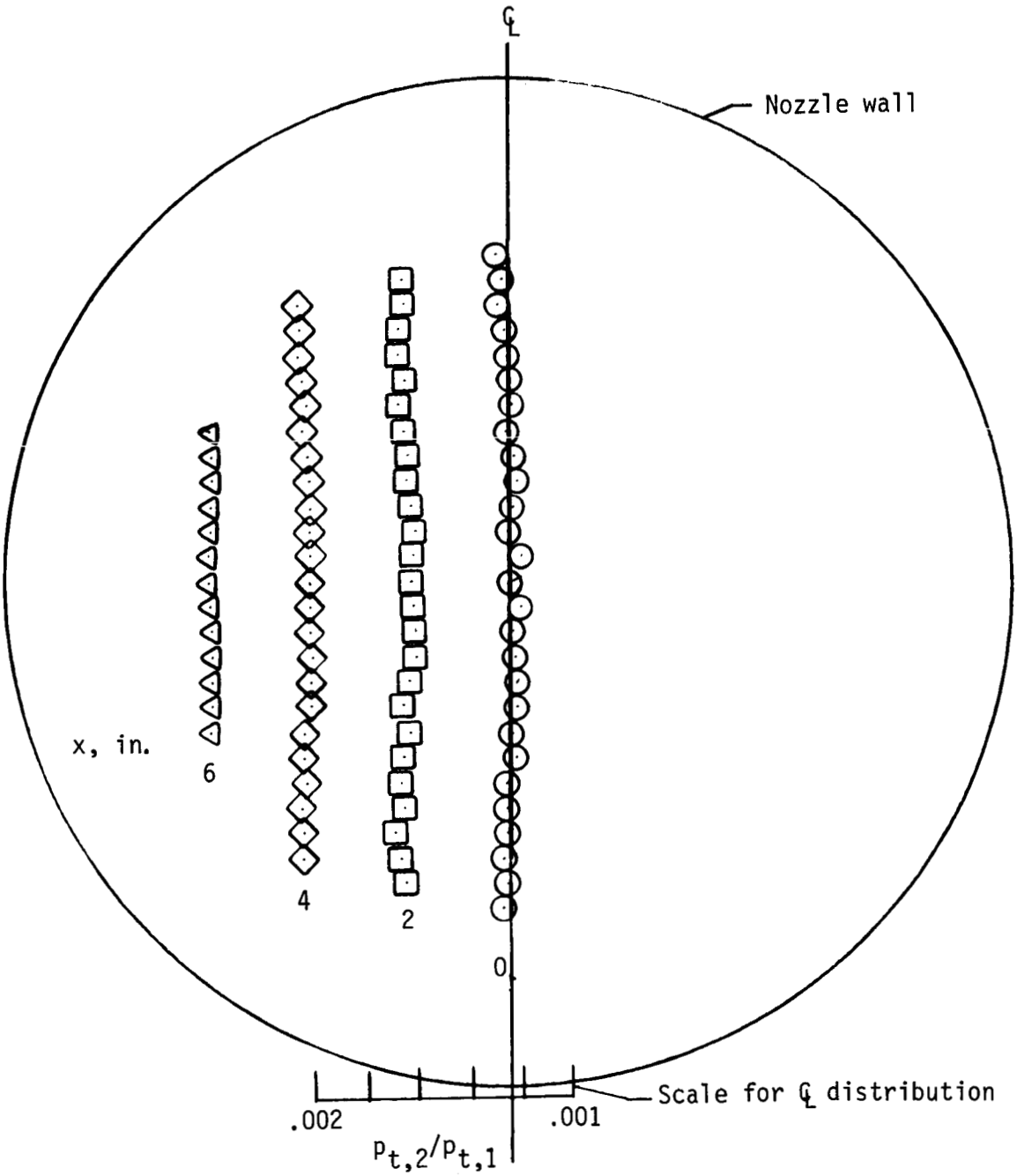

(c) $z = 8$ in.

Figure 23. Concluded.

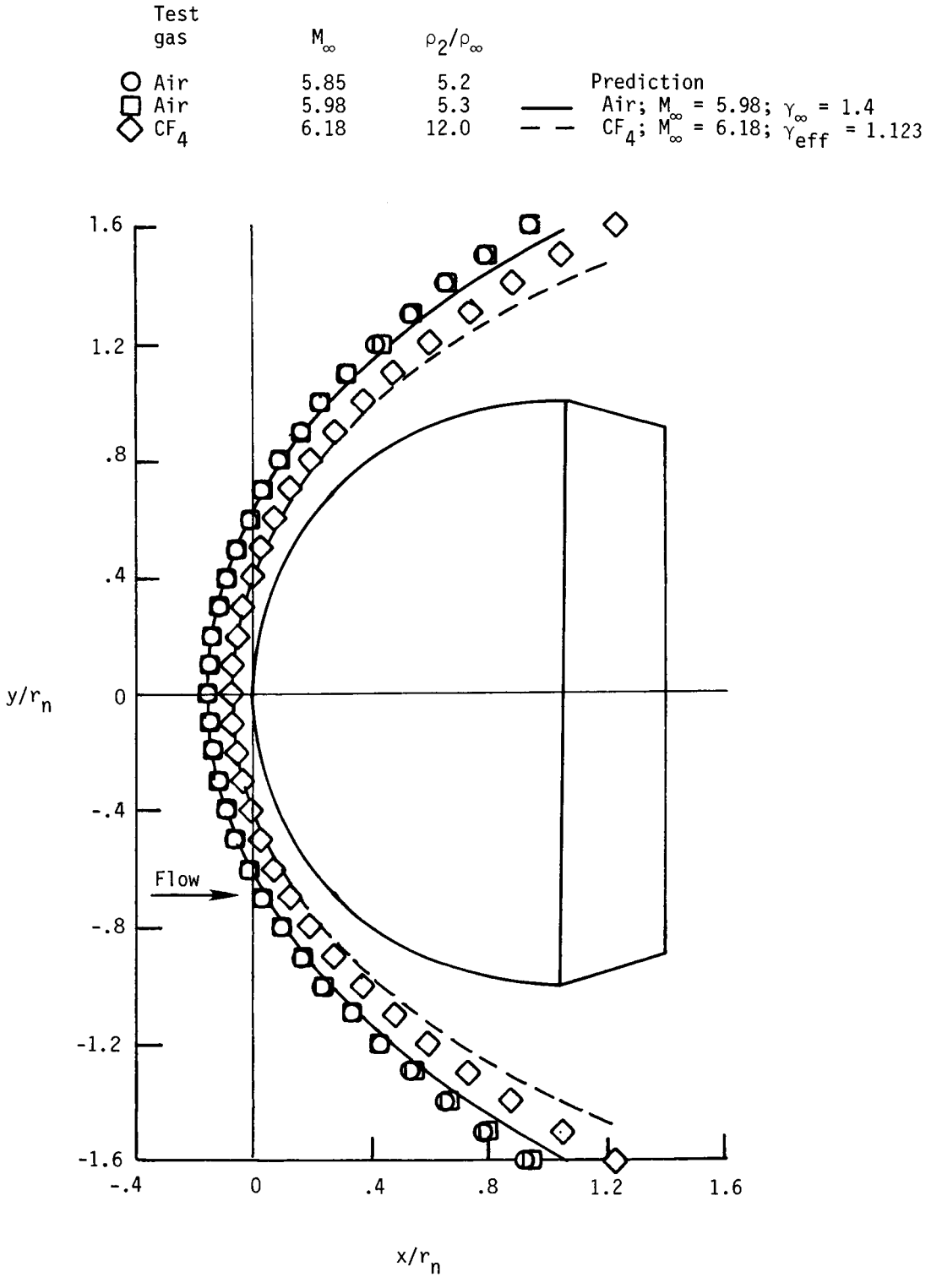

(a) 4-in-diameter hemisphere. Figure taken from reference 14.

Figure 24. Comparison of measured shock detachment distance at Mach 6 in air and CF_4 for various configurations.

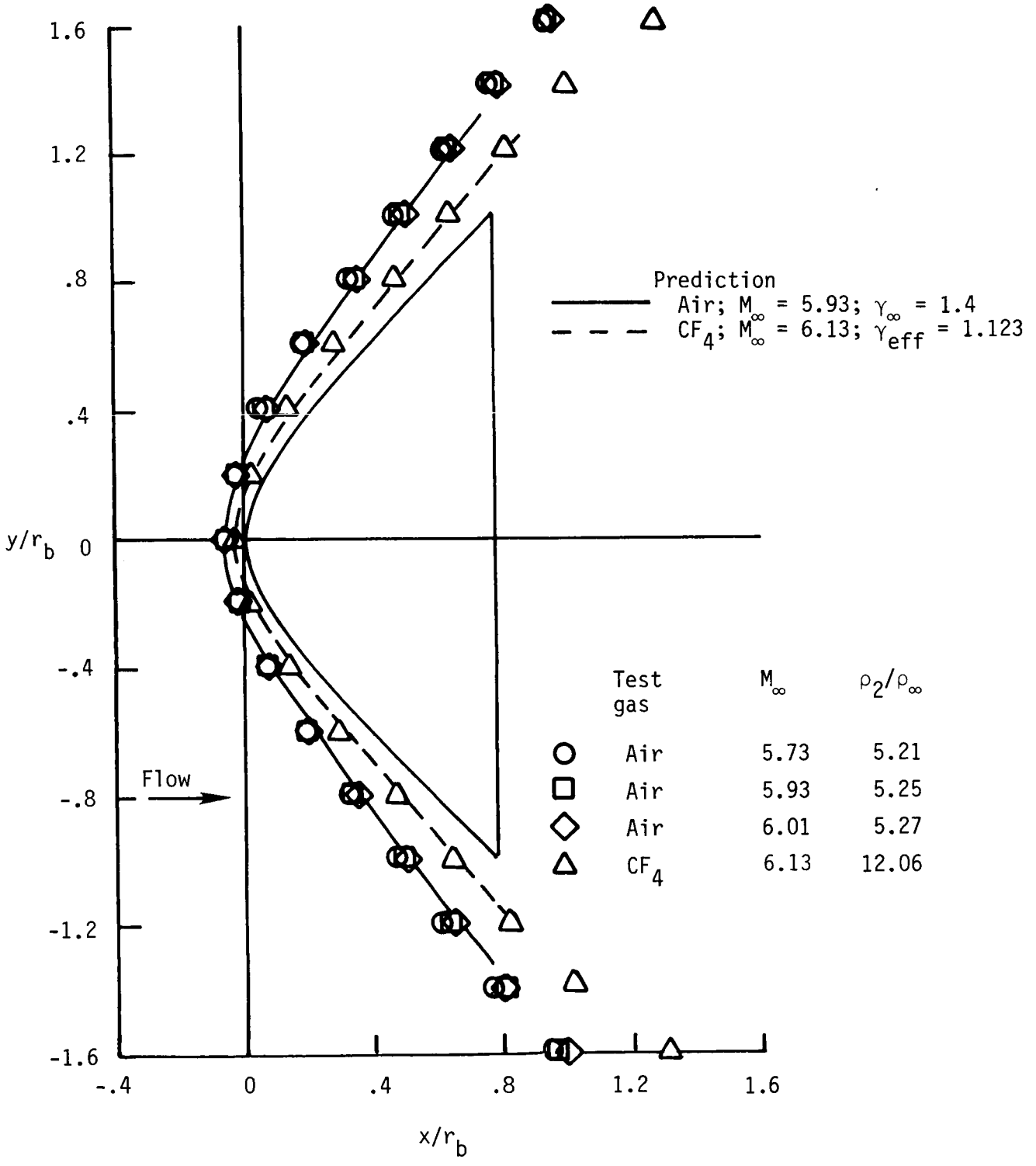

(b) Representative planetary aeroshell. Figure taken from reference 14.

Figure 24. Continued.

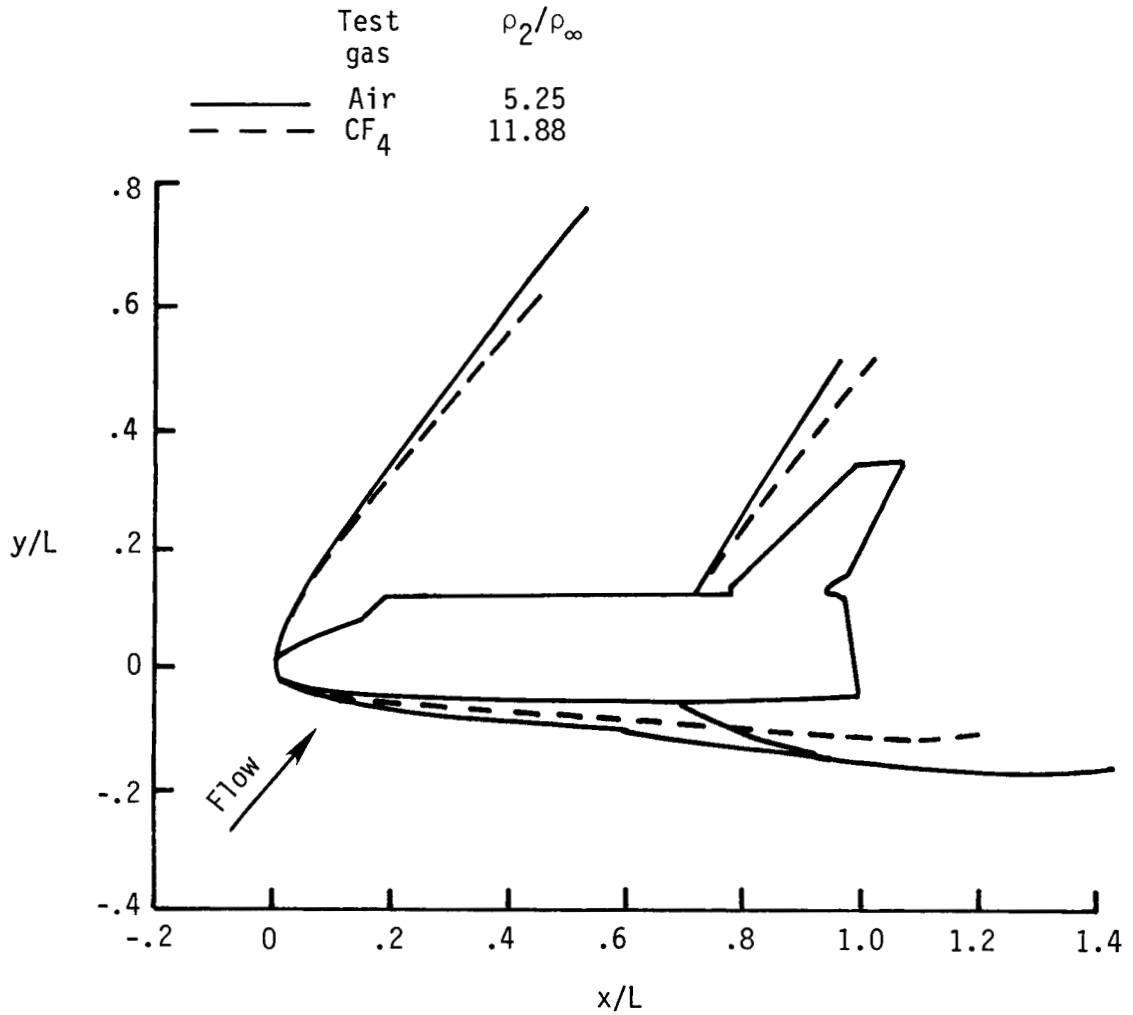

(c) 0.006-scale Shuttle orbiter at $\alpha = 40°$. Figure taken from reference 15.

Figure 24. Continued.

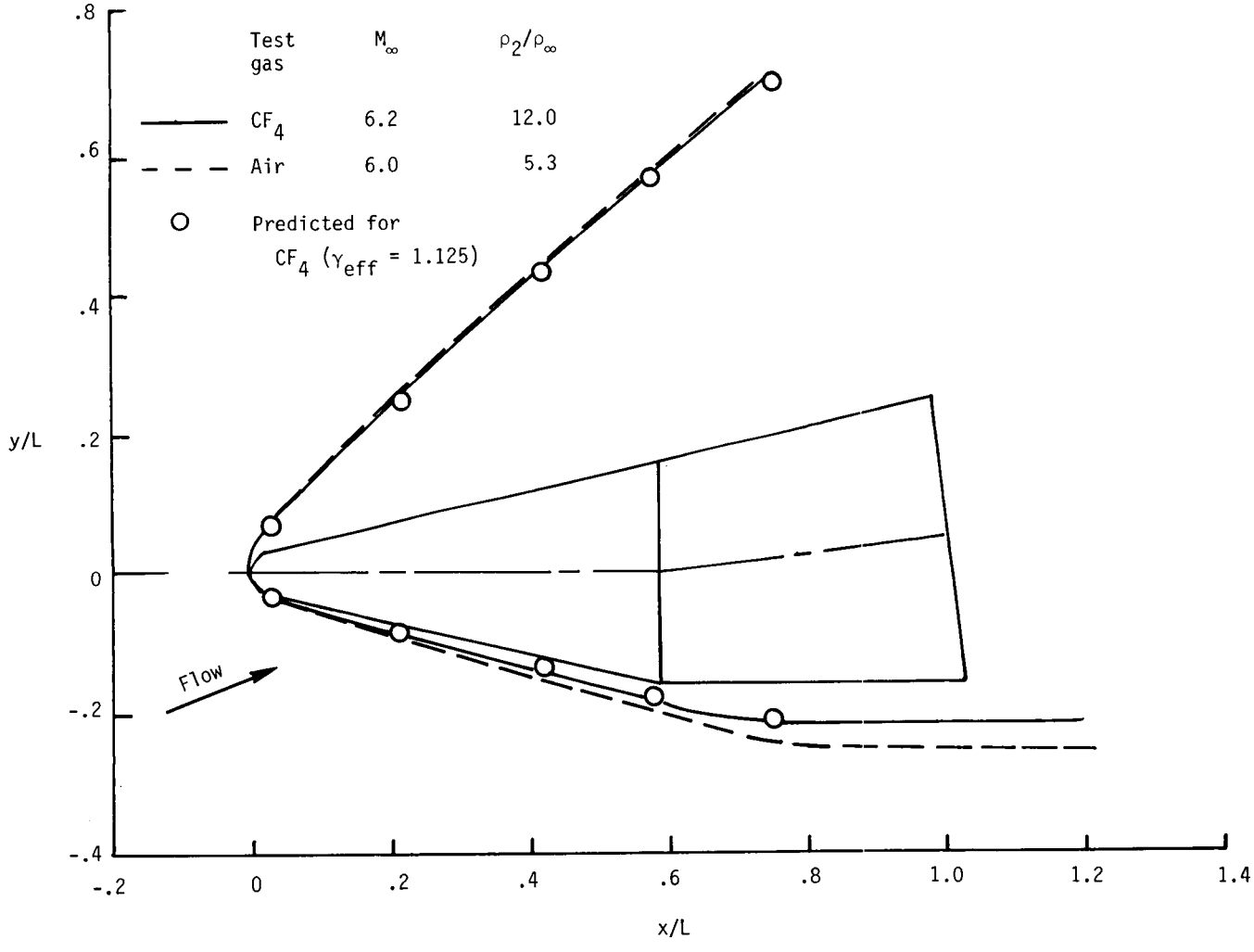

(d) Proposed planetary aerocapture vehicle. Figure taken from reference 16.

Figure 24. Concluded.

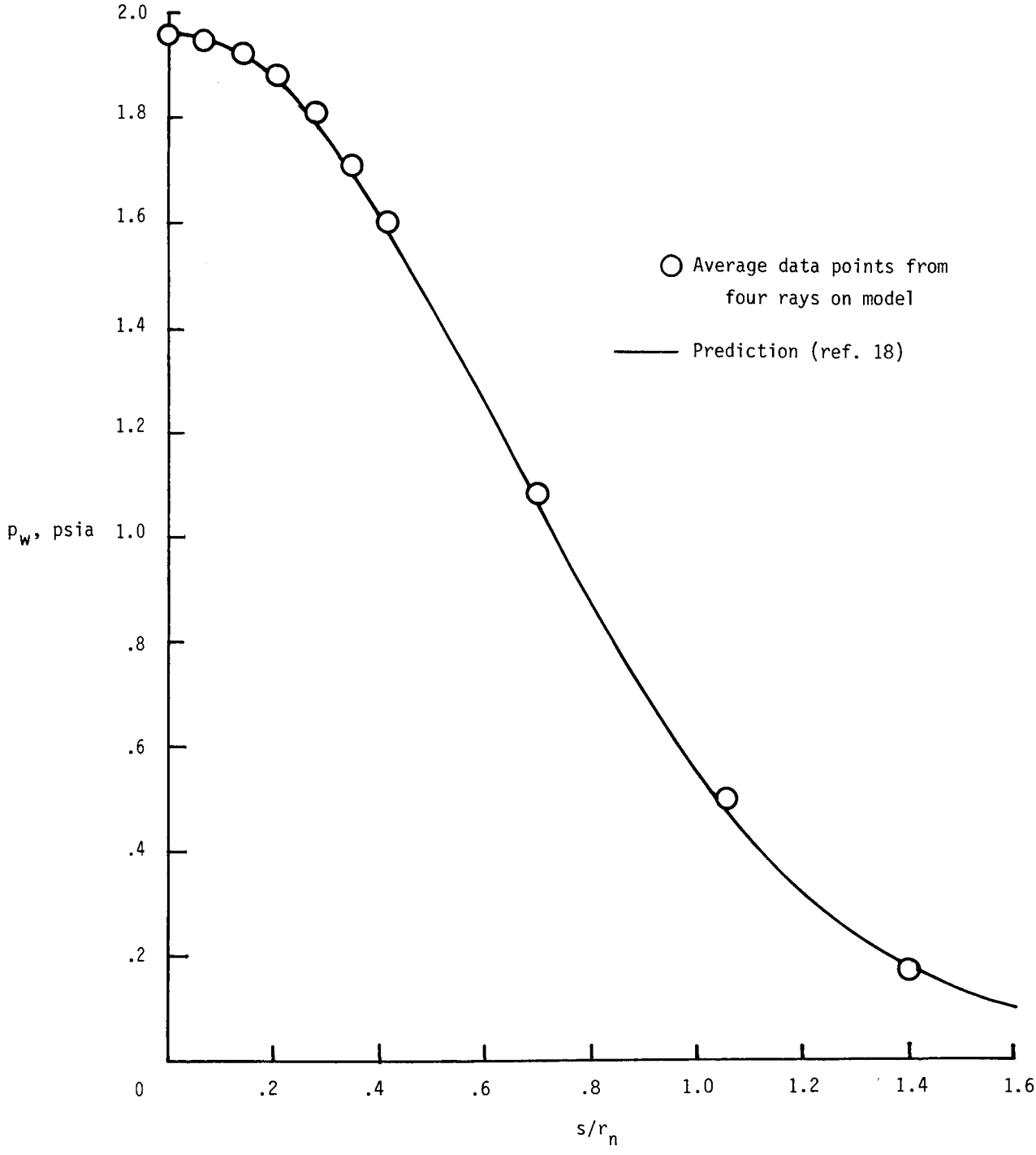

(a) 4-in-diameter hemisphere.

Figure 25. Pressure distributions on various configurations.

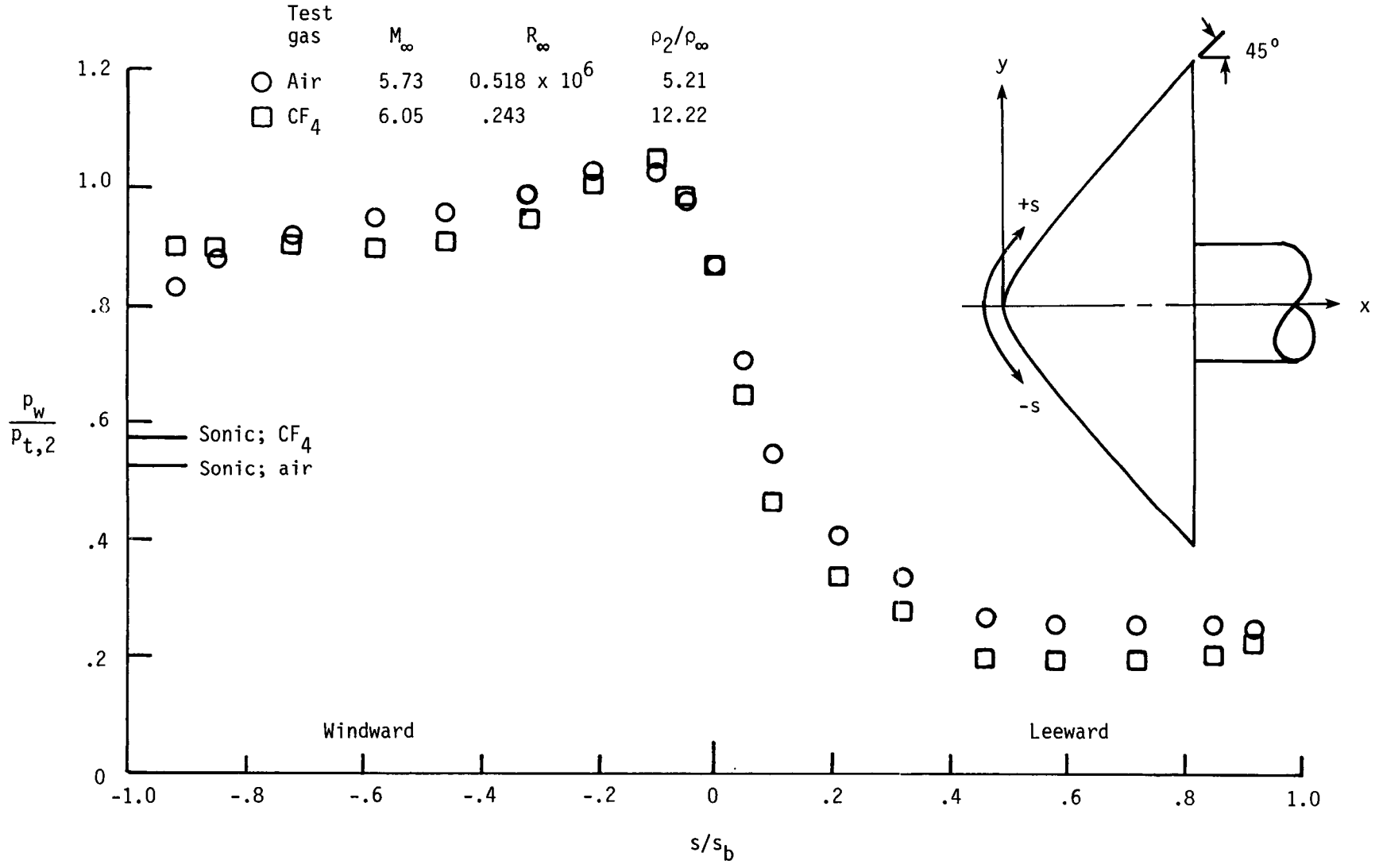

(b) Representative planetary aeroshell (hyperboloid). $\alpha = 20°$. Data taken from reference 14.

Figure 25. Continued.

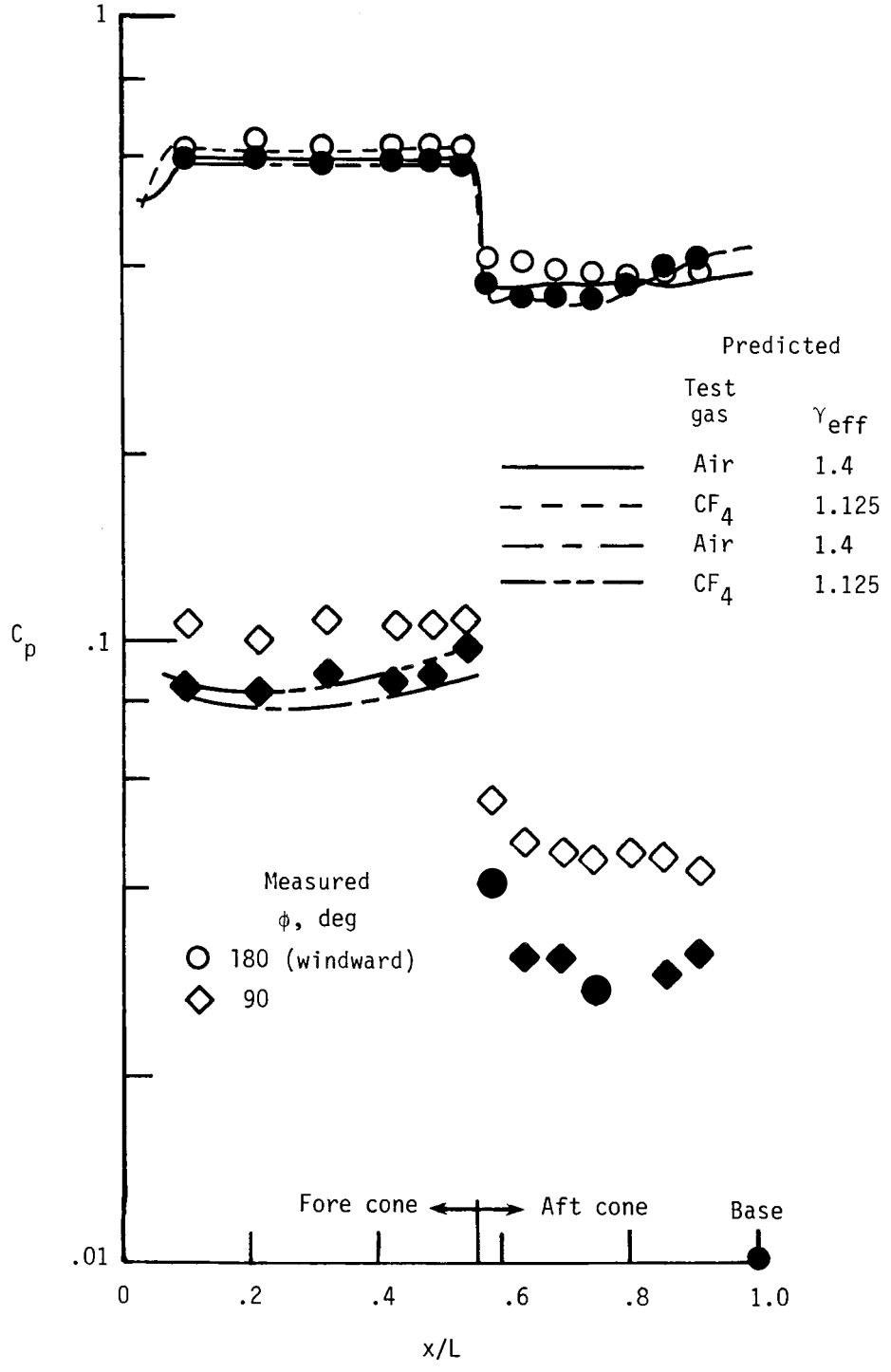

(c) Straight, spherically blunted, 13°/7° biconic. $\alpha = 20°$. Figure taken from reference 16. Open symbols indicate air data; closed symbols indicate CF_4 data.

Figure 25. Concluded.

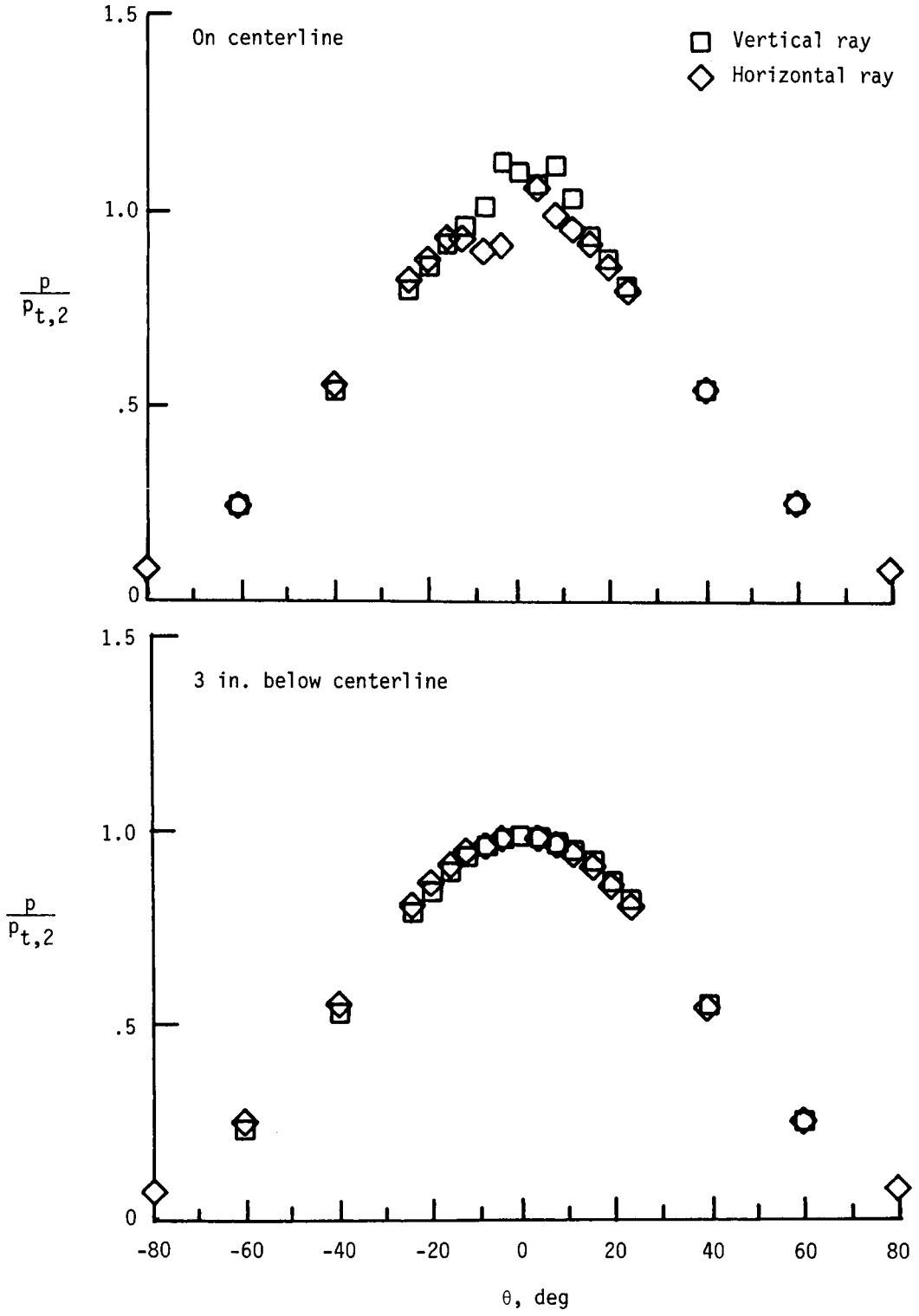

(a) $p_{t,1} \approx 1000$ psia; $T_{t,1} \approx 1185°$R; $z = 0.5$ in.

Figure 26. Pressure distributions on 4-in-diameter hemisphere.

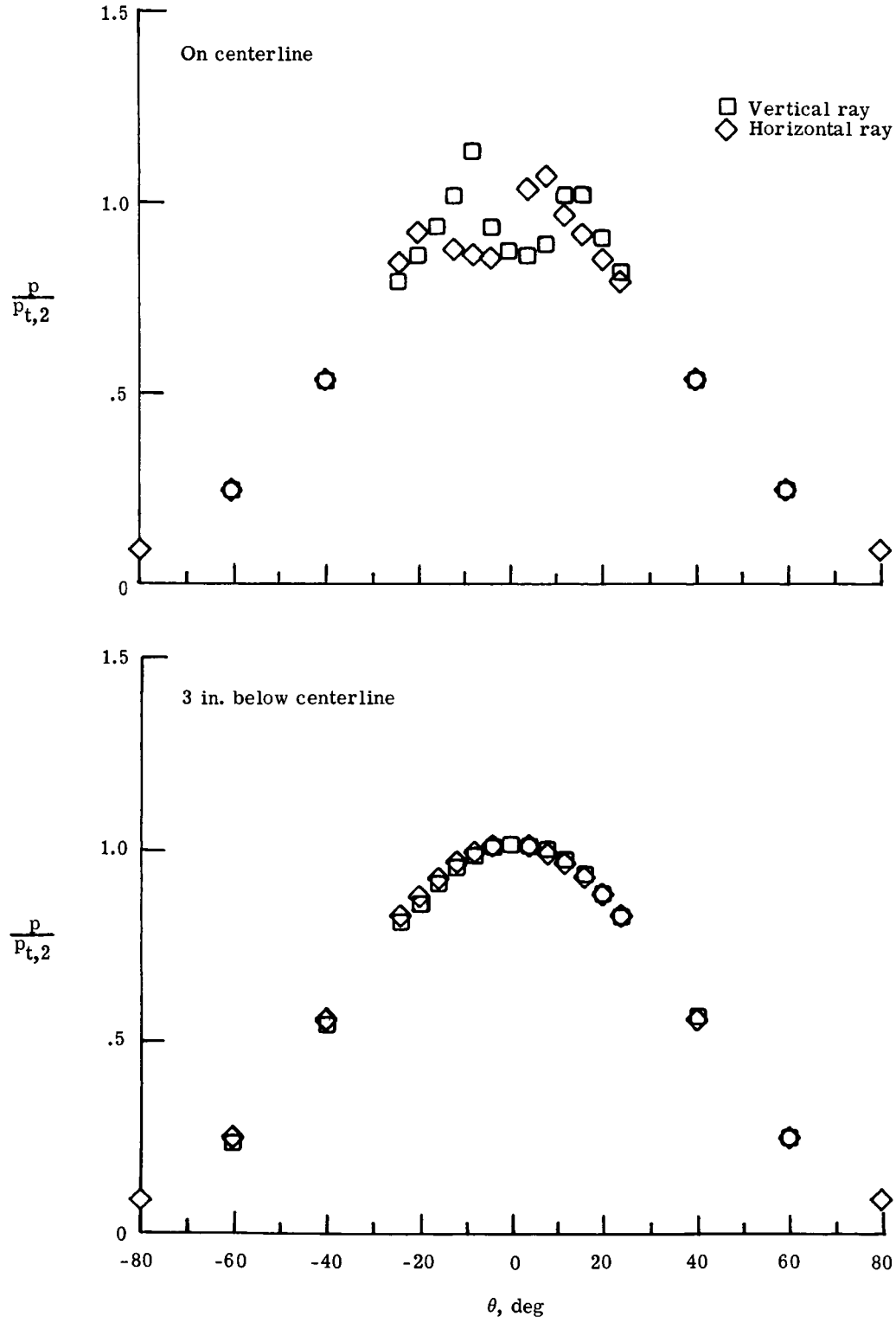

(b) $p_{t,1} \approx 1540$ psia; $T_{t,1} \approx 1179°$R; $z = 0.5$ in.

Figure 26. Continued.

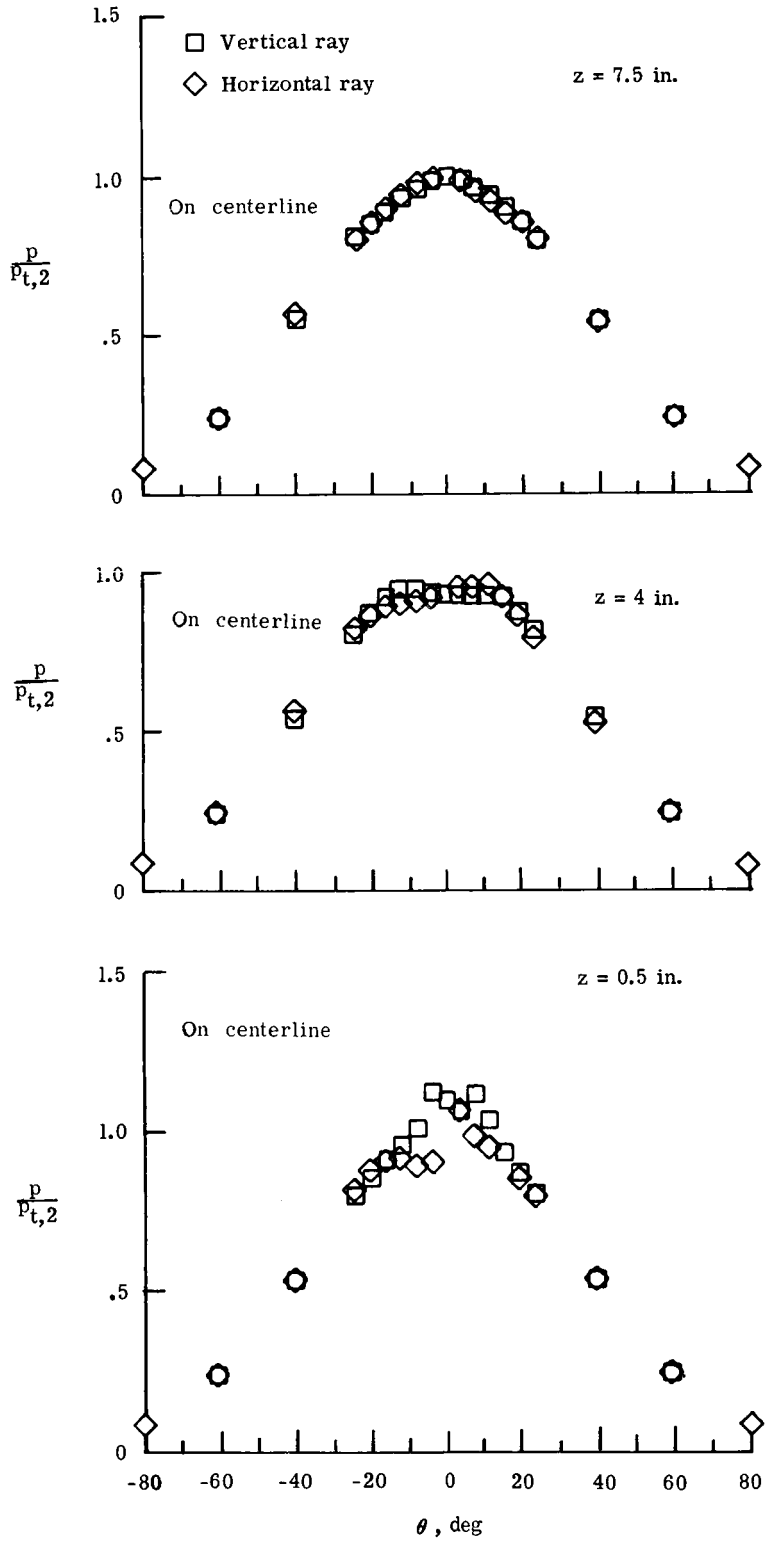

(c) $p_{t,1} \approx 1000$ psia; $T_{t,1} \approx 1179°$R; on centerline.

Figure 26. Continued.

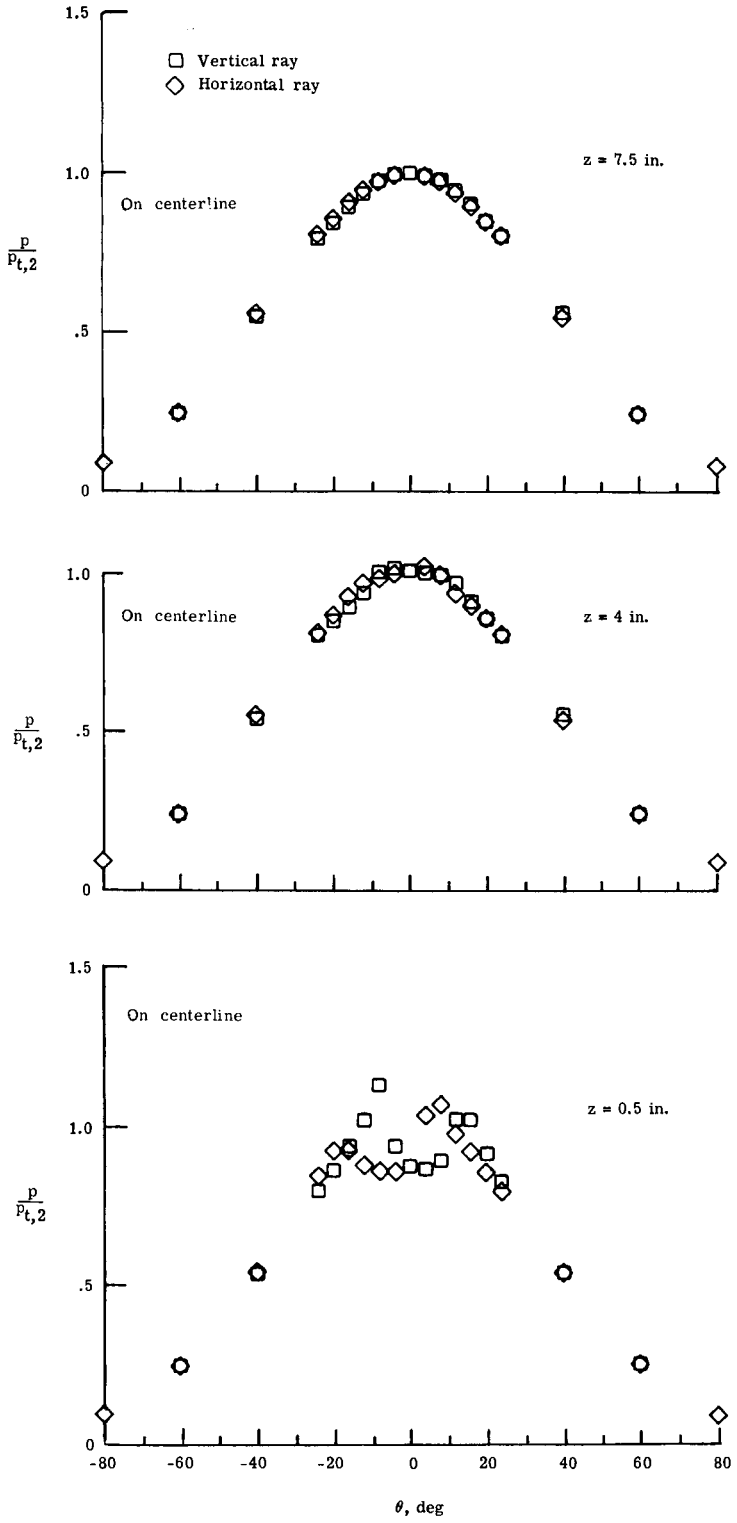

(d) $p_{t,1} \approx 1540$ psia; $T_{t,1} \approx 1179°$R; on centerline.

Figure 26. Concluded.

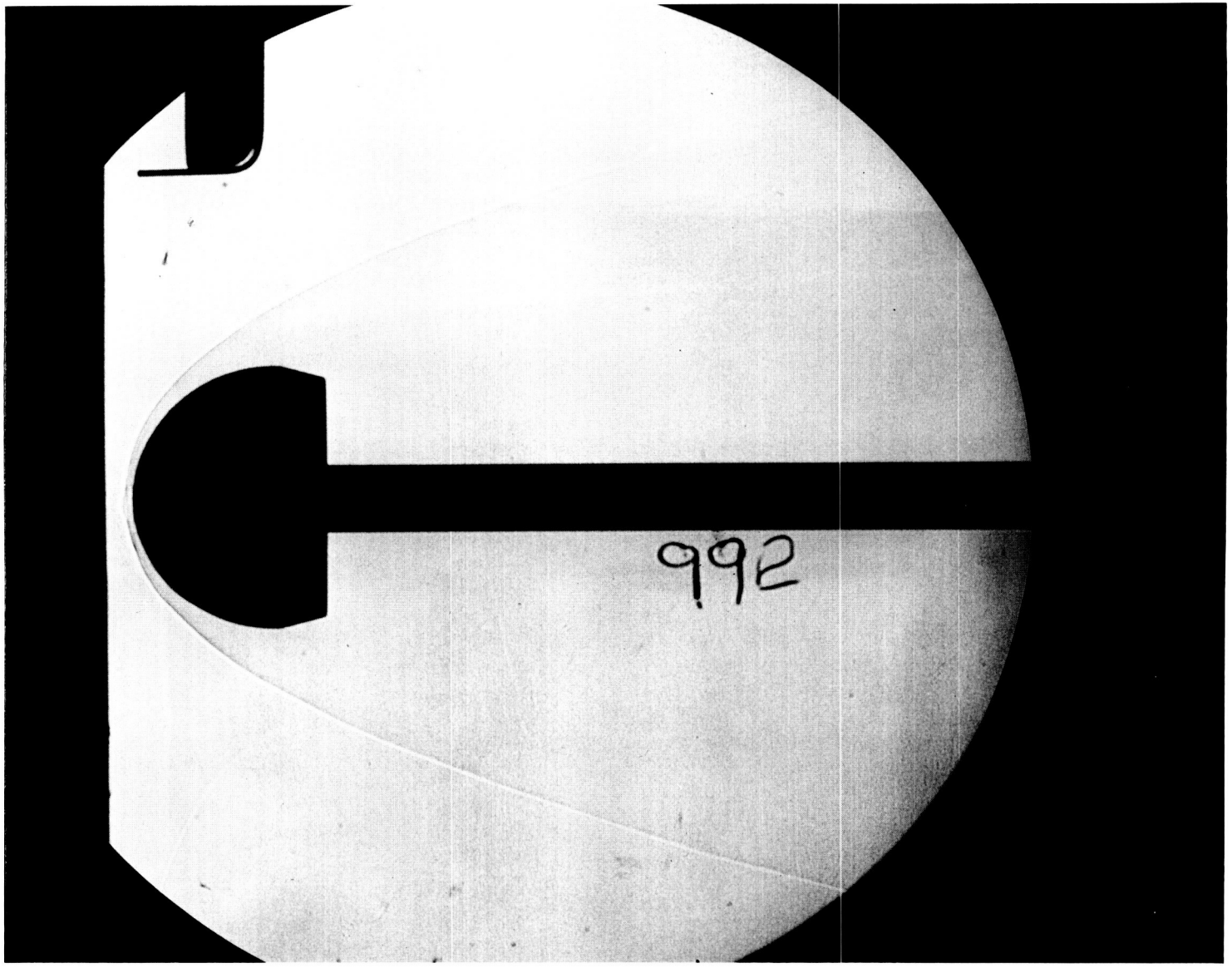

L-84012,909

(a) Shock shape.

Figure 27. Effect of nozzle centerline disturbances on shock shape and heating distribution for 4-in-diameter hemisphere. Model centerline coincident with nozzle centerline.

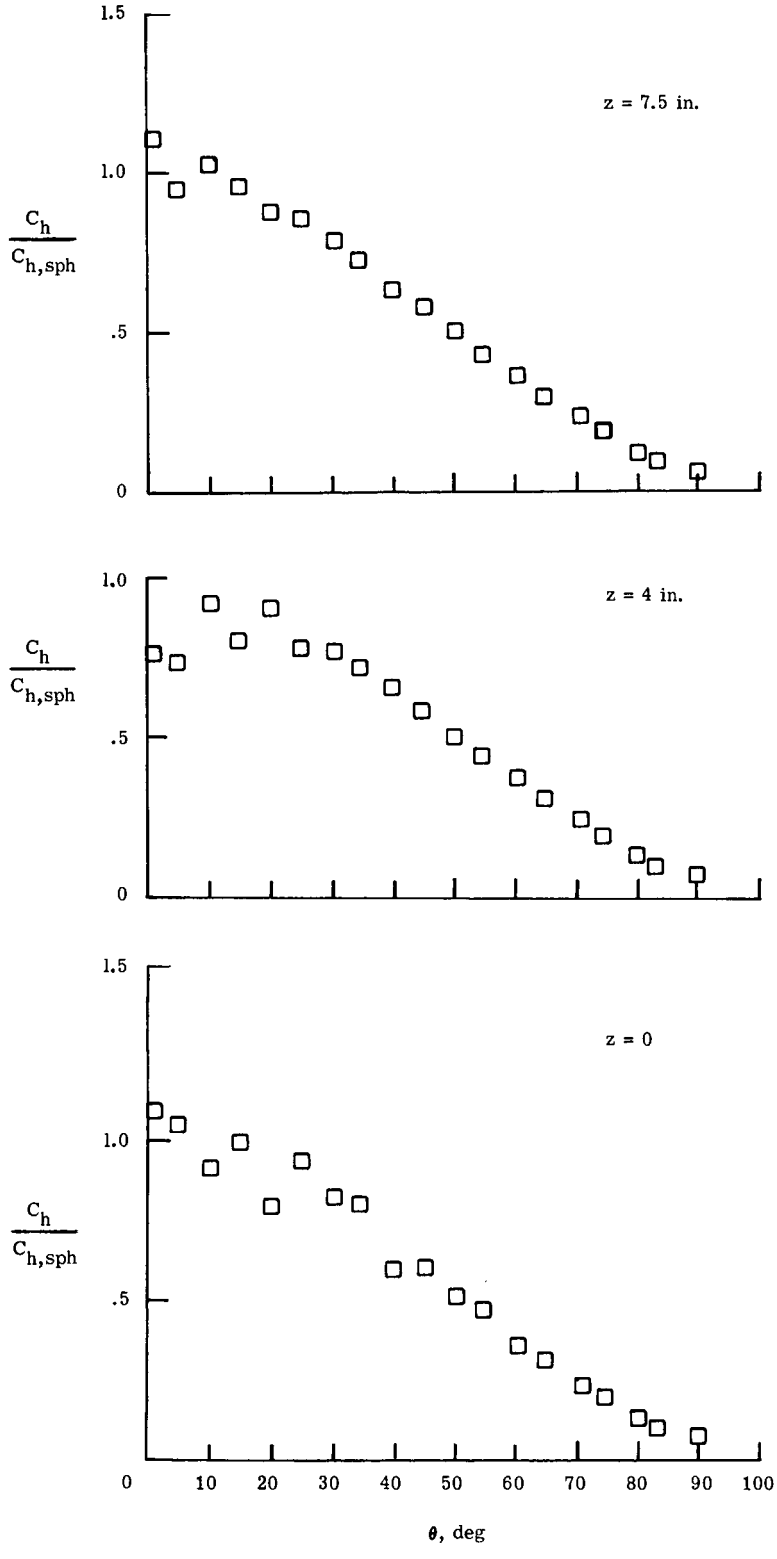

(b) Heat-transfer distributions for various distances z. $p_{t,1} \approx 1560$ psia; $T_{t,1} \approx 1180°$R.

Figure 27. Concluded.

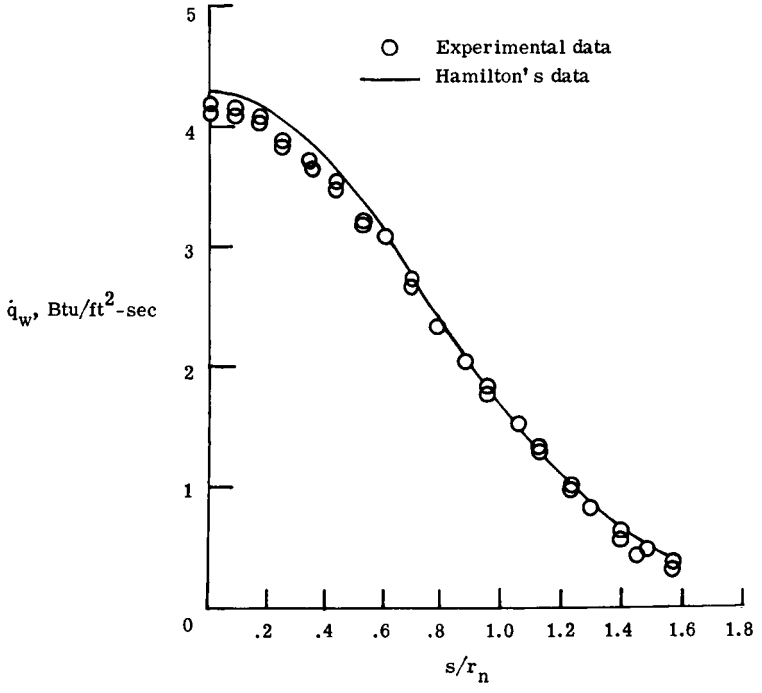

(a) $M_\infty = 6.24$; $R_{2,r_n} = 1.65 \times 10^4$.

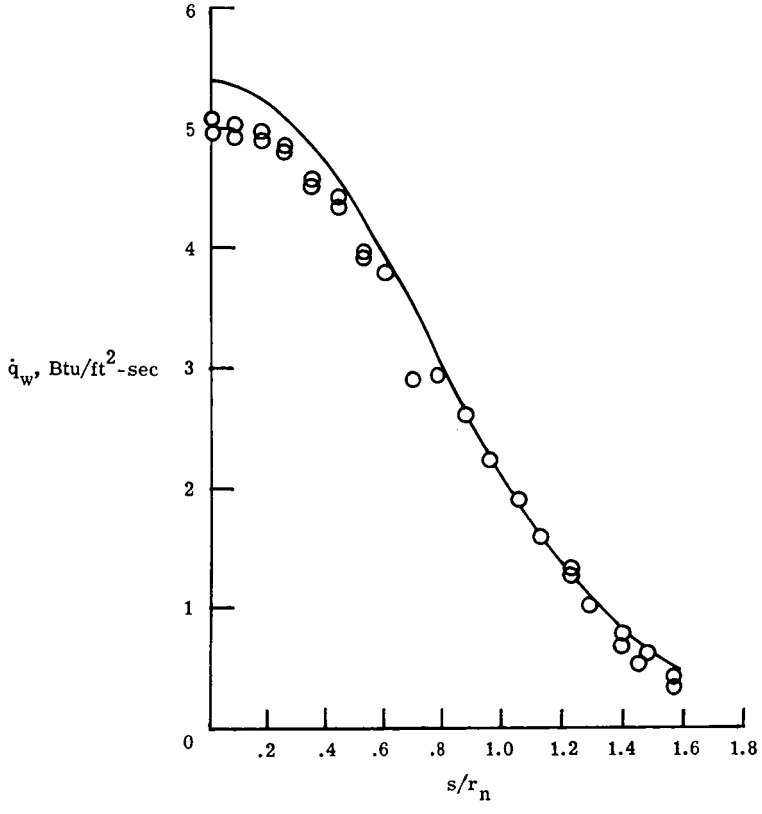

(b) $M_\infty = 6.23$; $R_{2,r_n} = 2.42 \times 10^4$.

Figure 28. Comparison of predicted and measured heat-transfer distributions on 4-in-diameter hemisphere.

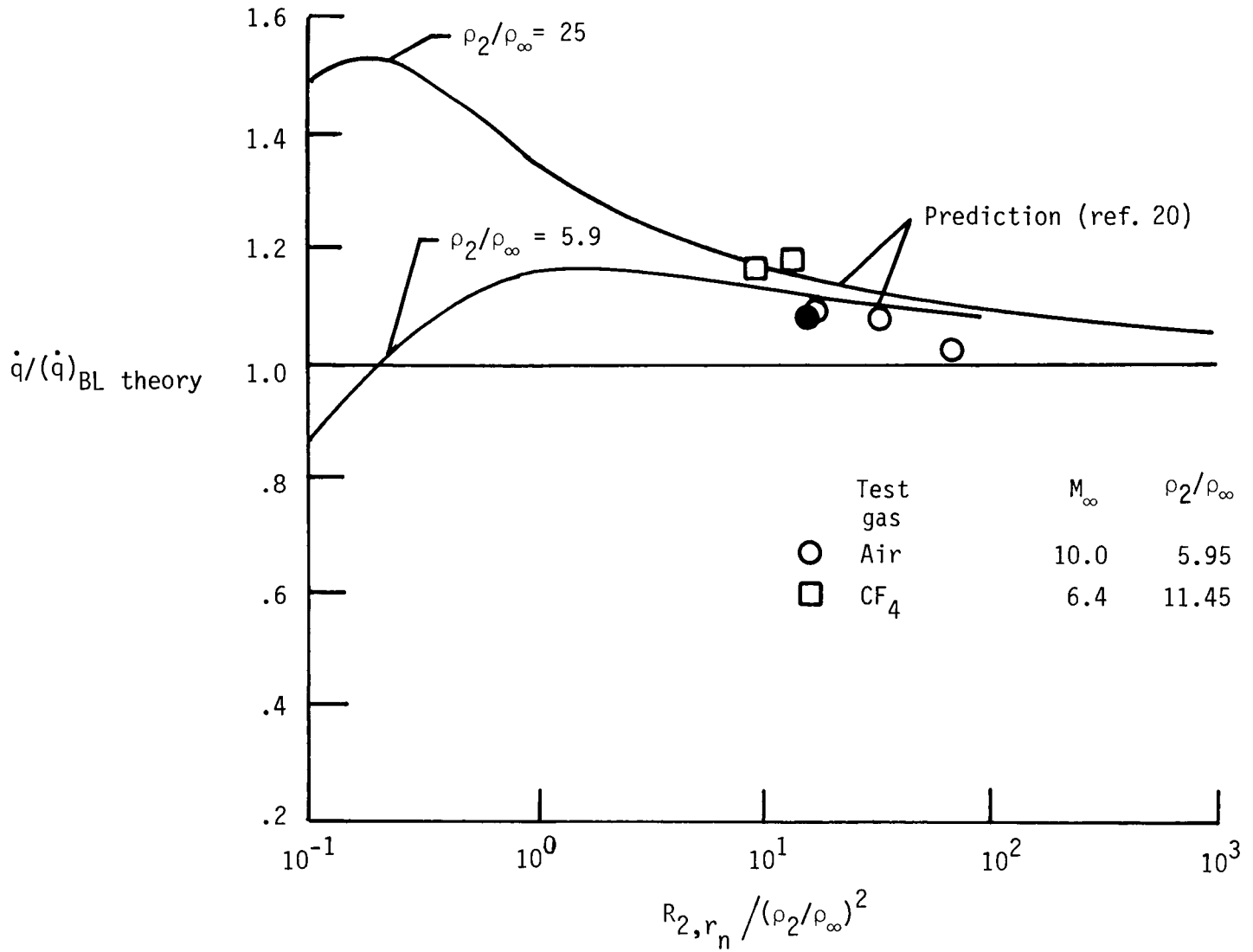

Figure 29. Low Reynolds number effects on stagnation-point heat-transfer rate to hemisphere. Open symbols indicate quartz hemisphere; closed symbol indicates MACOR nose tip.

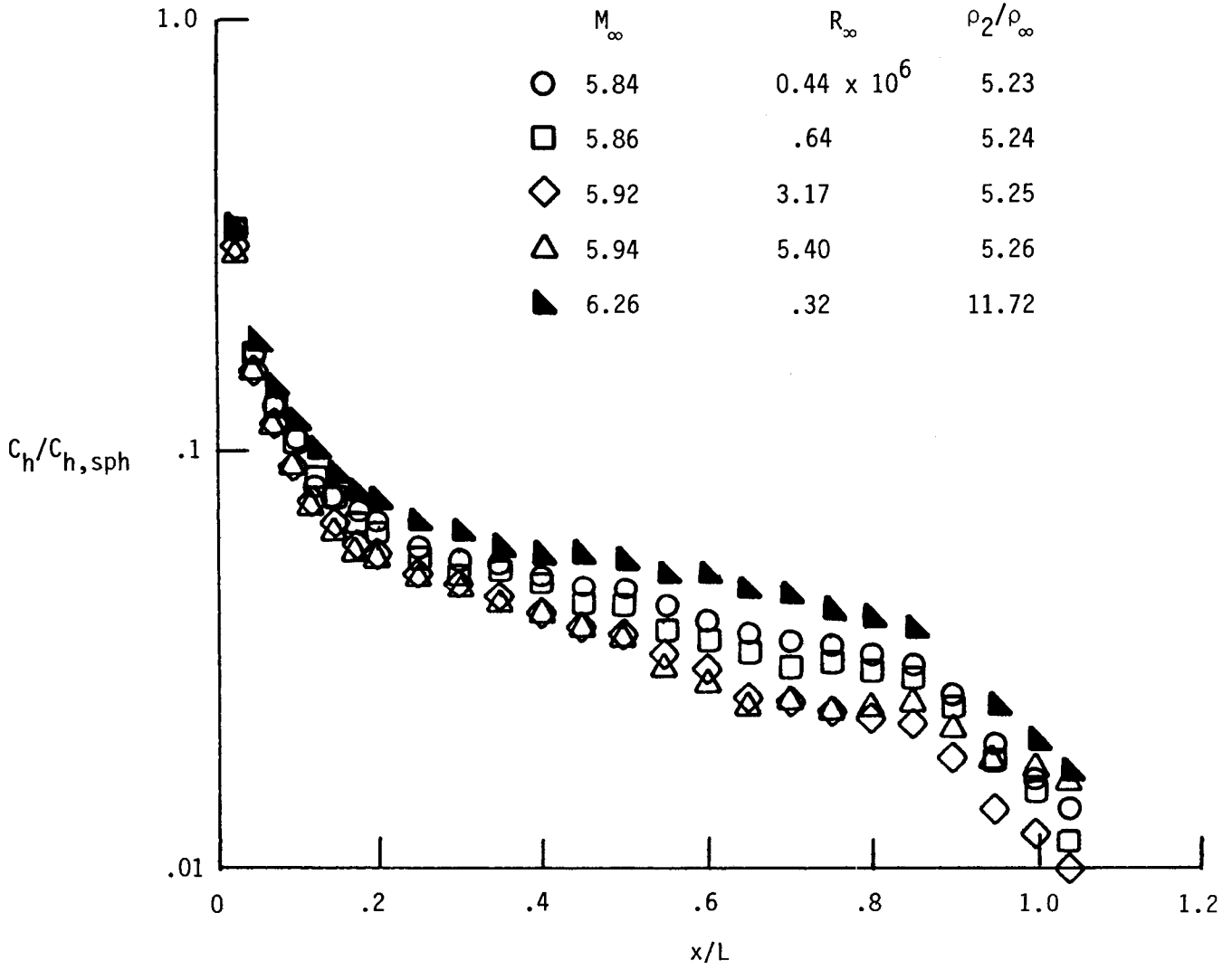

(a) $\alpha = 20°$.

Figure 30. Effect of density ratio on windward centerline heating distribution for a 0.006-scale Shuttle orbiter. Figures taken from reference 15.

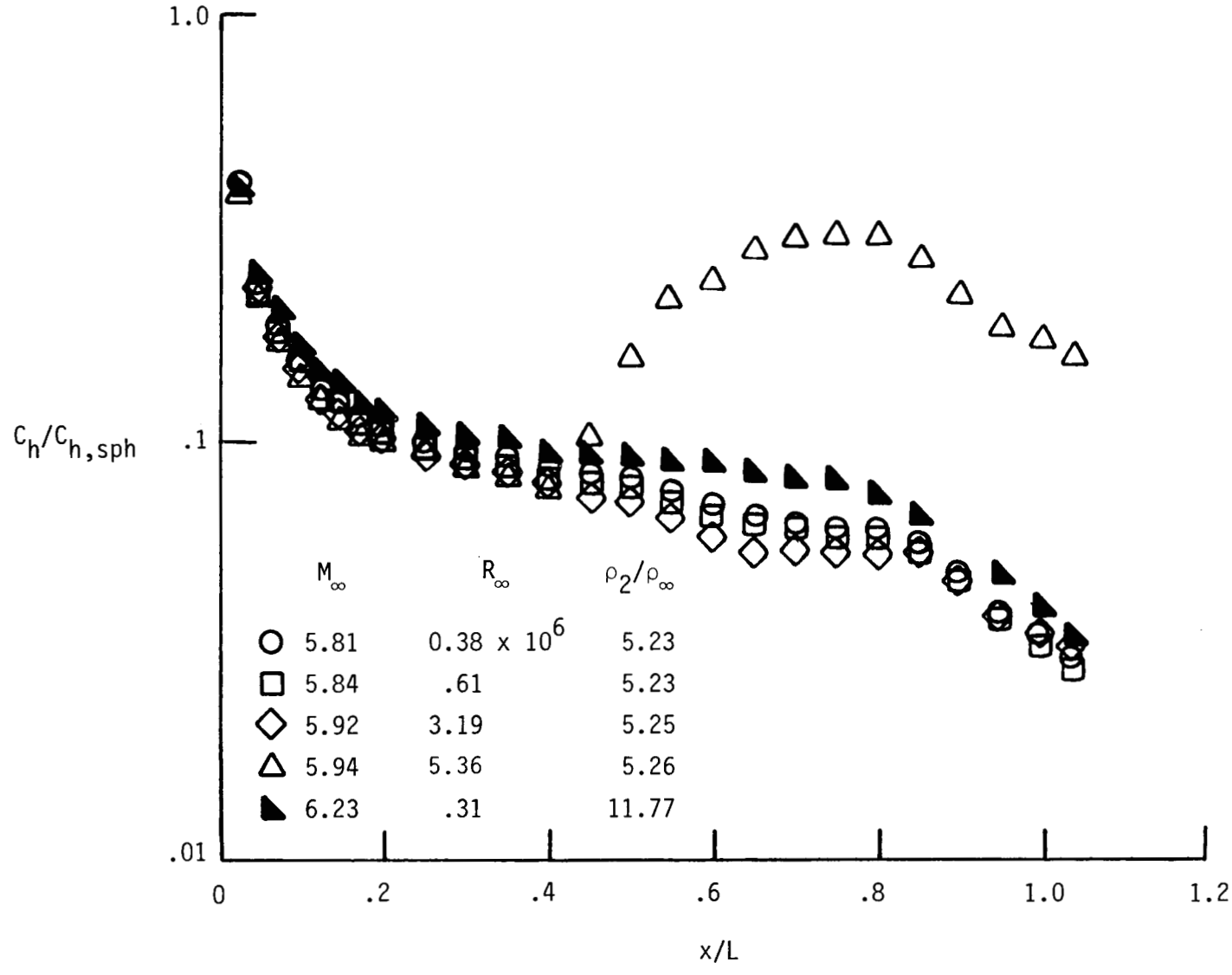

(b) $\alpha = 30°$.

Figure 30. Continued.

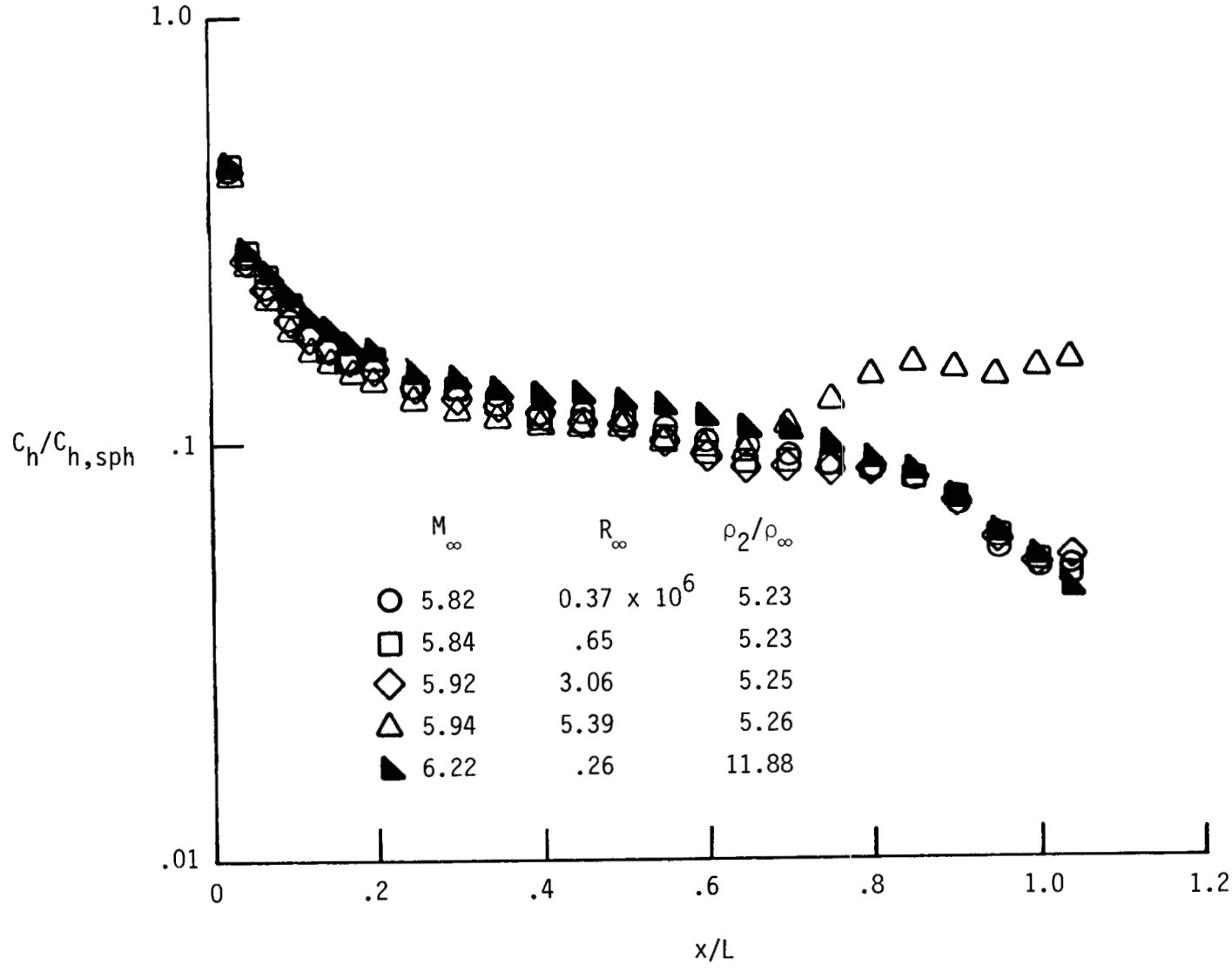

(c) $\alpha = 40°$.

Figure 30. Concluded.

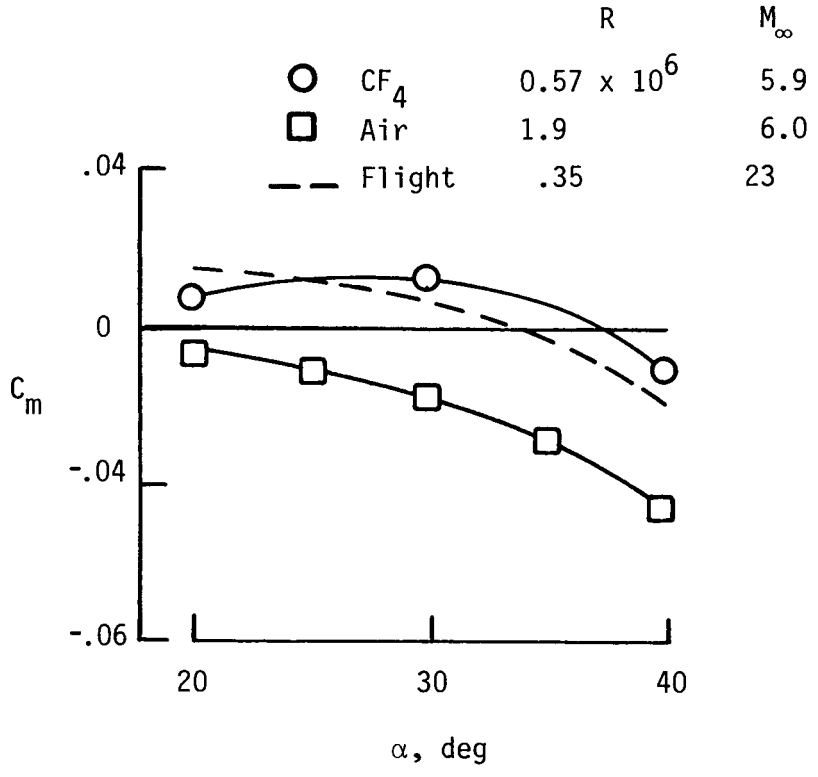

Figure 31. Comparison of wind-tunnel and flight-derived pitching-moment coefficients for Shuttle orbiter in CF_4 and air. Figure taken from reference 22.

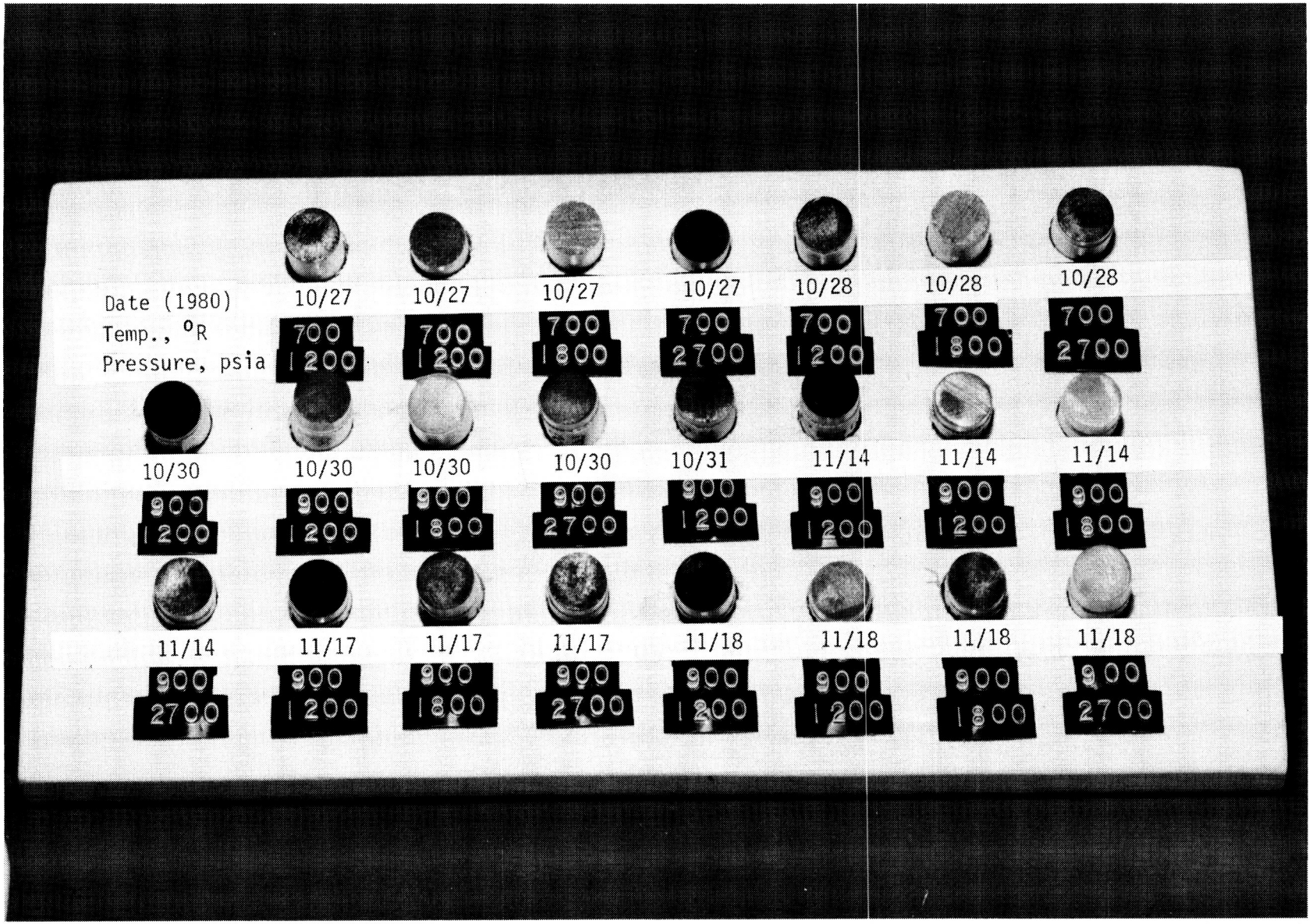

L-80-10,887

Figure 32. Teflon flat-faced-cylinder particle collector for various dates, reservoir pressures, and reservoir temperatures.

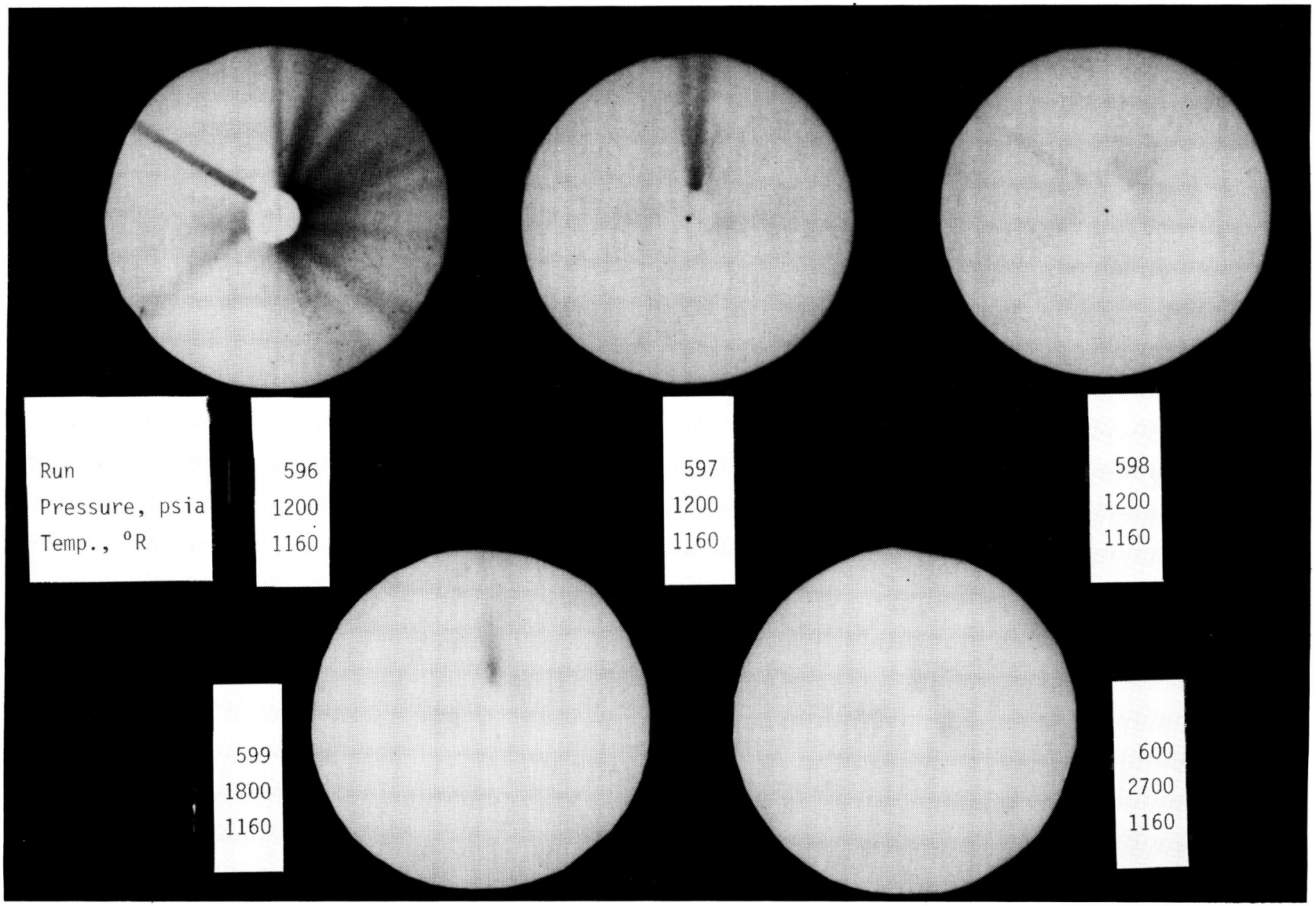

Figure 33. Time history of contamination arrival at test section.

1. Report No. NASA TP-2384	2. Government Accession No.	3. Recipient's Catalog No.

4. Title and Subtitle	5. Report Date
Description and Calibration of the Langley Hypersonic CF_4 Tunnel—A Facility for Simulating Low γ Flow as Occurs for a Real Gas	March 1985
	6. Performing Organization Code 506-51-13-01
7. Author(s) Raymond E. Midden and Charles G. Miller III	8. Performing Organization Report No. L-15798
9. Performing Organization Name and Address NASA Langley Research Center Hampton, VA 23665	10. Work Unit No.
	11. Contract or Grant No.
12. Sponsoring Agency Name and Address National Aeronautics and Space Administration Washington, DC 20546	13. Type of Report and Period Covered Technical Paper
	14. Sponsoring Agency Code

15. Supplementary Notes

16. Abstract

The Langley Hypersonic CF_4 Tunnel is a Mach 6 facility which simulates an important aspect of dissociative real-gas phenomena associated with the reentry of blunt vehicles, that is, the decrease in the ratio of specific heats (gamma) that occurs within the shock layer of the vehicle. A general description of this facility is presented along with a discussion of the basic components, instrumentation, and operating procedure. Pitot-pressure surveys were measured at the nozzle exit and downstream of the exit for reservoir temperatures from 1020°R to 1495°R and reservoir pressures from 1000 to 2550 psia. A uniform test core having a diameter of approximately 11 in. (0.55 times the nozzle-exit diameter) exists at the maximum value of reservoir pressure and temperature. The corresponding free-stream Mach number is 5.9, the unit Reynolds number is 4×10^5 per foot, the ratio of specific heats immediately behind a normal shock is 1.10, and the normal-shock density ratio is 12.6. When the facility is operated at reservoir temperatures below 1440°R, irregularities occur in the pitot-pressure profile within a small region about the nozzle centerline. These variations in pitot pressure indicate the existence of flow disturbances originating in the upstream region of the nozzle. This necessitates testing models off centerline in the uniform flow between the centerline region and either the nozzle boundary layer or the lip shock originating at the nozzle exit. Samples of data obtained in this facility with various models are presented to illustrate the effect of gamma on flow conditions about the model and the importance of knowing the magnitude of this effect.

17. Key Words (Suggested by Authors(s))	18. Distribution Statement
Langley Hypersonic CF_4 Tunnel Real-gas simulation Nozzle flow	Unclassified—Unlimited Subject Category 34

19. Security Classif.(of this report)	20. Security Classif.(of this page)	21. No. of Pages	22. Price
Unclassified	Unclassified	76	A05

For sale by the National Technical Information Service, Springfield, Virginia 22161

NASA-Langley, 1985